

**MoDOT**

Organizational Results

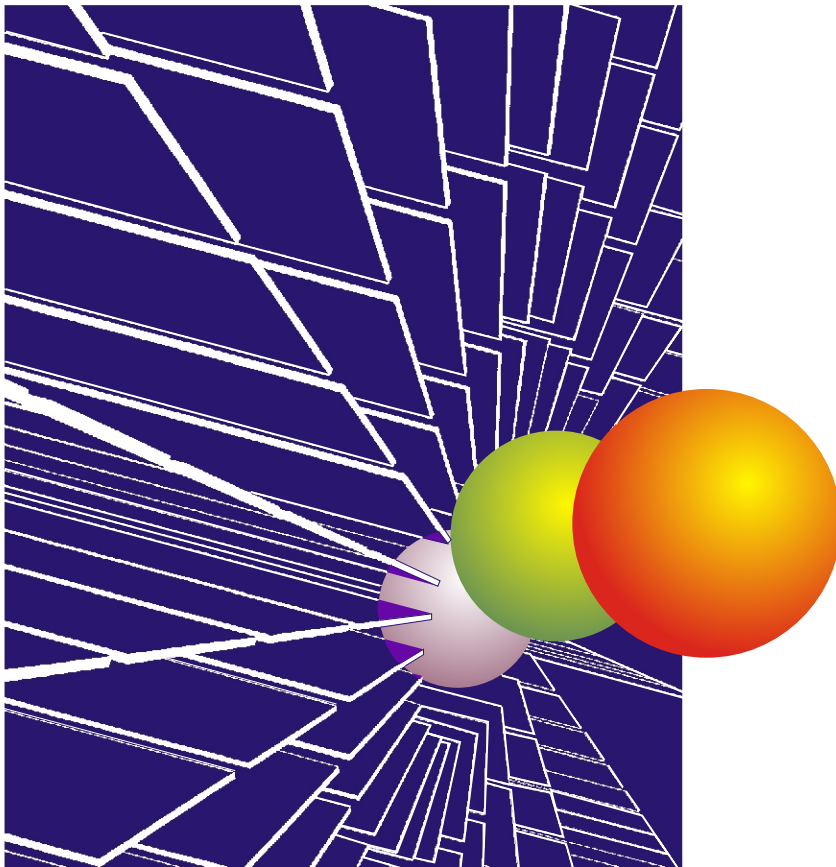
---

University of Missouri/Rolla

RDT 05-008

# **Failure Investigation of the Steel Strut on the Paseo Suspension Bridge**

RI 03-015



June, 2005

## TECHNICAL REPORT DOCUMENTATION PAGE

1. Report No. RDT 05-008	2. Government Accession No.	3. Recipient's Catalog No.	
4. Title and Subtitle FAILURE INVESTIGATION OF THE STEEL STRUT OF PASEO SUSPENSION BRIDGE		5. Report Date June 15, 2005	
		6. Performing Organization Code UMR	
7. Author(s) G. Chen, C. Courtright, L. R. Dharani, and B. Xu		8. Performing Organization Report No. RDT 05-008 /RI03-015	
9. Performing Organization Name and Address University of Missouri-Rolla 328 Butler-Carlton Civil Engineering Hall 1870 Miner Circle, Rolla, MO 65409-0030		10. Work Unit No.	
		11. Contract or Grant No.	
12. Sponsoring Agency Name and Address Missouri Department of Transportation Research, Development and Technology P. O. Box 270-Jefferson City, MO 65102		13. Type of Report and Period Covered Final Report	
		14. Sponsoring Agency Code MoDOT	
15. Supplementary Notes This investigation was conducted in cooperation with the U. S. Department of Transportation.			
16. Abstract A vertical strut of the 1232-foot long, self-anchored Paseo Suspension Bridge fractured when the temperature hit at a record low of 9°F below zero. During inspection the following day, it was found that its lower pin was frozen and did not allow for free movement of the superstructure. The objective of this study is to pinpoint one of the four reasons for this incidence or their combination: overstressing, thermal contraction, fatigue, and reduction in fracture toughness at low temperatures. To achieve this objective, material property and fatigue testing was performed on samples of strut material while the bridge and strut were analyzed under service loading conditions. This study indicated that the strut material practically has an infinite life under normal conditions. The root cause of the failure is overstressing of the vertical strut due to a frozen pin that became frozen because the design of the bridge did not allow the pin to be maintained. The mechanically frozen pin condition was attributable to salt and sand accumulation in the strut housing. To prevent this to the new struts and other similar structures, it is recommended that both upper and lower pins be greased during special inspections and the lower housings be partially sealed to prevent salt and sand accumulation near the pins. Alternatively, a rotation monitoring system can be installed to remotely monitor the rotation of all four vertical struts and alert officials should the pins become mechanically frozen.			
17. Key Words Fracture, fatigue resistance, suspension bridge, frozen pin, crack initiation life, crack propagation life		18. Distribution Statement No restrictions. This document is available to the public through National Technical Information Center, Springfield, Virginia 22161	
19. Security Classification (of this report) Unclassified	20. Security Classification (of this page) Unclassified	21. No. of Pages 86	22. Price

**Final Report**

RDT 05-008 (RI03-015)

**FAILURE INVESTIGATION OF THE STEEL STRUT  
OF PASEO SUSPENSION BRIDGE**

MISSOURI DEPARTMENT OF TRANSPORTATION  
RESEARCH, DEVELOPMENT AND TECHNOLOGY

BY: G. Chen, Ph.D., P.E.  
C. Courtright, EIT.  
L. R. Dharani, Ph.D.  
B. Xu, Ph.D.

Acknowledgments:

University Transportation Center at the University of Missouri-Rolla

JEFFERSON CITY, MISSOURI  
DATE SUBMITTED: June 15, 2005

The opinions, findings, and conclusions expressed in this publication are those of the principal investigators and the Missouri Department of Transportation; Research, Development and Technology. They are not necessarily those of the U.S. Department of Transportation, Federal Highway Administration. This report does not constitute a standard or regulation.

## **ACKNOWLEDGMENTS**

The authors would like to express their deepest gratitude to continuing coordination and support by Bryan Hartnagel, Ph.D., P.E., Structural Special Assignment Engineer, Jefferson City, and assistance over the duration of the project by Terry Stowell, Bridge Inspection Technician, District 4, from the Missouri Department of Transportation. Special thanks are due to Steve Gabel and Jeff Bradshaw from the Department of Civil, Architectural, and Environmental Engineering at the University of Missouri-Rolla (UMR) for their assistance in preparation of test specimens and apparatus, Dr. David C. Van Aken from the Materials Science and Engineering Department for his advise on the V-notch Charpy impact tests, and Jeffrey Thomas from the Basic Engineering Department for his assistance in tensile tests.

## EXECUTIVE SUMMARY

On January 22, 2003, the Paseo Bridge was hurriedly closed to traffic during the Wednesday afternoon rush hours when a pronounced gap between sections of the bridge's deck sparked fears about the span's safety. At the time, temperatures were reported to have hit a record low of 9°F below zero. During inspection the following day, the strut in the southeastern link anchorage assembly was found to be fractured. Field inspectors found the lower pin in the southeastern hanger was frozen and did not allow for free movement of the superstructure. As a result, the strut was subjected to both tension/compression and bending. The damage of the strut was likely caused by one of the following reasons or their combination: overstressing, thermal contraction, fatigue, and reduction in fracture toughness associated with low temperatures.

MoDOT requested an analysis of the bridge to determine the cause(s) of the failure. This report presents findings from an effort to understand why the southeastern vertical strut of the bridge fractured after 50 years of service. **The root cause of the failure is overstressing of the vertical strut due to a frozen pin that became frozen because the design of the bridge did not allow the pin to be maintained.** The mechanical freezing of the lower link pin has been attributed to salt and sand accumulation in the lower link housing, discovered during the bridge inspection two months prior to failure. Several relatively simple **recommendations** to prevent similar incidences to other bridges and the new struts installed on the Paseo Bridge are provided:

1. Greasing the upper and lower pins during special pin inspections and maintenances to ensure continued free rotation of the struts. This would have prevented the freezing and allows for the free rotation. It is recognized that the design of the bridge had limited access to the lower link pin housing. Therefore, although the two cycle of inspection is adequate, special pin maintenance may be done over a longer time period such as every ten years.
2. Partial sealing the lower housings to prevent salt and sand accumulation near the pins or providing traps under the finger expansion joints to stop salt and sand debris from dropping to the lower link housing. These corrosive materials damage and/or clog free rotation.
3. Installation of a problem alarming device at a cost of less than \$10k to remotely monitor the rotation of all four vertical struts and immediately alert officials should the pins become mechanically frozen. In light of the limited access to the lower link area, greasing pins could be costly, and this recommendation can be a practical solution.

### **Background and Issues:**

The Paseo Bridge is a self-anchored suspension bridge located in Kansas City, MO, spanning the Missouri River. The bridge supports Interstates I-29 and I-35 as well as US Highway 71 with an average daily traffic volume of 89,000 vehicles in 2003. Built in 1952, the total length of the bridge is 1232 ft., consisting of two side spans measuring 308 ft. each, and a main span length of 616 ft. At each end of the bridge, two stiffening girders are independently tied down to a bridge pier with two vertical hangers, or struts. Each hanger consists of a lower and an upper link connected with bolts by a strut (S24×120). The links are connected with the stiffening girder and the bridge pier by two 11-inch diameter pins, respectively.

The purpose of the study is to understand why the southeastern vertical strut of the bridge fractured after 50 years of service. To achieve this objective, material and fatigue tests were performed on samples of the strut material according to several ASTM standards. Results from the investigative testing were combined with finite element models of the bridge and strut under service loading conditions to determine why fracture occurred on January 22, 2003. The scope of this study and findings included:

1. Determine basic material properties from static tensile testing. The stress-strain curve of the material used in the fractured strut has been established with testing of five specimens. The Young's modulus of the material is 28,500 ksi, the yield stress is 36.2 ksi, and the ultimate stress is 61 ksi. The material was identified as A36 steel.
2. Establish a stress and cycles-to-failure (S-N) relation for crack initiation life estimation, taking into account mean stress effects. The fatigue constants necessary to predict the residual crack initiation life of the bridge strut with the strain-life method have been determined with testing of 25 specimens. The fatigue strength coefficient and exponent are 70.71 ksi and -0.066, respectively, while the fatigue ductility coefficient is 0.0077 and the fatigue ductility exponent is -0.28. Fatigue tests on the failed strut material indicated an infinite life under normal service conditions when the strut were free to rotate, had no initial defects or small cracks inherent to steel structures.
3. Establish the relation between fracture toughness and temperature. The goal of this exercise would be to determine the critical flaw size at the design stress as a function of the operating temperature using a fracture mechanics criterion. Charpy impact testing was conducted at nine temperatures since the thickness of specimens would be prohibitively large for direct fracture toughness testing. Based on testing of 45 specimens at temperatures ranging from -10° to 136°F, the breaking energy of various specimens was related to the temperatures to which the specimens are exposed. The fracture toughness was then converted from the breaking energy with an empirical relation. It ranges from 24 to 110 ksi\*in<sup>1/2</sup>.
4. Establish crack growth rate for crack propagation life estimation. This information allows for determination of the life to fracture given an initial crack length and known loading conditions. Five compact tension specimens were tested to establish the Paris crack growth law with two material constants:  $C=7 \times 10^{-10}$  and  $m=2.8$ . It was found that nearly 1,000,000 cycles (approximately 12 years) of 100% design loading or over 2,500,000 cycles of 50% design loading are required for an initial defect of 0.005 inches in the strut to propagate to a critical length (over 1.3 or 2.4 inches) causing sudden fracture under normal loading conditions if the pin were free to rotate. Since no visual cracks were recorded during the inspection two months prior to the failure, crack propagation was unlikely the reason for the failure. On the other hand, sudden fracture occurred as a result of the mechanically frozen pin condition at the lower link of the southeastern strut.
5. Estimate service loading conditions and number of cycles. Dead load, live load, and thermal effects on the failed strut as a result of a frozen pin condition were estimated. The dead plus live load on the failed strut is 145 kips in tension only when the pin is free to rotate. With a frozen pin condition, the dead plus live load includes a tension force of 145 kips and a moment of 4,250 kip-in at a design temperature of 60°F. When the temperature drops to -10°F (when the strut failed), the thermal effects associated with the frozen pin condition amount the load on the strut to a total of 200 kips in tension and 40,800 kip-in

in bending moment. From the recent traffic count records collected in the bridge area, each strut was subjected to approximately 230 cycles of live loading per day.

6. Establish a detailed finite element model and simulate the strut failure process. This allows for accurate calculation of the stress concentration (3.76) in the area of flange coping and the stress intensity factor as a function of crack length. Simulation results indicated that the strut would never have fractured even at low temperatures and with a 0.005-inch initial defect if the pin in the lower link were free to rotate. Low temperature makes the strut material behave more brittle with low fracture toughness and is thus a secondary contributor to the fracture of the strut after the pin was frozen. The load transferred through the web of the strut is likely 50% of design loading as supported by the fact that the strut did not fracture under the combined dead plus live load and thermal effect at a temperature of higher than 10°F during the bridge inspection in November, 2002. This fact also suggests that the initial defect (crack) in the coping flange area of the failed strut seems more than 0.001 inches.

### **Conclusion and Recommendations:**

Better design of lower link pin housing areas that allows preventative maintenance of the pins between vertical struts and the bridge foundation or special maintenance of the pins is required to prevent similar occurrences here or on other structures. The overstressing, thermal contraction, fatigue, and reduction in fracture toughness associated with low temperatures were all real conditions, but they would not have caused the failure if the preventative maintenance was done. They are contributory factors.

Once again the recommendations are:

1. Greasing the upper and lower pins during special pin inspections and maintenances to ensure continued free rotation of the struts. This would have prevented the freezing and allows for the free rotation. It is recognized that the design of the bridge had limited access to the lower link pin housing. Therefore, although the two cycle of inspection is adequate, special pin maintenance may be done over a longer time period such as every ten years.
2. Partial sealing the lower housings to prevent salt and sand accumulation near the pins or providing traps under the finger expansion joints to stop salt and sand debris from dropping to the lower link housing. These corrosive materials damage and/or clog free rotation.
3. Installation of a problem alarming device at a cost of less than \$10k to remotely monitor the rotation of all four vertical struts and immediately alert officials should the pins become mechanically frozen. In light of the limited access to the lower link area, greasing pins could be costly, and this recommendation can be a practical solution.

## TABLE OF CONTENTS

	Page
LIST OF ILLUSTRATIONS .....	x
LIST OF TABLES .....	xii
1. INTRODUCTION .....	1
1.1 GENERAL .....	1
1.2 RESEARCH SIGNIFICANCE .....	6
1.3 RESEARCH OBJECTIVES .....	6
2. LITERATURE REVIEW .....	7
2.1 GENERAL .....	7
2.2 STATIC TENSILE TESTING .....	7
2.3 FATIGUE TESTING .....	7
2.4 CHARPY IMPACT TESTING .....	8
2.5 FATIGUE CRACK GROWTH .....	9
2.6 PASEO BRIDGE INSPECTION REPORTS .....	9
2.7 AMBIENT TEMPERATURE HISTORY .....	9
3. STATIC TENSILE TESTING .....	11
3.1 GENERAL .....	11
3.2 SPECIMEN DESIGN .....	11
3.3 TEST PROCEDURE .....	11
3.4 FINDINGS .....	13
4. FATIGUE TESTING .....	15
4.1 GENERAL .....	15
4.2 SPECIMEN DESIGN .....	15
4.3 TEST PROCEDURE .....	15
4.4 FINDINGS .....	18
5. CHARPY IMPACT TESTING .....	23
5.1 GENERAL .....	23
5.2 SPECIMEN DESIGN .....	23
5.3 TEST PROCEDURE .....	24

5.4	FINDINGS .....	25
6.	FATIGUE CRACK GROWTH .....	29
6.1	GENERAL .....	29
6.2	SPECIMEN DESIGN .....	29
6.3	TEST PROCEDURE .....	31
6.4	FINDINGS .....	32
7.	LOAD AND CYCLE ESTIMATION .....	35
7.1	GENERAL .....	35
7.2	DEAD LOAD CALCULATION .....	35
7.3	LIVE LOAD CALCULATION .....	35
7.4	THERMAL LOAD CALCULATION .....	37
7.5	CYCLE DETERMINATION .....	38
8.	FINITE ELEMENT MODELING .....	40
8.1	GENERAL .....	40
8.2	FINITE ELEMENT MODELS .....	40
8.3	FINITE ELEMENT MODEL LOADING .....	42
8.4	J-INTEGRAL EVALUATION .....	44
8.5	FINDINGS .....	44
9.	CONCLUSIONS AND RECOMMENDATIONS .....	49
10.	BIBLIOGRAPHY .....	51
APPENDICES		
A.	STATIC TENSILE TESTING DATA .....	53
B.	FATIGUE DATA .....	55
C.	CHARPY V-NOTCH IMPACT DATA .....	80
D.	FATIGUE CRACK GROWTH DATA .....	81
E.	INFLUENCE LINES FOR SOUTHEASTERN STRUT .....	84
F.	SPECIFICATIONS FOR REMOTE TILTMETER .....	86

## LIST OF ILLUSTRATIONS

	Page
Figure 1.1 Plan and Elevation View of Paseo Bridge.....	2
Figure 1.2 Link Anchorage Details.....	2
Figure 1.3 Rise in Southern Span .....	3
Figure 1.4 Point of Strut Failure .....	3
Figure 1.5 Fractured Strut Web Detail.....	3
Figure 1.6 Lower Link Anchorage.....	4
Figure 1.7 Shear Damage of Rivets and Fracture Surface.....	4
Figure 1.8 Fracture Pattern of SE Strut Web .....	4
Figure 1.9 Comparison of Pin Conditions .....	5
Figure 1.10 Cracking in Northeastern Strut.....	5
Figure 2.1 Charpy V-Notch Impact Test Results (Frank, 1974).....	8
Figure 2.2 Temperature History for Downtown Kansas City Airport .....	11
Figure 3.1 Instron 4485 and Data Acquisition System .....	12
Figure 3.2 Calibrated Extensometer .....	12
Figure 3.3 Verification of Test Validity .....	13
Figure 3.4 Engineering Stress-Strain Curves.....	14
Figure 4.1 Fatigue Specimen Dimensions .....	15
Figure 4.2 MTS 880 and Data Acquisition System .....	16
Figure 4.3 Longitudinal Strain Measurement Devices .....	16
Figure 4.4 Failure of Fatigue Specimen.....	17
Figure 4.5 Typical Hysteresis Loop for Specimen 15 .....	18
Figure 4.6 Power Law Curve Fit for Stress Amplitude vs. Reversals to Failure.....	19
Figure 4.7 Power Law Curve Fit for Plastic Strain vs. Reversals to Failure .....	20
Figure 4.8 Finite Element Model to Determine Stress Concentration Factor.....	20
Figure 4.9 Strain Life Curve for Paseo Bridge Struts.....	22
Figure 4.10 Residual Life Estimation Curve for Paseo Bridge Struts .....	22
Figure 5.1 Standard Charpy V-Notch Specimens.....	23
Figure 5.2 Tinius Olsen Model 84 Universal Impact Tester .....	24
Figure 5.3 Dry-Ice and Alcohol Bath .....	24
Figure 5.4 Temperature as Measured from Alcohol Bath .....	25
Figure 5.5 Placing Charpy V-Notch Specimen in Anvil .....	25
Figure 5.6 Absorbed Energy at Temperatures Tested .....	29
Figure 5.7 Prediction of Fracture of Southeastern Strut .....	28
Figure 6.1 Compact Tension Specimen Orientation.....	30
Figure 6.2 Compact Tension Specimen Dimensions.....	30
Figure 6.3 Compact Tension Specimen .....	30
Figure 6.4 Crack Growth Test Set-up.....	31
Figure 6.5 Crack Measurement During Growth .....	31
Figure 6.6 Plot Showing Regions I and II.....	32
Figure 6.7 Power Law Curve Fit to Determine Paris Law Constants.....	33
Figure 6.8 Crack Propagation Life Estimation Curves.....	34
Figure 7.1 Dead Load Ballast Used During Deck Repositioning.....	35
Figure 7.2 SAP 2000 Model of Paseo Suspension Bridge.....	36

Figure 7.3 Cross Section of Deck, Stringers, and Girder.....	36
Figure 7.4 Deflected Shape of Paseo Bridge Due to Thermal Contraction.....	36
Figure 8.1 ABAQUS Model of Middle Plate of Strut Assembly .....	40
Figure 8.2 Front and Back Views of Modeled Strut.....	41
Figure 8.3 Local Model Relationship to Global Model.....	41
Figure 8.4 Three Dimensional Mesh of Local Model.....	42
Figure 8.5 Mesh around Crack Tip of Local Model .....	42
Figure 8.6 Cross Section Dimension of Global Model.....	43
Figure 8.7 Illustration of Stress Application to the Global Model .....	43
Figure 8.8 Progression of Plastic Deformation Areas for Selected Load Cases.....	46
Figure 8.9 Mises Stress Contour in Load Case 1 for Crack Initiation Location Determination...	47
Figure 8.10 Crack Patterns.....	47
Figure 8.11 Mises Stress Distribution for Different Patterns in Load Case 1 .....	48
Figure 8.12 Actual Crack Propagation Pattern .....	48

## LIST OF TABLES

	Page
Table 2.1 Material Properties of Various Steels at Room Temperature .....	7
Table 3.1 Tensile Specimen Dimensions.....	11
Table 3.2 Results of Static Tensile Testing .....	14
Table 4.1 Fatigue Testing Test Matrix.....	17
Table 4.2 Experimentally Determined Fatigue Constants .....	20
Table 5.1 Predicted Fracture Toughness Using Barsom.....	26
Table 7.1 Possible Permutations for Lane Loading .....	37
Table 7.2 Calculated Live Loads Due to AASHTO HS 20-44 Lane Loading .....	37
Table 7.3 Calculated Thermal Induced Loads .....	38
Table 7.4 Longitudinal Displacements of Selected Points in Figure 7.5.....	38
Table 7.5 Average Daily Traffic Count for Paseo Bridge .....	39
Table 8.1 Loading Matrix for Chosen Test Cases .....	43
Table 8.2 Comparison of $J_{IC}$ to $J$ for Selected Load Cases (100% Loading).....	45
Table 8.3 Comparison of $J_{IC}$ to $J$ for Selected Load Cases (50% Loading).....	46

# 1. INTRODUCTION

## 1.1 GENERAL

The Paseo Bridge in Kansas City, MO, is a self-anchored suspension bridge, see Figure 1.1. The total length of the main bridge is 1232 feet, including one main span of 616 feet and two side spans of 308 feet each. At each end of the bridge, two stiffening girders are independently tied down to a bridge pier with two vertical hangers, or struts as shown in Figure 1.2. Each hanger consists of a lower and an upper link connected with bolts by a strut (24I120 or S24x120). The links are connected with the stiffening girder and the bridge pier by two 11-inch diameter pins, respectively.

The construction of the bridge began in 1952. Currently the bridge supports Interstates I-29 and I-35, and US Highway 71, and as of 2003 data carries an average of 89,000 vehicles daily. On January 22, 2003, the Paseo Bridge was hurriedly closed to traffic during the Wednesday afternoon rush hours when a pronounced gap between sections of the bridge's deck sparked fears about the span's safety. At the time, temperatures were reported to hit a record low of 9°F below zero and wind chills approached 25°F below zero. As shown in Figure 1.3, the bridge deck of the southern side span rose approximately 8 inches above the approach deck. The following day, it was found that the strut (web) in the southeastern link anchorage assembly was fractured, see Figure 1.4. Close-up views are presented in Figures 1.5 and 1.6. During fracture, several rivets were sheared off as seen from Figure 1.7. Also seen in Figure 1.7 as well as Figure 1.8 is a view of the fractured surface, indicating a brittle failure.

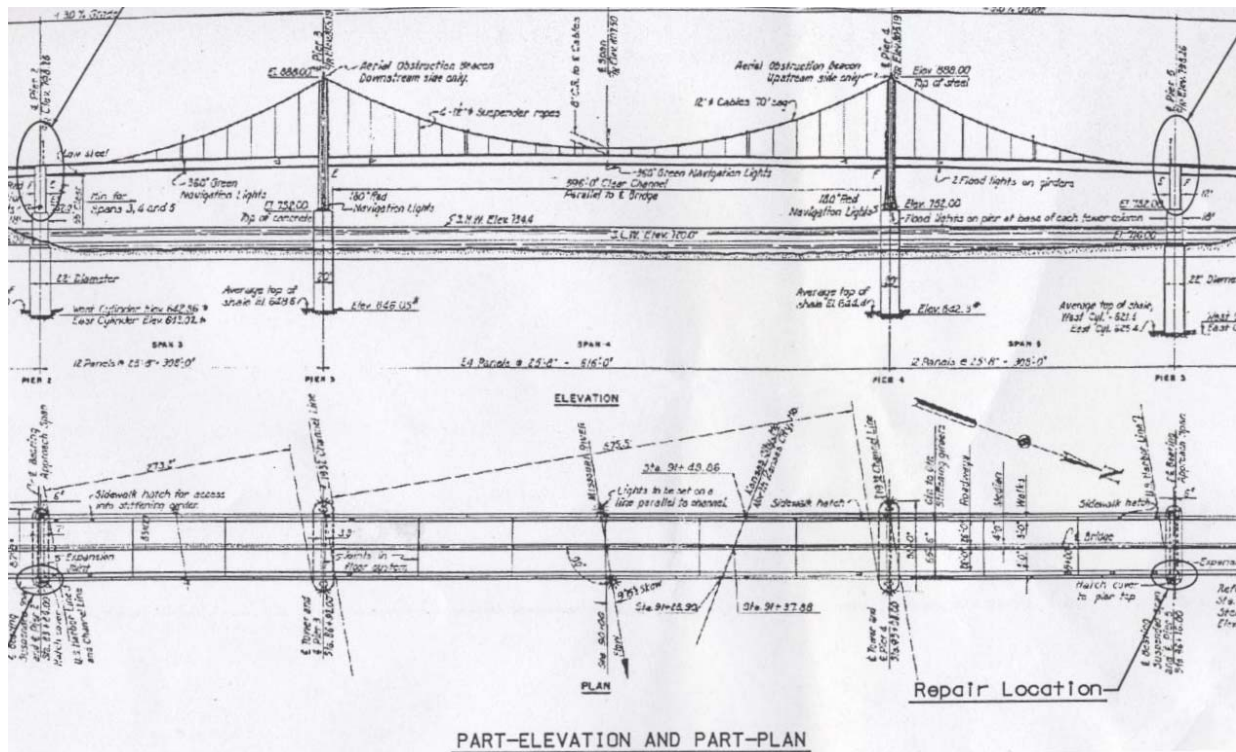


Figure 1.1. Plan and Elevation View of Paseo Bridge

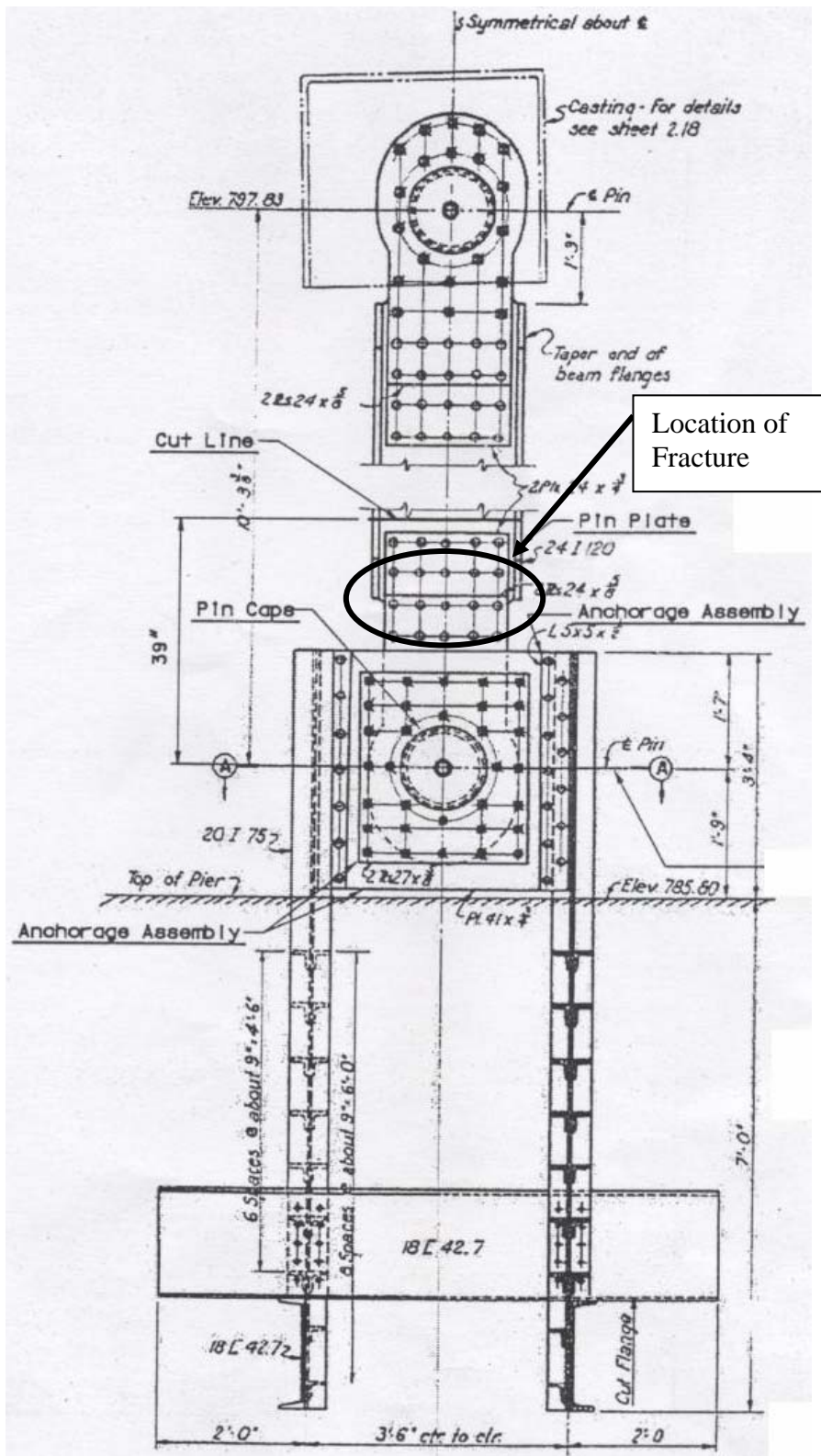


Figure 1.2 Link Anchorage Details



Figure 1.3 Rise in Southern Span



Figure 1.4 Point of Strut Failure



Figure 1.5 Fractured Strut Web Detail

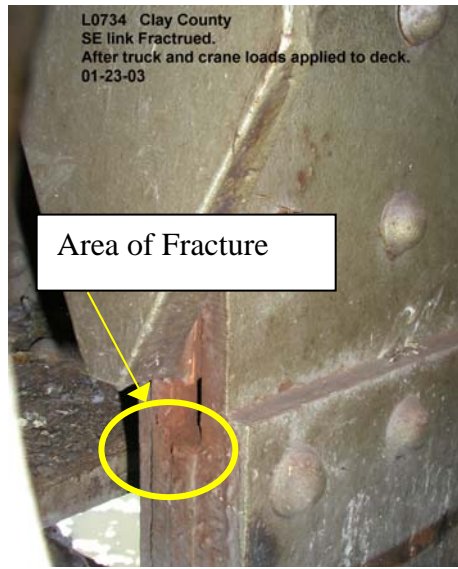


Figure 1.6 Lower Link Anchorage

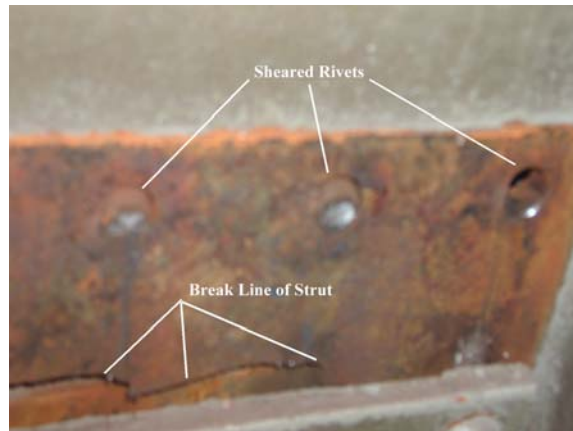


Figure 1.7 Shear Damage of Rivets and Fracture Surface



Figure 1.8 Fracture Pattern of SE Strut Web

Based on the reports from field inspectors, the lower pin in the southeastern hanger was frozen and did not allow for free rotation of the superstructure. The surface condition of the pin on the Southeastern side was severely corroded. This can be seen from the comparison between two pins (Southeastern (a) vs. Southwestern (b) sides) in Figure 1.9.



(a) Southeastern Pin

(b) Southwestern Pin

Figure 1.9 Comparison of Pin Conditions

The decision was made to replace all four hangers of the bridge including the fractured one. When the strut on the Northeastern hanger was removed, it was also found to have been cracked, see Figure 1.10. However, careful inspection by engineers revealed that this crack was due mainly to overstressing as a result of fracturing of the southeastern strut.

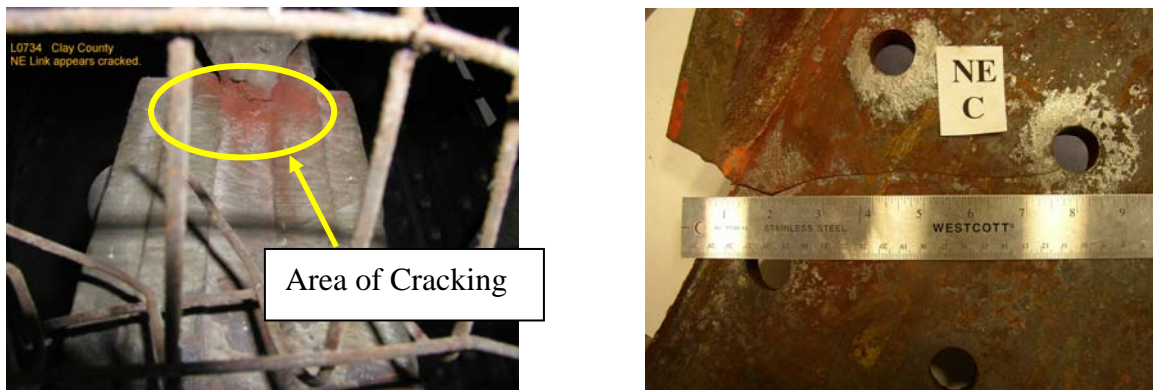


Figure 1.10 Cracking in Northeastern Strut

As a result of the frozen condition in the southeastern pin, the strut was subjected to both tension/compression and bending. The damage of the strut was likely caused by one of the following reasons or their combination: overstressing, thermal contraction, fatigue, and reduction in fracture toughness associated with low temperatures.

## **1.2 RESEARCH SIGNIFICANCE**

Numerous bridges in the nation's inventory are constructed of steel. An understanding of the conditions causing fracture in the Paseo Bridge could better inform bridge inspectors as to signs to look for. Prevention of a similar occurrence elsewhere through better understanding of material and structural behavior is crucial to maintaining normal traffic volume and flow throughout the country's transportation infrastructure.

## **1.3 RESEARCH OBJECTIVES**

The objective of this project is to understand the plausible reason(s) why the southeastern vertical strut of the Paseo Suspension Bridge in Kansas City, MO, fractured on January 22, 2003 after nearly 50 years of service. The research conducted at the University of Missouri-Rolla and provided in this report includes:

- Determine basic material properties,
- Establish a stress and cycles-to-failure (S-N) relation for crack initiation life estimation,
- Establish the relation between fracture toughness and temperature,
- Establish the crack growth rate data for crack propagation life estimation,
- Estimate the average dead plus live load, range and number of cycles of live load,
- Establish a detailed finite element model and simulate strut failure process.

## 2. LITERATURE REVIEW

### 2.1 GENERAL

Conventional methods were employed in this investigation to study fatigue and fracture of the failed strut. They are reviewed in this section, particularly those that have been used in previous studies involving fracture and fatigue of steel bridge components. Some of the findings specific to this grade of steel and materials believed to be similar in composition as well as function are summarized and discussed below.

### 2.2 STATIC TENSILE TESTING

ASTM A 36 steel is typically used for general construction applications such as for the fabrication of bridges and buildings (Holt et al., 1996). The specification provides a minimum yield strength of 36 ksi. The typical modulus of elasticity is  $29 \times 10^3$  ksi and the coefficient of thermal expansion within the range of  $-50^\circ\text{F}$  to  $150^\circ\text{F}$  has been reported as  $6.5 \times 10^{-6}$  in./in./ $^\circ\text{F}$  (Holt et al., 1996). Mechanical tests have been performed on bridge material and reported by Frank (1974) in a report to the Federal Highway Administration. The material specifications for these tests were A 7 and A 373 which are very similar to the current A 36 designation. A summary of material properties from bridge components of the same era as the Paseo Bridge given in Structural Alloys Handbook from Frank's findings are listed in Table 2.1.

Table 2.1 Material Properties of Various Steels at Room Temperature

Bridge Type	Type of Member	Decade of Manufacture	Material Specification	Yield Strength (ksi)	Ultimate Strength (ksi)	RA (%)
Simple-Span Truss	Rolled Beam	1950	A 7	36.3	69.3	42
Stringer Bridge	Welded Girder	1950	A 373	37.5	66.8	-
Continuous-Stringer Bridge	Welded Girder	1940	A 374	36.8	60.9	43
Stringer Bridge	Welded Girder	1950	A 375	36.5	58.1	-

### 2.3 FATIGUE TESTING

Initial flaws exist in all manufactured and fabricated bridge members and details (Fisher et al., 1980). These initial flaws combined with cyclic fluctuations of thermal and live loads can lead to fatigue crack growth and eventual fracture of steel bridge components. Cyclic fatigue properties of a material are obtained from completely reversed constant amplitude strain-controlled tests. Bridge components seldom experience this type of loading; rather some mean stress due to dead load is usually present. Mean stresses have a significant effect on fatigue life, and their effects are seen predominantly at longer lives (Bannantine et al., 1990). A significant amount of fatigue data exists for A 36 steel; however, with each individual case, specific loading history is crucial to predicting fatigue life. Many tests of a given detail are necessary to generate

a statistically significant stress-life relationship (Fisher et al., 1980). It is not possible to predict directly the fatigue performance of large members from the results of laboratory tests on small specimens. Although crack initiation tests conducted on small specimens do not precisely establish the fatigue life of a large part, such tests do provide data on the intrinsic fatigue crack initiation behavior of a metal (ASM, 1985). Small specimen tests change the surface to volume ratio which is important because fatigue cracking usually initiates on the outer surface of structural members. Other factors affecting the fatigue initiation life are stress-concentrations due to geometry and environmental exposure (ASM, 1985), which are unique to the specific application. Additionally, surface residual stresses from specimen preparation such as machining and surface grinding can influence the fatigue strength, although there is no generalization that predicts the extent of improved fatigue strength (ASM, 1985).

## 2.4 CHARPY IMPACT TESTING

Many correlations between fracture toughness and Charpy impact energy have been published. However, owing to the critical nature of many fracture mechanics assessments, combined with the many uncertainties associated with the application of Charpy-toughness correlations, such correlations should be applied with caution (Phaal, 1997). The relations, empirical in nature, are specific to temperature ranges and material heats. Barsom (1974) developed equations specific to bridge steels in the lower shelf and transition regions of temperature-absorbed energy plots, the temperatures experienced during normal service conditions. His correlations were used in AASHTO fracture toughness requirements for bridge steels.

Charpy V-notch impact test results for A-36 steel can be found in Structural Alloys Handbook (Holt et al., 1996). The specimens were from service failure, brittle fracture of a stringer bridge, and reported by Frank (1974). Results from his findings, interpreted from a plot, are shown in Figure 2.1.

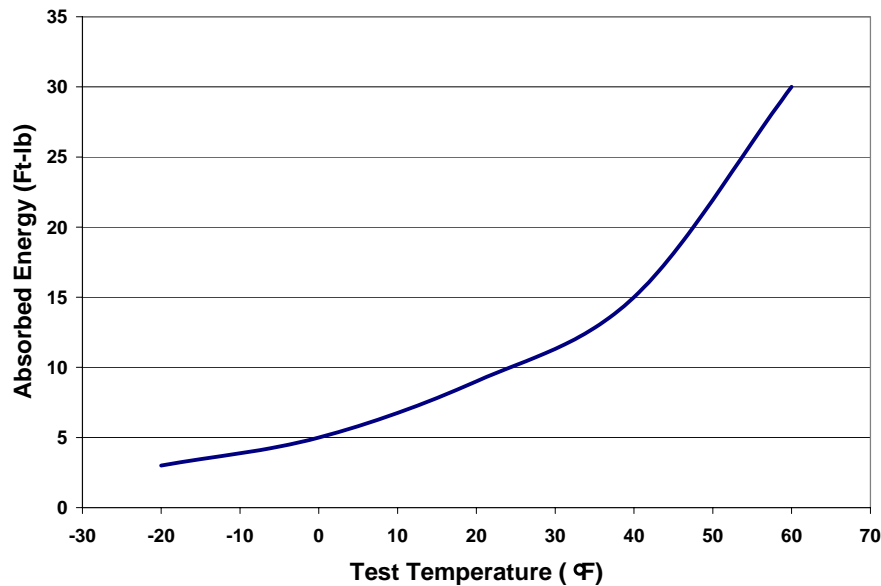


Figure 2.1 Charpy V-Notch Impact Test Results (Frank, 1974)

## 2.5 FATIGUE CRACK GROWTH

Numerous published reports of crack growth rates can be found in the literature. The most accepted model to describe crack growth behavior, proposed in the early 1960's is the Paris Equation (Bannantine et al., 1990). The primary factor affecting fatigue crack growth rates in structural steels is the applied stress intensity factor range,  $\Delta K_I$  (Barsom, 1971). Barsom found that conservative estimates for ferrite-pearlite steels (A 36) concerning crack growth per cycle could be obtained by the relationship given in Equation 2.1. This conservative estimate was confirmed by Fisher (1989).

$$\frac{da}{dN} = 3.6 * 10^{-10} (\Delta K_I)^3 \quad (2.1)$$

## 2.6 PASEO BRIDGE INSPECTION REPORTS

A thorough inspection of the Paseo Bridge in Kansas City, MO, was performed by the Parsons engineering group in November, 2002, approximately two months prior to fracture of the southeastern vertical strut. Referred to as links in the Parsons evaluation, it was reported that longitudinal motion of the links was observed (Parsons, 2003). This gives indication that at the time of inspection the pins were in working condition, allowing free rotation of the superstructure. It was reported, upon inspection, no section loss or corrosion to the links was visible. Additionally, the lower link housings were observed to be accumulated with debris and rust (Parsons, 2003). Fretting rust was also noticed at top pins of links on the south side. No mention of similar observable fretting rust on the lower pins was found, however pack rust was observed between the plates at the bottom pin of the southeastern link (Parsons, 2003).

## 2.7 AMBIENT TEMPERATURE HISTORY

The temperature at the time fracture occurred on the Southeastern vertical strut was reported to be approximately 9°F below zero. Daily temperature data, reported for the downtown airport in Kansas City, MO, was obtained to analyze what temperatures the bridge was exposed to during the period following the Parson's inspection. The day fracture occurred was the coldest day since the Parson's report that longitudinal motion was observed for the links. Figure 2.2 shows the temperature history giving the daily high and low for the months of November, 2002 until January, 2003.

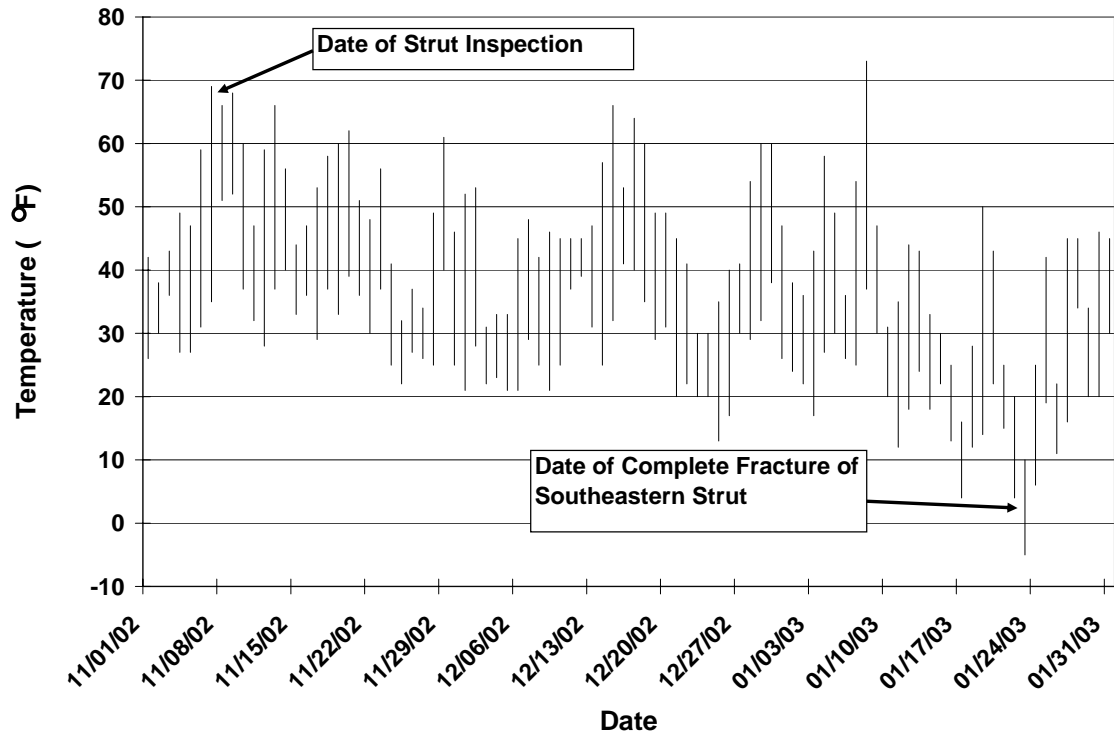


Figure 2.2 Temperature History for Downtown Kansas City Airport

### 3. STATIC TENSILE TESTING

#### 3.1 GENERAL

Basic material properties are necessary to perform calculations in the following sections. The documents available for the steel members on the Paseo Bridge do not contain information regarding these material properties. Static tensile testing of the material, following ASTM E 8, will provide the necessary information.

#### 3.2 SPECIMEN DESIGN

Tensile coupons for static testing were obtained from the fractured southeastern vertical strut according to ASTM E 8. The specimens were first saw cut slightly oversized in vertical sections whereby the direction of tensile force in the coupon corresponded to the vertical axis in the strut during service loading conditions. The coupons were then precision milled and finished to a polished surface on a surface grinder. The specimens measured 10 in. in length and had an approximate prismatic cross section measuring 0.71 in. by 0.22 in. Table 3.1 lists specific specimen dimensions obtained using precision calipers.

The cross section dimensioning on the larger face correlated to the thickness of the plate material from which the specimen was produced, 0.75 in., minus material removed during the surface grinding procedure. Thus, the completed specimens were free of surface imperfections caused by scratches and environmental exposure. The smaller cross section dimensioning or thickness was determined from allowances given in the standard as determined from the aforementioned 0.75 in. dimension.

Prismatic cross sections are allowed by ASTM E 8 as long as fracture occurs a distance greater than two times the width (0.71 in.) away from the gripping device. The minimum acceptable fracture distance from the gripping device in this case corresponded to 1.42 in.

Table 3.1 Tensile Specimen Dimensions

<b>Specimen</b>	<b>Width (in)</b>	<b>Thickness (in)</b>
1	0.713	0.226
2	0.714	0.259
4	0.714	0.219
5	0.714	0.216
6	0.714	0.240

#### 3.3 TEST PROCEDURE

A total of six specimens were tested in the Materials Testing Lab of the Basic Engineering Department at the University of Missouri-Rolla. An Instron 4485 displacement controlled testing machine, Figure 3.1, was used in combination with automated data retrieval software. Following ASTM E 8, the testing was displacement controlled at a rate of 0.2 inches per minute. Specimen dimensions were input into the software. As seen in Figure 3.2, a

calibrated one inch extensometer was attached to each specimen to measure longitudinal strain. After failure, measurements were taken on each specimen to ensure fracture occurred at a minimum of two widths away from the grips, Figure 3.3. The third specimen was determined as an invalid test due to this criterion.



Figure 3.1 Instron 4485 and Data Acquisition System



Figure 3.2 Calibrated Extensometer



Figure 3.3 Verification of Test Validity

### 3.4 FINDINGS

Upon completion of five valid tests at room temperature, material constants were determined by the automated data retrieval software. The constants were then verified from the raw data. These material constants included yield stress,  $\sigma_y$ , ultimate stress,  $\sigma_u$ , and Young's Modulus,  $E$ . Yield stress was determined by 0.2% offset method, whereby stress deviation from the linear portion of the stress-strain curve by more than 0.2% resulted in the return of a value for  $\sigma_y$ . Ultimate stress was found using the peak value on the engineering stress-strain curve. Young's Modulus was calculated as the slope of the linear portion of the stress-strain curve prior to yield stress. Measurements were taken using precision calipers on the cross section of the fractured area. These measurements were used to calculate fracture stress,  $\sigma_f$ , and percent reduction in area, %RA. Figure 3.4, shows the engineering stress-strain curves obtained from valid tests for this material. Individual specimen stress-strain curves as well as additional data generated by the data acquisition system are available in Appendix A. Table 3.2, lists the aforementioned constants found from testing. Averages from the five valid tests were determined and used as the accepted constants. These values compare well to Frank's findings of tensile properties from bridge components (Frank, 1974) of the same decade mentioned in the Literature Review section of this report.

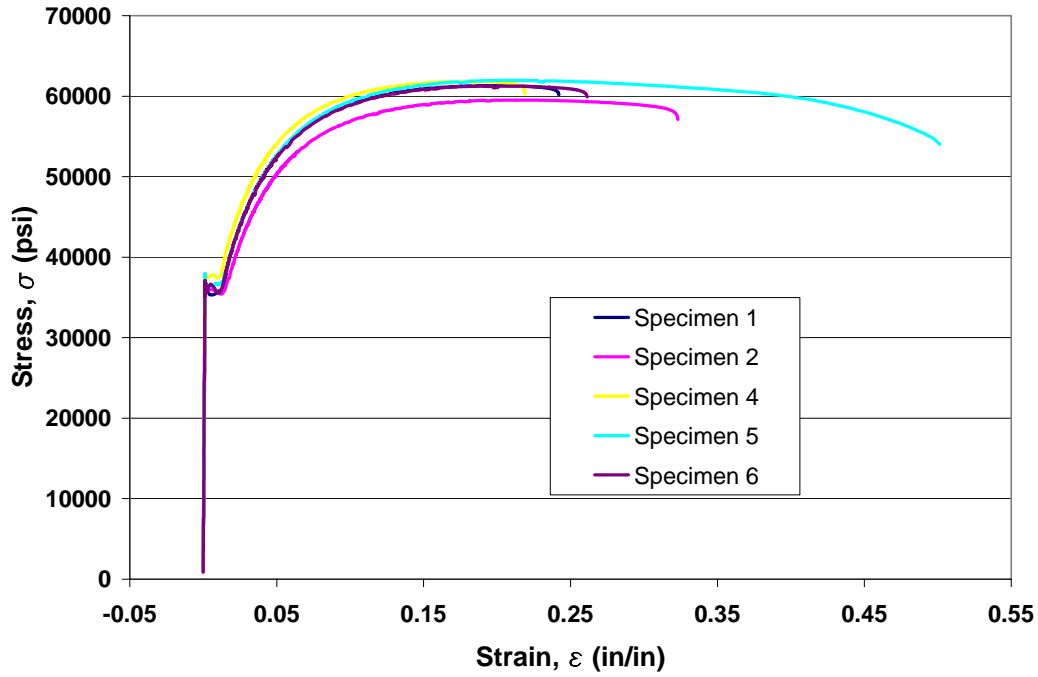


Figure 3.4 Engineering Stress-Strain Curves

Table 3.2 Results of Static Tensile Testing

Specimen	Young's Modulus E (ksi)	Yield Stress $\sigma_y$ (psi)	Ultimate Stress $\sigma_u$ (psi)	Fracture Stress $\sigma_f$ (psi)	Reduction in Area RA (%)
1	27500	35200	61300	96700	46.7
2	27700	35700	59500	92400	49.5
4	27700	37600	61800	94900	44.0
5	29700	36400	62000	97800	47.3
6	29700	36000	61300	101000	48.6
<b>AVG.</b>	28500	36200	61000	95400	46.9

## 4. FATIGUE TESTING

### 4.1 GENERAL

Fatigue of structural components is a process by which premature failure or damage of a component may occur when subjected to repeated loading. The magnitude of this loading may be well below the design stress of the component. The loading type, i.e. zero mean, versus non-zero mean reversed stress loading significantly affects the fatigue life of the specimen. Additionally, geometry plays an important role in fatigue life, thus considerations due to the coped flange of the strut must be taken into account to more accurately predict the fatigue life in this case. The material tested here is not virgin material. It was subjected to 50 years of service conditions, therefore the data generated from these samples can only be used to generate residual life predictions rather than the total initiation life.

### 4.2 SPECIMEN DESIGN

Specimens were machined according to ASTM E 606 under the provisions of flat-sheet fatigue specimens with rectangular cross sections. As with the static tensile testing specimens, the long axis or length of the specimens were oriented so that tensile loads during testing corresponded to the vertical axis in the strut during service loading conditions. Again, the limiting dimension was the width of the specimen which correlates to plate thickness, 0.75 in., minus material removed during surface grinding processes to remove any surface imperfections which would significantly reduce the fatigue life of the specimen. A total of 30 specimens were produced from the material. It should be noted that the specimens here were not fabricated from the fractured Southeastern strut, rather the Southwestern strut. Figure 4.1, shows the fatigue specimen dimensioning.

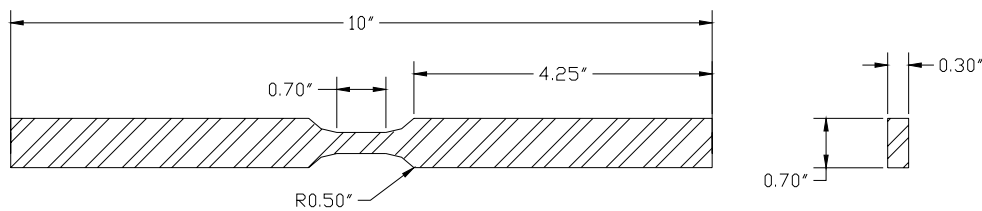


Figure 4.1 Fatigue Specimen Dimensions

### 4.3 TEST PROCEDURE

Testing was done in the High Bay Structural Lab of the Civil Engineering Department at the University of Missouri-Rolla on an MTS 880 equipped with digital data acquisition interfaced with LabView. Figure 4.2, shows the MTS 880 and data acquisition system. Longitudinal strain was measured two ways in the specimen, using a calibrated two inch extensometer and 0.5 in. strain gages. Since the available extensometer gage length was longer than the specimen gage length, strain data collected from it was always lower than that collected from the strain gages, thus extensometer measurements were used only to verify strain gage values. Figure 4.3 shows the test set-up with the strain devices attached.

The loading of specimens was determined from a predefined stress value in the reduced area. Each specimen was tested with cyclic stress fluctuations in the form of a sine wave at a rate of 5 Hz starting at the mean stress value.



Figure 4.2 MTS 880 and Data Acquisition System



Figure 4.3 Longitudinal Strain Measurement Devices

Maximum stress for each case was a predetermined value ranging from 37.5 ksi to 55 ksi in increments of 2.5 ksi depending on the particular specimen. Errors were generated in the Data Acquisition System as the load approached zero, thus the minimum value was selected so as to be near zero but not initiate the errors in calculation. A specific test matrix is supplied in Table 4.1. The number of cycles on each specimen was recorded by the MTS system and failure was defined as complete specimen separation, see Figure 4.4. Run-out was determined as 2,000,000 cycles and the testing terminated at this point, given specimen survival.

Table 4.1 Fatigue Testing Test Matrix

Report Specimen	Minimum Stress (ksi)	Maximum Stress (ksi)	Stress Range (ksi)	Mean Stress (ksi)	Cycles to Failure (experimental)
1	3.1	37.5	34.4	20.3	250629
2	2.5	37.5	35.0	20.0	975562
3	2.5	37.5	35.0	20.0	2000000
4	2.8	40.0	37.2	21.4	105100
5	2.8	40.0	37.2	21.4	654333
6	2.2	40.0	37.8	21.1	2000000
7	2.9	42.5	39.6	22.7	215775
8	2.7	42.5	39.8	22.6	218153
9	2.5	42.5	40.0	22.5	461638
10	2.6	45.0	42.4	23.8	158235
11	2.8	45.0	42.2	23.9	307591
12	2.4	45.0	42.6	23.7	742383
13	2.5	47.5	45.0	25.0	65398
14	2.9	47.5	44.6	25.2	142807
15	3.1	47.5	44.4	25.3	168714
16	3.1	47.5	44.4	25.3	185761
17	3.4	50.0	46.6	26.7	43352
18	3.4	50.0	46.6	26.7	54794
19	2.6	50.0	47.4	26.3	58569
20	3.0	50.0	47.0	26.5	169772
21	2.7	52.5	49.8	27.6	5496
22	0.5	52.5	52.0	26.5	13968
23	2.7	52.5	49.8	27.6	21971
24	3.0	55.0	52.0	29.0	3335
25	3.0	55.0	52.0	29.0	12172



Figure 4.4 Failure of Fatigue Specimen

Load and longitudinal strain data were recorded at a rate of 60 Hz. Initial loading was recorded as well as the first 3000 cycles on each specimen. It was found that stable hysteresis loops were generated after the first 1000 cycles for those specimens below the maximum stress level of 47.5 ksi. The hysteresis loops for specimens at the higher maximum stress levels never stabilized. Data was recorded for each specimen periodically after the first 3000 cycles to monitor hysteretic loop stabilization.

#### 4.4 FINDINGS

Load data was converted to stress,  $\sigma$ , and plotted versus strain,  $\varepsilon$ , for each specimen to obtain hysteresis loops. Hysteresis loops for each member are provided in Appendix B. Maximum and minimum values for both parameters were determined from each hysteresis loop, see Figure 4.5, and used to calculate amplitudes,  $\Delta\sigma/2$  and  $\Delta\varepsilon/2$ . Plastic strain amplitude,  $\Delta\varepsilon_p/2$ , was calculated using Equation 4.1 (Bannantine et al., 1990).

$$\frac{\Delta\varepsilon_p}{2} = \frac{\Delta\varepsilon}{2} - \frac{\Delta\sigma}{2E} \quad (4.1)$$

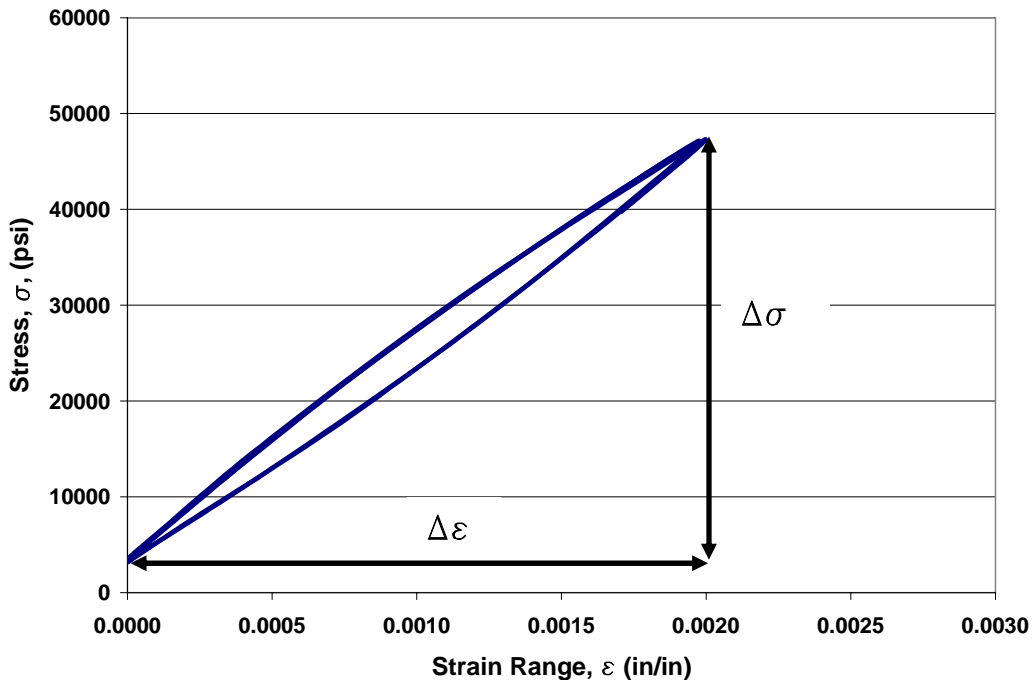


Figure 4.5 Typical Hysteresis Loop for Specimen 15

The basis of the strain-life method is given by Equation 4.1 (Bannantine et al., 1990). Total strain amplitude is divided into two terms one representing the elastic portion of strain and the other the plastic portion. The strain-life method requires four empirical constants that are material properties. These constants are the fatigue strength coefficient,  $\sigma'_f$ , the fatigue strength exponent,  $b$ , the fatigue ductility coefficient,  $\varepsilon'_f$ , and the fatigue ductility exponent,  $c$ . Equation 4.2 is valid for fully reversed loading or zero mean stress.

$$\frac{\Delta \varepsilon}{2} = \frac{\sigma'_f}{E} (2N_f)^b + \varepsilon'_f (2N_f)^c \quad (4.2)$$

The previously undefined term in Equation 4.2 is the reversals to failure,  $2N_f$ . For sinusoidal loading the number of reversals to failure is two times the cycles to failure. To account for the mean stress effects in this test, the Smith, Watson, and Topper equation, Equation 4.3 is employed (Smith et al., 1970).

$$\sigma_{\max} \frac{\Delta \varepsilon}{2} = \frac{(\sigma'_f)^2}{E} (2N_f)^{2b} + \sigma'_f \varepsilon'_f (2N_f)^{b+c} \quad (4.3)$$

The  $\sigma_{\max}$  in Equation 4.3 is defined by Equation 4.4 with mean stress,  $\sigma_o$ , calculated by averaging the maximum and minimum stress values from the hysteresis loop.

$$\sigma_{\max} = \frac{\Delta \sigma}{2} + \sigma_o \quad (4.4)$$

The empirical material constants, as defined in the Smith, Watson, Topper equation, were determined from fitting power law relationships to the plots of stress amplitude versus reversals to failure and plastic strain amplitudes versus reversals respectively on log-log scales. Figures 4.6 and 4.7 show these plots and the corresponding power law curve fit produced in Excel. Table 4.2 lists the empirical constants found from the curve fits. The empirical constants are needed to predict the crack initiation life.

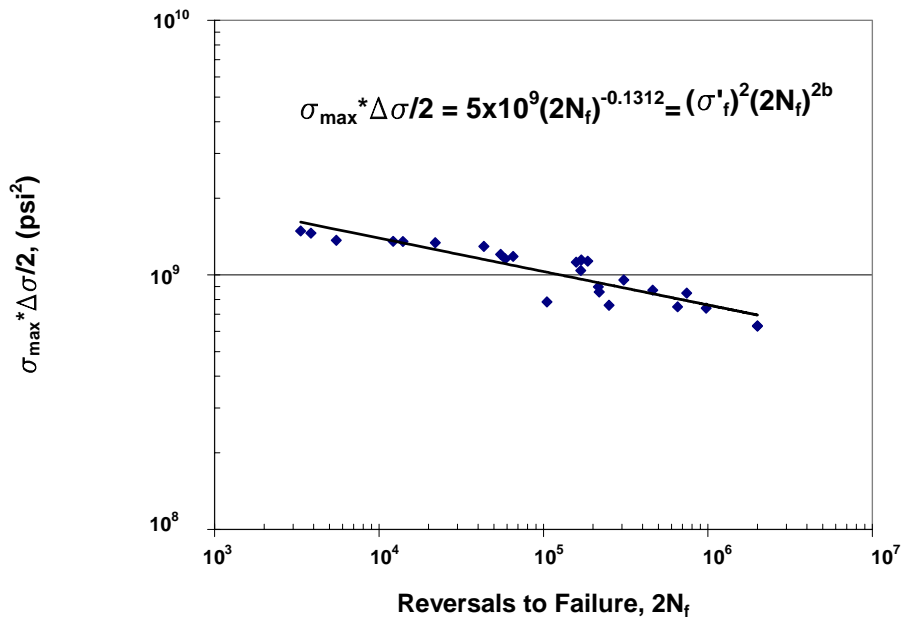


Figure 4.6 Power Law Curve Fit for Stress Amplitude vs. Reversals to Failure



Considering the coped flange on the Southeastern strut to act as a notch, Neuber's rule (Bannantine et al., 1990) was applied to determine residual life of the vertical struts. Neuber's rule takes into account the local stress-strain at the notch root may vary from the nominally applied load at a remote location. The stress concentration factor,  $K_t$ , necessary to convert nominal stress,  $S$ , to local stress,  $\sigma$ , was found to be approximately 3.76. This value was determined from a finite element (FE) model as shown in Figure 4.8, which was subjected to the dead plus live axial load when the pin in the lower link is free to rotate. The stress concentration factor was found by dividing the nominal stress applied by the notch root stress supplied by the FE model.

Strain Life curves for the Paseo Bridge were developed employing the following method. With a given nominal stress, the local stress was found by applying Equation 4.5

$$K_t^2 \frac{\Delta S}{2} \left[ \frac{\Delta S}{2E} + \left( \frac{\Delta S}{2K'} \right)^{1/n'} \right] = \frac{\Delta \sigma}{2} \left[ \frac{\Delta \sigma}{2E} + \left( \frac{\Delta \sigma}{2K'} \right)^{1/n'} \right] \quad (4.5)$$

and solving for the local stress amplitude,  $\Delta \sigma/2$ . The cyclic strength coefficient,  $K'$ , and the cyclic strain hardening exponent,  $n'$ , in Equation 4.5, can be determined from the values in Table 4.1 using Equations 4.6 and 4.7.

$$K' \approx \frac{\sigma_f'}{(\varepsilon_f')^n} \quad (4.6)$$

$$n' \approx \frac{b}{c} \quad (4.7)$$

Local strain amplitude was then calculated from the hysteresis curve, Equation 4.8. Finally, reversals to failure were found by using the strain-life equation accounting for mean stress, Equation 4.9. This method was repeated for different nominal stress levels and used to predict the residual life curves depicted in Figures 4.9 and 4.10.

$$\frac{\Delta \varepsilon}{2} = \frac{\Delta \sigma}{2E} + \left( \frac{\Delta \sigma}{2K'} \right)^{1/n'} \quad (4.8)$$

$$\frac{\Delta \varepsilon}{2} = \frac{\sigma_f' - \sigma_o}{E} (2N_f)^b + \varepsilon_f' (2N_f)^c \quad (4.9)$$

Using the residual life curve in Figure 4.10, the predicted residual life of the vertical struts, assuming the pin was not mechanically frozen, is found to be practically infinite. This is calculated by taking the number of cycles for 100% live load,  $10^8$ , and dividing by the daily number of cycles, 230, found in Section 7.5 of this report. The resulting value is nearly 1200 years. It should be noted, that this value is for fully reversed loading at 100% of the design live load and a constant dead load value of 120 kips.

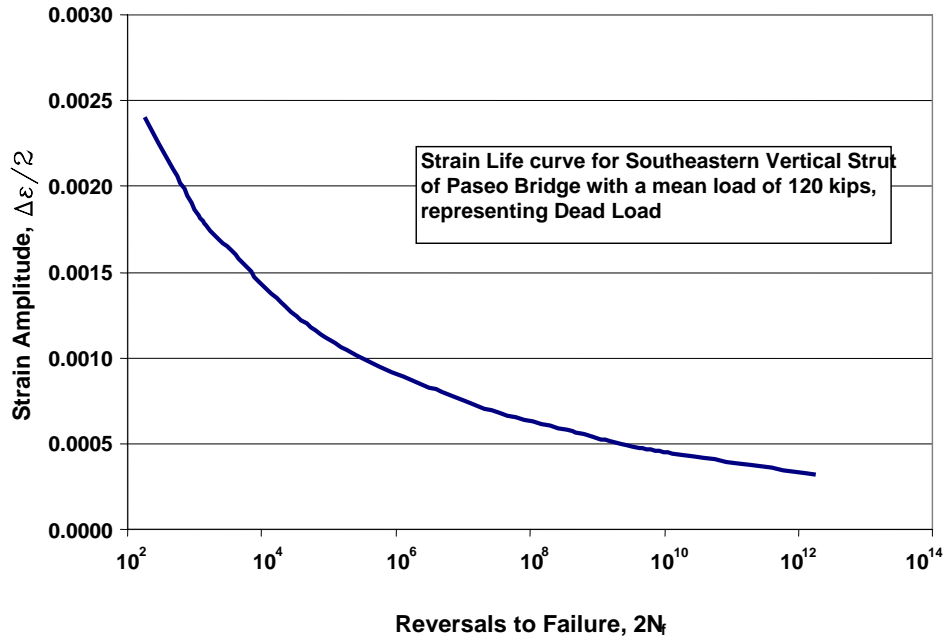


Figure 4.9 Strain Life Curve for Paseo Bridge Struts

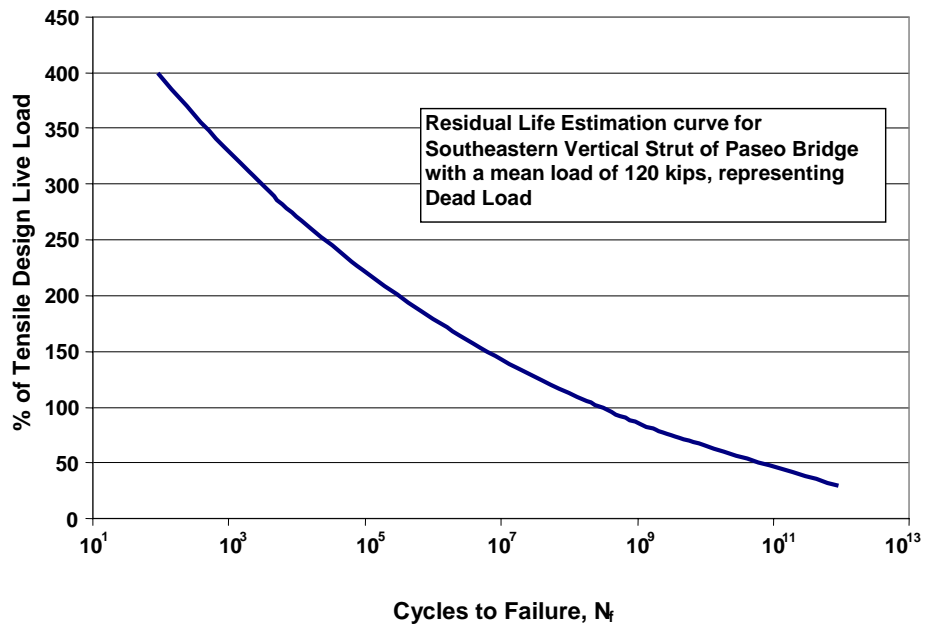


Figure 4.10 Residual Life Estimation Curve for Paseo Bridge Struts

## 5. CHARPY IMPACT TESTING

### 5.1 GENERAL

With the value of yield stress,  $\sigma_y$ , equal to 36.2 ksi (Table 3.2), specimen thickness would be prohibitively large for fracture toughness,  $K_{IC}$ , testing according to ASTM 399. Therefore, instead of determining  $K_{IC}$  using standard plane strain fracture toughness testing, Charpy V-notch testing was performed following ASTM E 23. The results obtained from Charpy V-notch testing at different temperatures when correlated with service conditions have been found to predict the likelihood of brittle fracture accurately (ASM, 1978).

### 5.2 SPECIMEN DESIGN

Charpy V-notch specimens were machined from the strut material according to ASTM E 23. Specimens were oriented so that the long axis of the specimens correlated to the tensile/compressive axis of loading in the service conditions of the struts. The V-notch was oriented so fracture would occur transverse to the rolled direction of the material, the same plane of cracking and fracture that occurred in the southeastern strut. It has been found that little difference in transition temperature and the energy absorbed can be observed in the brittle range when the notch of the specimens is oriented longitudinally versus transversely (Bucher 1967). In the ductile fracture range, however, significant differences between specimen orientations do exist.

Standard dimensions were used for the Charpy V-notch specimens, measuring 2.165 in. in length and having a cross section of 0.394 in. by 0.394 in. The V-notch is located midspan, with regards to length having a depth of 0.079 in. with a notch angle of 45°. Charpy V-notch impact specimens can be seen in Figure 5.1.

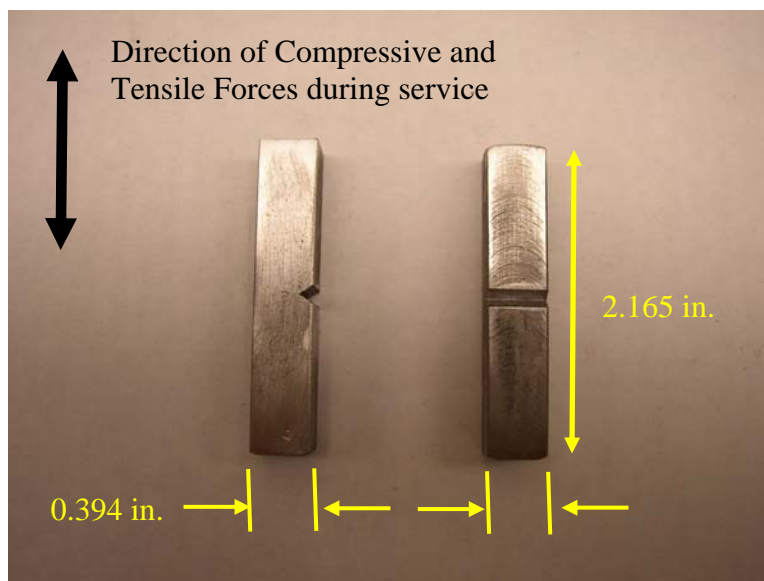


Figure 5.1 Standard Charpy V-Notch Specimens

### 5.3 TEST PROCEDURE

Charpy V-notch impact testing was done in a metallurgical lab at the University of Missouri-Rolla. Tests were performed using a calibrated Tinius Olsen Model 84 Universal Impact Tester, Figure 5.2. The tester has an anvil where specimens are placed and a swinging pendulum which rotates down to fracture the specimen. Data in the form of breaking energy is displayed and is calculated from the change of kinetic energy of the swinging pendulum after impact.



Figure 5.2 Tinius Olsen Model 84 Universal Impact Tester

The temperature range chosen,  $-10^{\circ}\text{F}$  to  $140^{\circ}\text{F}$ , represents the temperature range the material was likely exposed to during service. Temperatures below room temperature were obtained using an alcohol bath and dry ice, see Figure 5.3. The specimens were submerged in the alcohol in an insulated container and the temperature monitored using a submersible probe as flakes of dry ice were put in the bath. Figure 5.4 shows the temperature being measured at the lower end of the scale  $-10^{\circ}\text{F}$ . Temperatures were monitored in the bath and kept relatively constant for 20 minutes prior to impact to minimize temperature gradients within the specimen material. Temperatures above room temperature were obtained using a laboratory oven and again sufficient time given for stabilization of internal temperatures.



Figure 5.3 Dry-Ice and Alcohol Bath



Figure 5.4 Temperature as Measured from Alcohol Bath

Upon reaching equilibrium of the desired temperature, specimens were quickly removed from the bath or oven and placed in the anvils of the impact tester, Figure 5.5. The pendulum was released from its starting position and allowed to swing through and strike the specimen causing fracture. The breaking energy,  $C_v$ , was recorded and the test repeated until five valid tests had been performed at each temperature. Test validity, given in ASTM E 23, was determined as complete fracture of the specimen.



Figure 5.5 Placing Charpy V-Notch Specimen in Anvil

## 5.4 FINDINGS

When breaking energy was plotted versus temperature the curve took on a shape characterized by what is termed the lower-shelf and transition region of breaking temperature. The plotted data can be seen in Figure 5.6, and is consistent with Frank's findings referenced in the Literature Review section of this report. It should be noted that approximately 20 times the energy was required for fracture between the extremes of the chosen temperature range. Literature was consulted and a suitable equation found that would relate fracture energy to fracture toughness. Equation 5.1 was developed by Barsom (1974) and is applicable to the aforementioned lower-shelf and transition regimes.

$$\frac{K_{IC}^2}{E} = 5Cv \quad (5.1)$$

Since this is an empirically derived equation, Equation 5.1 is valid using the units of psi and inch for Young's Modulus, E, and fracture toughness,  $K_{IC}$ . Units of Charpy breaking energy, Cv, must be ft-lb. Barsom used this relationship in developing the AASHTO fracture toughness requirements for bridge steels (Phaal et al., 1997). Table 5.1 shows the fracture toughness,  $K_{IC}$ , calculated using Equation 5.1 and the average breaking energy of the five specimens at each temperature level tested.

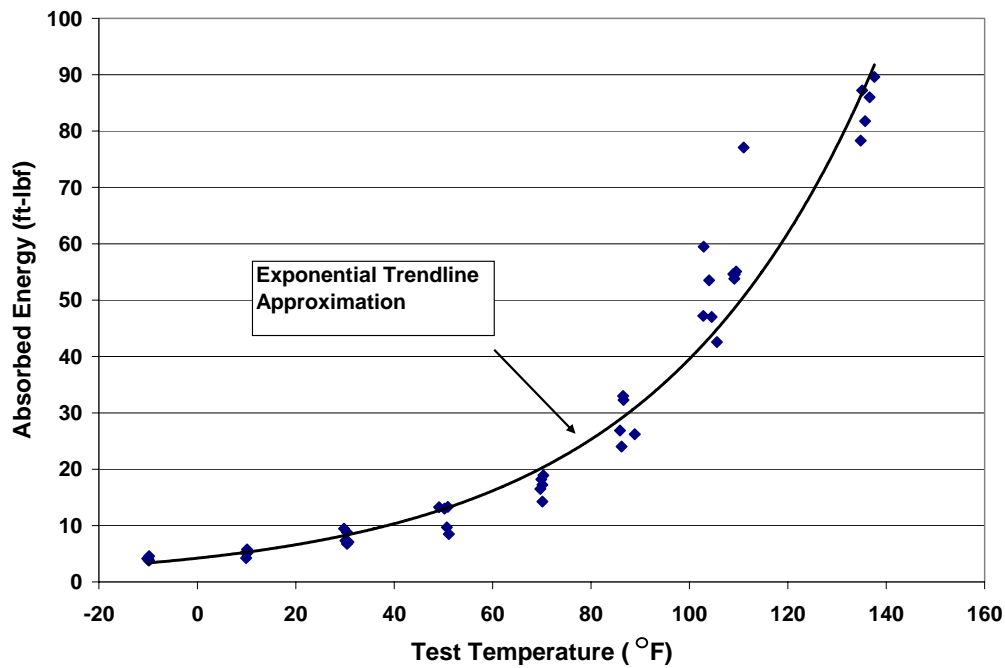


Figure 5.6 Absorbed Energy at Temperatures Tested

Table 5.1 Fracture Toughness Calculated from Equation 5.1

Temperature °F	Breaking Energy (Cv) ft-lbf	$K_{IC}$ ksi*in <sup>1/2</sup>
136.0	84.57	110
109.5	59.03	92
104.0	49.96	84
86.8	28.48	64
70.0	17.03	49
50.4	11.56	41
30.3	7.89	34
10.0	5.11	27
-9.9	4.11	24

Using the  $K_{IC}$  values from Table 5.1, it is possible to estimate the temperature that would cause sudden fracture on the Southeastern Paseo Bridge strut with a frozen pin condition, using textbook equations. For this purpose, an edge cracked plate subject to tension and bending were used to determine the stress intensity factors at the notch root. These equations are given as Equation 5.2 for the contribution of the axial force, Equation 5.3 for the contribution of the moment, and Equation 5.4 for their combined loading effects to calculate the stress intensity factor. The term  $a$ , refers to crack length,  $W$ , the plate width,  $B$ , plate thickness, with  $P$  and  $M$  the applied axial force and moment respectively.

$$f_t\left(\frac{a}{W}\right) = \frac{\sqrt{2 \tan \frac{\pi a}{2W}}}{\cos \frac{\pi a}{2W}} \left[ 0.752 + 2.02\left(\frac{a}{W}\right) + 0.37\left(1 - \sin \frac{\pi a}{2W}\right)^3 \right] \quad (5.2)$$

$$f_b\left(\frac{a}{W}\right) = \frac{6\sqrt{2 \tan \frac{\pi a}{2W}}}{\cos \frac{\pi a}{2W}} \left[ 0.923 + 0.199\left(1 - \sin \frac{\pi a}{2W}\right)^4 \right] \quad (5.3)$$

$$K_I = \frac{1}{B\sqrt{W}} \left[ Pf_t\left(\frac{a}{W}\right) + \frac{M}{W} f_b\left(\frac{a}{W}\right) \right] \quad (5.4)$$

It should be noted that these equations are a non-conservative estimate to the actual condition. It does not take into account the coped flanges which would increase the stress intensity factors. On the other hand, consideration of plasticity around the root of a notch in actual conditions will reduce the stress intensity factors. Therefore, the prediction of the critical temperature is approximate and it will be verified with numerical analysis in Section 8.

The applied axial force was from dead load alone. The moments applied were a function of temperature, caused by thermal contraction of the bridge deck, assuming the lower pin was mechanically frozen such that the strut was in a completely vertical position. These moments were obtained from a SAP 2000 model of the bridge discussed in Section 7 of this report. A zero moment condition exists at 60°F, the temperature at which structural dimensions were given. Figure 5.7 shows the relation between stress intensity factor and temperature, as well as the fracture toughness obtained from the Charpy impact tests. This figure can be considered as a supply-demand diagram. The “supply” curve or the  $K_{IC}$  is the positively sloped curve in Figure 5.7. The “demand” curves are the negatively sloped lines, each representing the stress intensity factor,  $K_I$ , at the given temperature. Where the “demand” curves cross and lie above the “supply” curve sudden fracture occurs. For example, with an initial crack length of 0.001 inch, sudden fracture of the Southeastern strut would occur at 20°F with no live load present. It should be reminded that this is for the strut being mechanically frozen in the vertical position. Moments generated from the thermal contraction of the bridge are much lower as the frozen position of the strut is at an increasing angle toward the deck. This would shift the “demand” curves to the left in Figure 5.7, as would a less conservative estimate of the stress intensity factor.

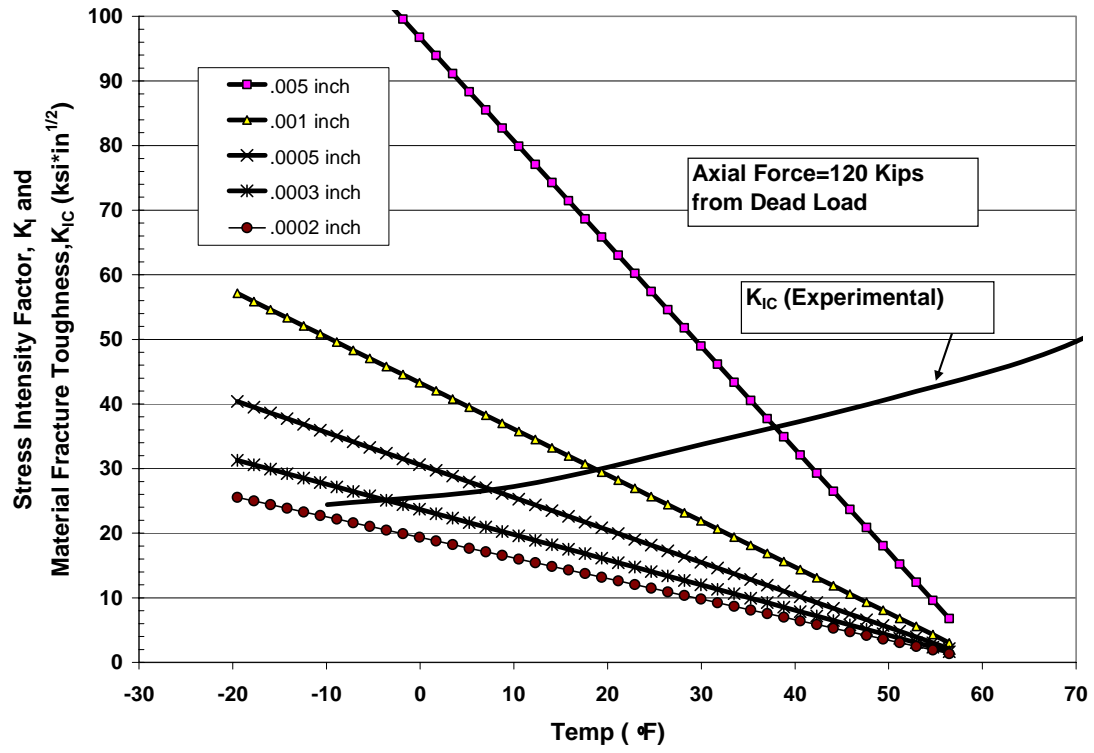


Figure 5.7 Prediction of Fracture of Southeastern Strut

## 6. FATIGUE CRACK GROWTH

### 6.1 GENERAL

A fatigue crack propagates primarily depending upon the stress intensity factor range it is subjected to. Crack propagation is a localized phenomenon that depends on boundary conditions at the crack tip. An empirical representation of this phenomenon has been shown as the Paris Crack Growth Law, Equation 6.1.

$$\frac{da}{dN} = C(\Delta K)^m \quad (6.1)$$

This law suggests the dependence upon the stress intensity factor range,  $\Delta K$ , for crack growth per loading cycle,  $da/dN$ . By finding the material constants  $C$  and  $m$ , and knowing loading conditions, one can accurately predict the rate at which cracks propagate through material. A procedure for finding the material constants for the strut material is performed here.

### 6.2 SPECIMEN DESIGN

Eight compact tension specimens were machined from the strut material according to ASTM E 647. The area where crack growth would occur was polished to a smooth finish on a surface grinder to remove any surface imperfections and make cracks more visible, resulting in a finished specimen thickness of 0.735 in. The specimens were oriented so the plane of crack growth was transverse to the rolled direction of the steel, as shown in Figure 6.1. Similar to the static tension specimens and the fatigue specimens the line of loading action corresponded to the service loading conditions. The standard requires that the condition of Equation 6.2 be met for the test to be considered valid.

$$(W - a) \geq \left( \frac{4}{\pi} \right) \left( \frac{K_{I\max}}{\sigma_y} \right)^2 \quad (6.2)$$

Based upon literature review of similar material, it was determined that the specimen's uncracked ligament,  $(W-a)$ , would be of sufficient magnitude that valid specimens could not be arranged between the existing rivet holes in the strut material.  $K_{I\max}$  is the stress intensity factor corresponding to the maximum load,  $P$ , and  $a$  is the crack length measured from the center of the loading holes. It was decided to use an existing rivet hole to load the specimen, thus other dimensions of the compact tension specimen were determined based on this 1 inch existing hole diameter. Figure 6.2 shows the dimensions chosen in inches for the compact tension specimens and Figure 6.3 is the finished specimen. It should be noted that the existing hole in the back face violates the standard but any stress intensity contribution from the hole would cause the crack to deviate by more than  $20^\circ$  from its initial plane, which would invalidate the test, regardless of the presence of the hole.

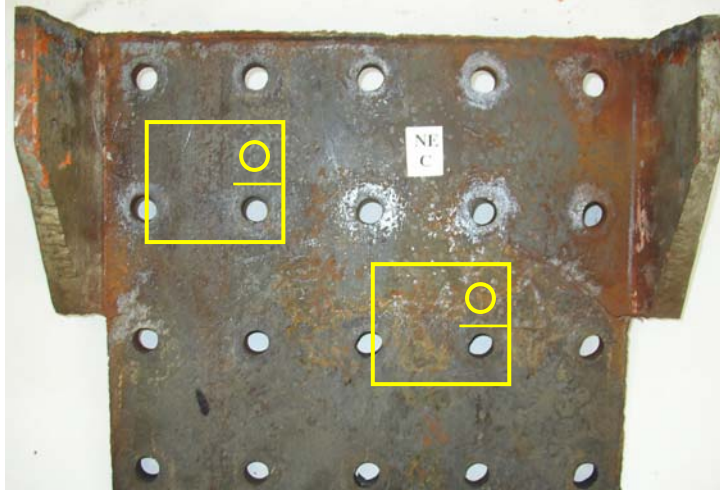


Figure 6.1 Compact Tension Specimen Orientation

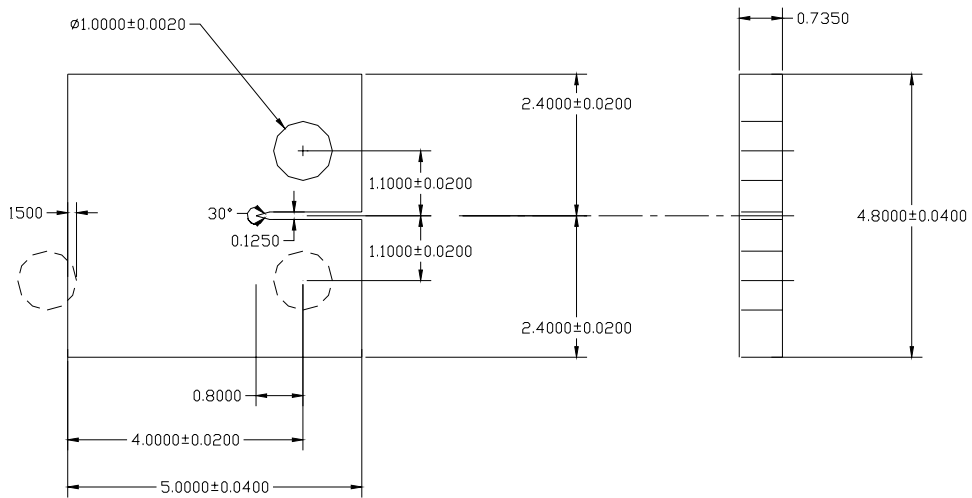


Figure 6.2 Compact Tension Specimen Dimensions

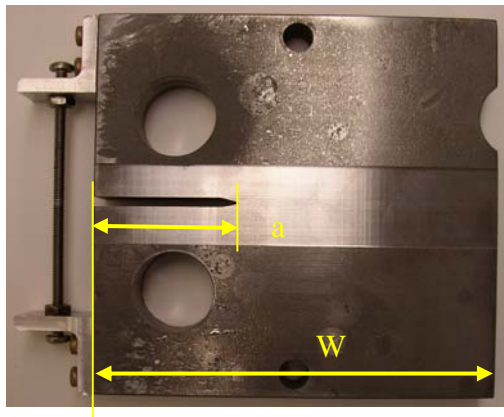


Figure 6.3 Compact Tension Specimen

### 6.3 TEST PROCEDURE

Specimens were tested in the Structural High-Bay Lab at the University of Missouri-Rolla using the same MTS 880 and data acquisition system as the fatigue specimens. Specimens were attached to the MTS grips using a clevis and pin assembly as outlined in ASTM E 647. Specimens were tested under cyclic loading fluctuations in the form of a sine wave at 5 Hz. The loading sine wave had a maximum value of 11,000 lbs. and a minimum value of 400 lbs. Again, due to errors generated in the data retrieval system, zero load was approached but avoided. An extensometer, as shown in Figure 6.4 can be used to check crack length by the compliance method (ASTM E 647). Figure 6.4, shows the test set up prior to testing. After measurable crack growth was noticed in the specimens, measurements were taken on both the front and rear faces using precision calibrated calipers. Measurements of crack length,  $a$ , were taken every 3000 cycles, see Figure 6.5, and repeated until the specimen failed. Data for the five valid tests is supplied in Appendix D.



Figure 6.4 Crack Growth Test Set-up

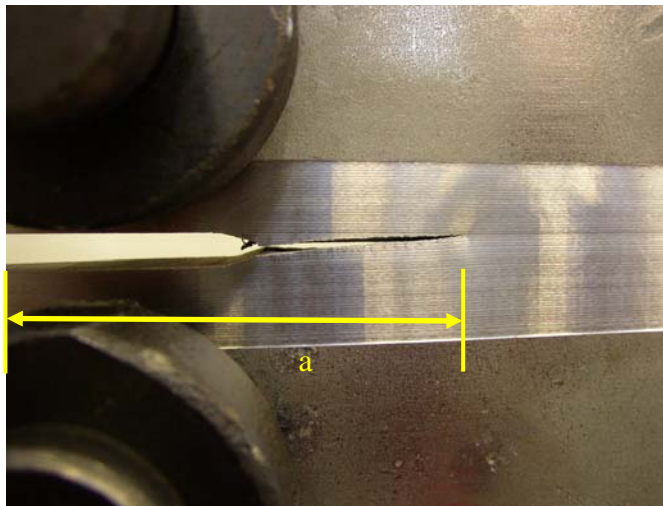


Figure 6.5 Crack Measurement During Growth

## 6.4 FINDINGS

The stress-intensity factor range,  $\Delta K$ , for compact tension specimens is proportional to the load range,  $\Delta P$ , as follows:

$$\Delta K = \frac{\Delta P}{B\sqrt{W}} \frac{\left(2 + \frac{a}{W}\right)}{\left(1 - \frac{a}{W}\right)^{\frac{3}{2}}} \left(0.886 + 4.64\left(\frac{a}{W}\right) - 13.32\left(\frac{a}{W}\right)^2 + 14.27\left(\frac{a}{W}\right)^3 - 5.6\left(\frac{a}{W}\right)^4\right) \quad (6.3)$$

The variable B is specimen width, plate thickness in this case, and W is dimension from load line to back face, see Figure 6.3. Stress-intensity factors were calculated for each crack length measured. The change in crack length per cycle,  $da/dN$ , was calculated by dividing the crack length measurements by the number of cycles elapsed between measurements. The stress-intensity factor ranges were then plotted versus the change in crack length per cycle calculations on a log-log scale and are given in Figure 6.6.

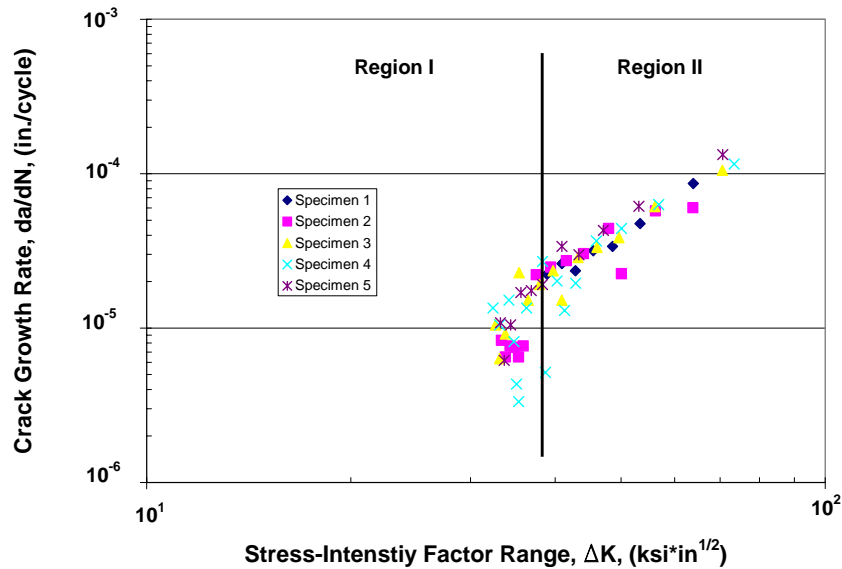


Figure 6.6 Plot Showing Regions I and II

A plot of  $\log da/dN$  versus  $\log \Delta K$  is a sigmoidal curve that can be divided into three distinct regions. Region I, at low stress intensities, is characterized by cracking behavior associated with threshold,  $\Delta K_{th}$ , effects. Region II consists of the linear portion of the data characterized by stable crack growth. Region III, not included in this data set has high  $\Delta K$  values, where crack growth rates are extremely high and little fatigue life is involved (Bannantine et al., 1990). As seen in Figure 6.6, Region I and Region II are distinctly visible. Data points in Region I were removed and a power-law curve fit performed on the data of Region II, see Figure 6.7. The material constants C and m from the Paris Crack Growth law are

revealed from this curve fit and are  $7 \times 10^{-10}$  and 2.8, respectively. These values are consistent with the findings of Barsom (1971) and confirmed by Fisher (1989).

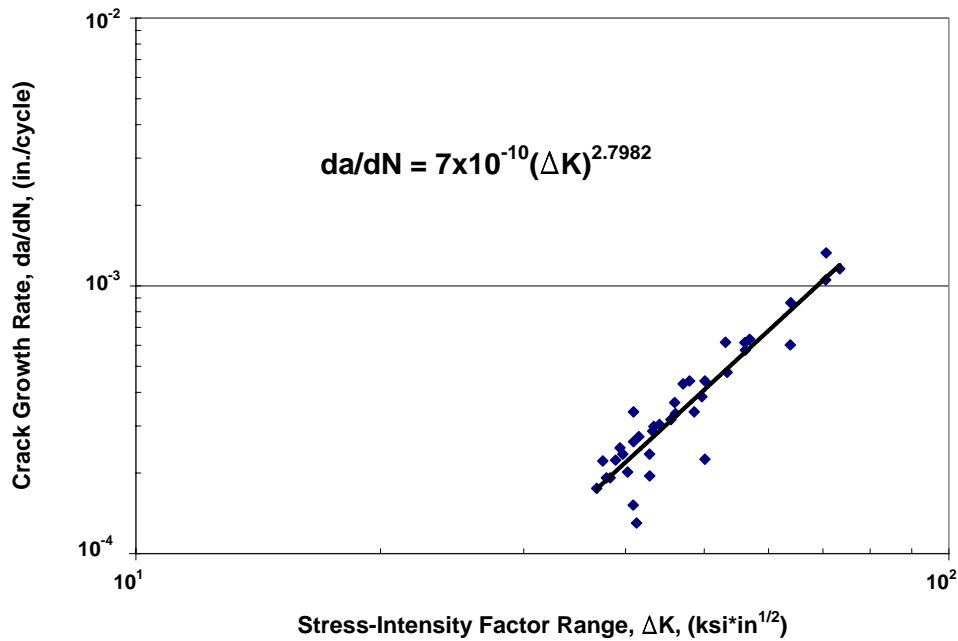


Figure 6.7 Power Law Curve Fit to Determine Paris Law Constants

The material constants  $C$  and  $m$  from the Paris Crack Growth Law allow for the determination of the crack propagation life. During crack propagation life estimation, it is assumed that fracture occurs when the stress intensity range,  $\Delta K$ , reaches a value corresponding to the material fracture toughness,  $K_{IC}$ . This allows an approximate method to predict the fatigue crack growth under constant amplitude loading (Bannantine et al., 1990).

To determine the crack propagation life for the vertical struts of the Paseo bridge, it was assumed they behave like an edge cracked plate subject to tension. This assumption allows the use of Equations 6.4 and 6.5.

$$\Delta K = f(g)\Delta\sigma\sqrt{\pi a_{avg}} \quad (6.4)$$

$$f(g) = 1.12 - 0.231\left(\frac{a_{avg}}{b}\right) + 10.55\left(\frac{a_{avg}}{b}\right)^2 - 21.72\left(\frac{a_{avg}}{b}\right)^3 + 30.39\left(\frac{a_{avg}}{b}\right)^4 \quad (6.5)$$

An initial crack length of 0.005 in. was assumed and the crack allowed to propagate at intervals of 0.005 in. until a critical crack length, one causing sudden fracture was reached. At each interval the corresponding average crack length,  $a_{avg}$ , between two successive intervals was calculated and  $f(g)$ , Equation 6.5, was evaluated for this average crack length. The term  $b$  represents the plate width, in this case the web of the strut, 20 inches. The stress intensity range,  $\Delta K$ , was then calculated for each interval. Rearranging the Paris Crack Growth Law, Equation 6.6, allowed solving for  $\Delta N$ , the number of cycles elapsed between successive crack length intervals.

$$\Delta N = \frac{\Delta a}{C(\Delta K)^m} \quad (6.6)$$

The number of cycles was then summed at each successive crack length interval to get the total number of elapsed cycles since initial crack length. Crack propagation life estimation curves were then generated for three different loading conditions on the struts. It should be noted that only tensile live loads were used, as compressive forces do not contribute to crack growth. So the stress range was from zero to max for each condition. The curves are given in Figure 6.8, and were calculated for a temperature of 60°F, where  $K_{IC}$  was estimated to be 45 ksi\*in<sup>1/2</sup>, that was interpolated from the values given in Table 5.1. The curves terminate at the critical crack length, or crack length corresponding to sudden fracture for the given loading conditions.

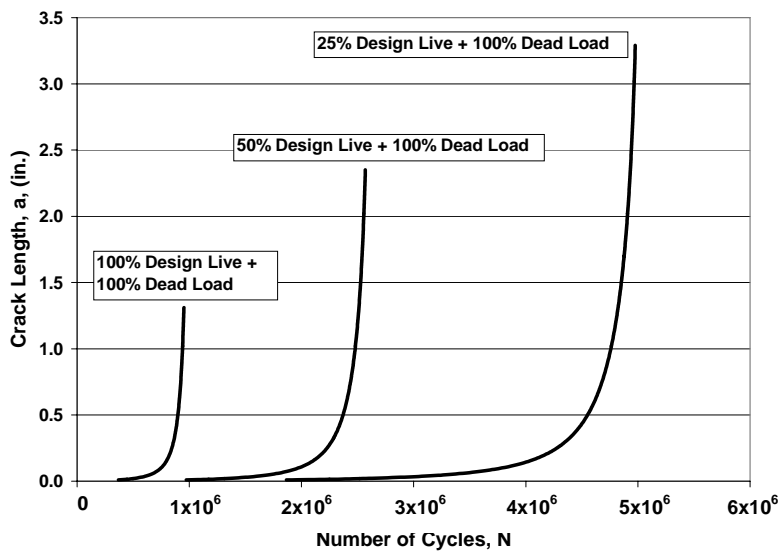


Figure 6.8 Crack Propagation Life Estimation Curves

With the frozen pin condition, and temperature of -10°F, ( $K_{IC}$  equal to 24, see Table 5.1) the same initial crack length of 0.005 in. was used to estimate crack propagation life. The stresses produced from thermal loading were calculated from values supplied in Table 7.3. It was found that sudden fracture would occur in less than 200 cycles of live loading, or within one day (see section 7.5), combined with the dead load and thermal loading effects. It should be reminded that this is a conservative estimate for the strut geometry, edge cracked plate subject to tension and bending. Taking the actual conditions into effect, rolled shape with a coped flange, the propagation life would be significantly shorter.

## 7. LOAD AND CYCLE ESTIMATION

### 7.1 GENERAL

Load on the fractured strut was estimated from three sources: the payload used on the bridge deck during repairing to reposition the raised deck, the calculation of live load using AASHTO HS 20-44 loading on a SAP2000 model of the bridge, and thermal effects on the failed strut as a result of the frozen pinned connection. Traffic flow records provided by the Missouri Department of Transportation (MoDOT) were used to estimate the number of cycles.

### 7.2 DEAD LOAD CALCULATION

Dead load on the strut was calculated from ballast payload that was placed on the bridge during replacement of the strut assemblies. Approximately 240 kips was placed on the end of the bridge during repositioning of the deck, see Figures 7.1. From this payload, and assuming equal load distribution between the two struts at each end of the bridge, the dead load on the failed strut equaled to 120 kips, the same as calculated during retrofit design.



Figure 7.1 Dead Load Ballast Used During Deck Repositioning

### 7.3 LIVE LOAD CALCULATION

A finite element model of the Paseo Bridge was constructed using SAP 2000, Figure 7.2. The model consists of 268 joints and 412 elements. Only frame elements were used, thus moments were released on the ends of each element representing a cable. The model consists of the same dimensioning as the actual structure and contains all of the major structural elements of the bridge including, the four vertical struts, two towers, two stiffening girders, including floor beams and vertical hangers spaced as they exist on the actual bridge. Properties such as cross sections and moments of inertia for both strong and weak axes were obtained from structural drawings of the bridge. An equivalent stiffness for the deck and stringers were calculated and lumped with the stiffening girders. A representation used to calculate this equivalent system can be seen in Figure 7.3.

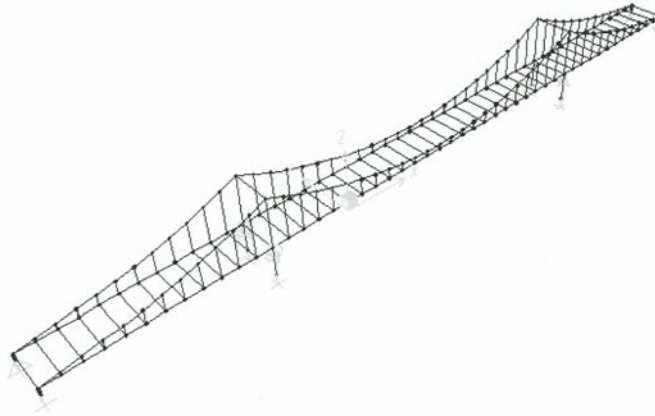


Figure 7.2 SAP 2000 Model of Paseo Suspension Bridge

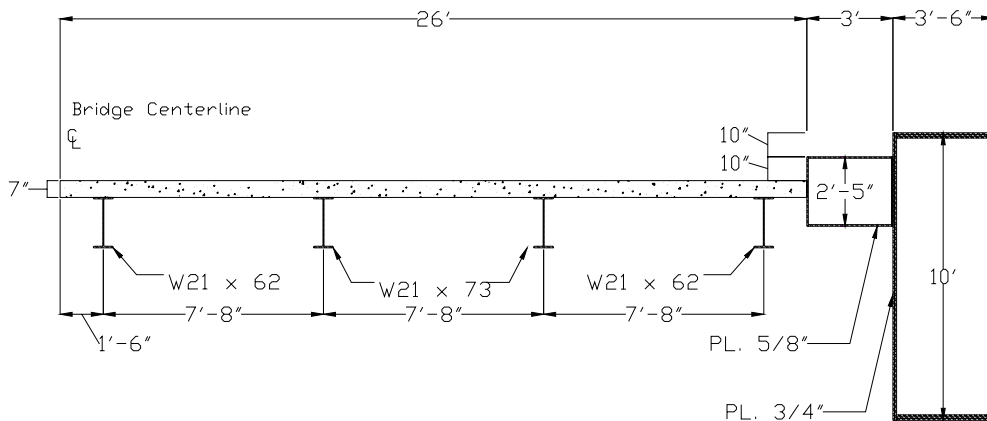


Figure 7.3 Cross Section of Deck, Stringers, and Girder

Four lanes were constructed on the model, two in each direction, with the same eccentricities about the stiffening girders as exist on the bridge. AASHTO HS 20-44 Truck and Lane Loads were applied to the model. The moving load case then seeks the maximum and minimum responses throughout the structure for the most severe of loading all four lanes, any three lanes, any two lanes or any single lane (SAP2000, 1997). Thus, there are fifteen possible permutations for assigning the vehicles the lanes with an appropriate scale factor which takes into account probability of the individual case existing. Table 7.1, displays these possible permutations with an appropriate scale factor. An x in the lane column indicates loading.

Influence lines were generated for the fractured strut for both axial force and moment from each lane during the frozen pin condition. Graphical representations of these conditions are supplied in Appendix E. The numerical influence line data, values for ends, 1/4 points, and midspan for each stiffening girder element in the model was extracted and supplied to Excel. AASHTO lane loads of 640 lbs./ft. were applied and one point load of either 18,000 lbs. for moment or 26,000 lbs. for shear (axial load in strut) at the location of maximum influence. The loads were then multiplied by the influence value and summed for positive and negative values.

The sign convention for axial influence on the strut was negative for compression and positive for tension. The sign convention for moments depended on the direction of the global Y axis of the model. The calculated live load values are summarized in Table 7.2. The values compare well with the load rating calculated during emergency repair design, 232 kips compression and 184 kips tension. Truck loads were also applied, but did not govern the axial force and bending moment on the strut. They are not shown in Table 7.2.

Table 7.1 Possible Permutation for Lane Loading

Permutation	Lane 1	Lane 2	Lane 3	Lane 4	Scale Factor
1	x				1.00
2		x			1.00
3			x		1.00
4				x	1.00
5	x	x			1.00
6		x	x		1.00
7			x	x	1.00
8	x			x	1.00
9	x		x		1.00
10		x		x	0.90
11	x	x	x		0.90
12	x	x		x	0.90
13	x		x	x	0.90
14		x	x	x	0.90
15	x	x	x	x	0.75

Table 7.2 Calculated Live Loads Due to AASHTO HS 20-44 Lane Loading

Lane	Frozen Pin Condition Axial Force in Strut (Kip)		Frozen Pin Condition Moment in Strut (Kip-in)	
	Compression	Tension	Negative	Positive
<b>1</b>	-82.2	38.4	-236	1176
<b>2</b>	-77.4	42.8	-250	1144
<b>3</b>	-34.7	42.3	-260	963
<b>4</b>	-29.7	46.4	-294	968
<b>Sum</b>	-224.0	170.0	-1040	4251

#### 7.4 THERMAL LOAD CALCULATION

Loads induced on the strut from thermal fluctuations under frozen pin conditions of the Southeast strut were also calculated with the aid of the SAP2000 model. To understand how the program works a simple model of just the girder, tower, and strut was constructed and thermal effects applied. Hand calculations verified the results returned by the simple model.

Thermal loads induced on the strut were calculated at temperatures designated by AASHTO for both moderate and cold climates, as well as the temperature the day fracture occurred. According to blueprints for the bridge, all measurements were given for 60°F. Table 7.3, displays the values calculated by the SAP 2000 model for bending moment and axial load at the fracture location of the Southeastern strut. The values are for the frozen pin condition due to thermal effects alone, at the chosen temperatures. The exaggerated deflected shape due to thermal contraction is provided in Figure 7.4. Table 7.4 provides the longitudinal displacements of selected points labeled in Figure 7.4 due to thermal contraction.

Table 7.3 Calculated Thermal Induced Loads

Temperature (°F)	Axial Force (kips)	Moment (kip-in)
-30	139	97800
-10	110	77200
0	95	66900
120	-80	-56600

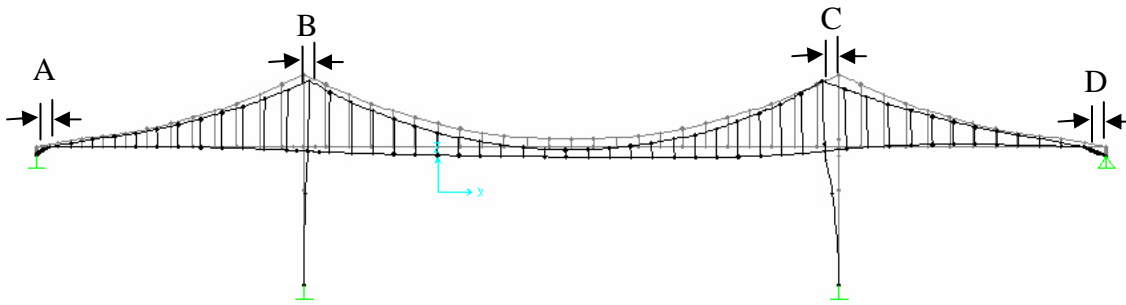


Figure 7.4 Deflected Shape of Paseo Bridge Due to Thermal Contraction

Table 7.4 Longitudinal Displacements of Selected Points in Figure 7.4

Temp °F	A (in)	B (in)	C (in)	D (in)
0	2.00	0.83	2.65	3.16
-10	2.34	0.96	3.09	4.22
-30	3.00	1.24	3.98	5.42

## 7.5 CYCLE DETERMINATION

Traffic data for the Paseo Bridge was supplied by the Missouri Department of Transportation (MoDOT). The average daily traffic volume was given for both the north and south bound lanes, and can be seen in Table 7.5. MoDOT suggested that approximately 11.5% of these vehicles to be trucks.

Table 7.5 Average Daily Traffic Count for Paseo Bridge

Year	North Bound		South Bound	
	All Vehicles	Trucks	All Vehicles	Trucks
1995	34968	4021	39506	4543
1998	40075	4609	43181	4966
1999	41828	4810	47161	5424
2003	45024	5178	43949	5054

Truck traffic was used to calculate the daily number of cycles on the struts, since they have a significantly greater influence on the loading than passenger cars. A cycle was defined by applying the maximum number of trucks of length, 28 feet, to each lane with a spacing of 84.5 feet in between trucks. The length of 28 feet corresponds to the minimum length of a standard AASHTO HS 20 truck and the 84.5 foot spacing was calculated, considering the minimum safety distance, and a loading equivalent to AASHTO lane loading of 640 lbs./ft. The total length of the span between struts is 1232 ft., thus 11 trucks could be in each lane at once. Using 4 lanes, 44 trucks traveling across the deck constituted a cycle.

According to the traffic counts in 1999 and 2003, the average number of trucks passing through the bridge is approximately 10,200 trucks per day. Dividing this total by 44, the number of trucks in one cycle, yields a minimum number of 230 cycles per day on the vertical struts.

## 8. FINITE ELEMENT MODELING

### 8.1 GENERAL

A finite element model of the strut was developed to better understand the stress intensity factor at the location of flange coping, the area of crack initiation in the failed strut, and the process of failure. Since the stress intensity factor and the failure process depend on the size of initial defect or crack length, several different crack lengths are modeled to determine this relationship. The modeling was performed using the commercially available software ABAQUS.

### 8.2 FINITE ELEMENT MODELS

As mentioned previously, the strut assemblies consist of a central rolled shape with two additional plates riveted to each side at the ends to provide bearing surface on the pins. Due to symmetry of the rolled shape, or middle plate,  $\frac{1}{2}$  of the shape is modeled. The middle plate is more likely stiffer than the side plates due to the continuity of the middle plate from pin to pin of the strut.

A model of the middle plate of the strut or the original S24 x 120 member was developed which consisted of the lower 43 inches as measured from the center of the lower pin. This length was chosen to provide four rows of rivet holes, two above, and two below the location of crack initiation. This model, referred to as the global model, consisted of 8835 nodes and 5408 hexahedral elements and can be seen in Figure 8.1.

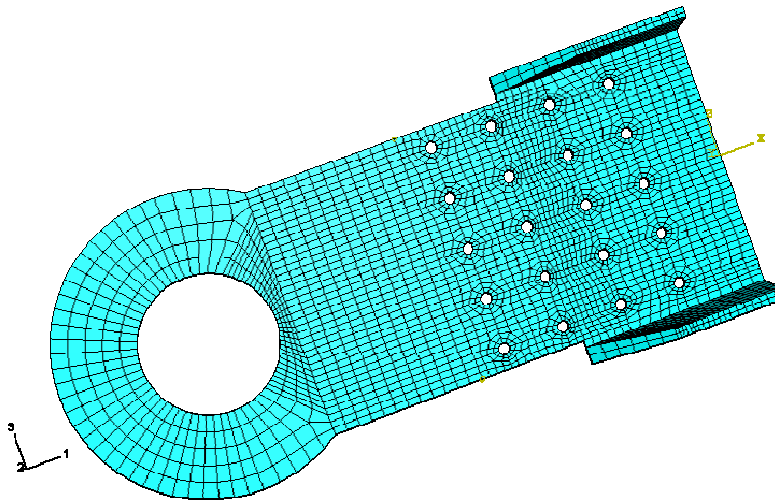


Figure 8.1 ABAQUS Model of Middle Plate of Strut Assembly

The surface of the hole for the 11-inch diameter pin is fully fixed in the global model and the back surface of the plate is constrained, as the model is only  $\frac{1}{2}$  of the middle plate. In other words, the plate thickness of the global model is 0.375 in. instead of 0.75 in., the thickness of the actual strut web. Front and back views of the global model are given in Figure 8.2.

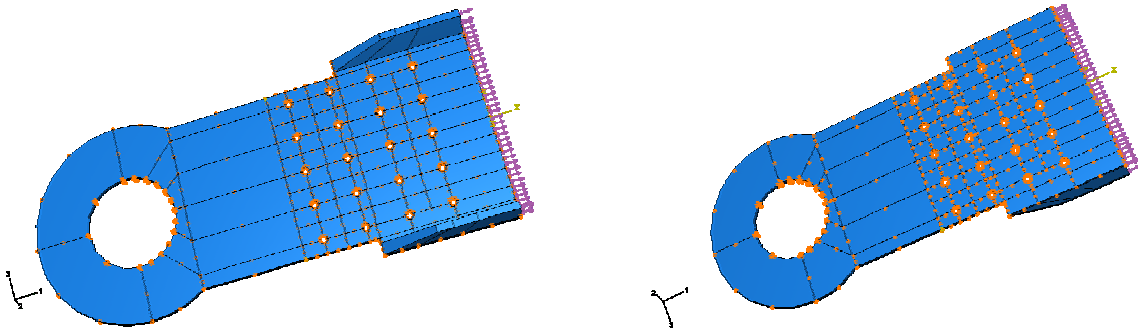


Figure 8.2 Front and Back Views of Modeled Strut

A local model of the area of crack initiation was produced from individual elements of the global model. This allowed for a finer mesh, thus more accurate calculations in the area of crack initiation. The location of the local model in relation to the global model is shown in Figure 8.3. Two global elements were chosen from the global clusters of elements and used as the boundaries for the local model elements.

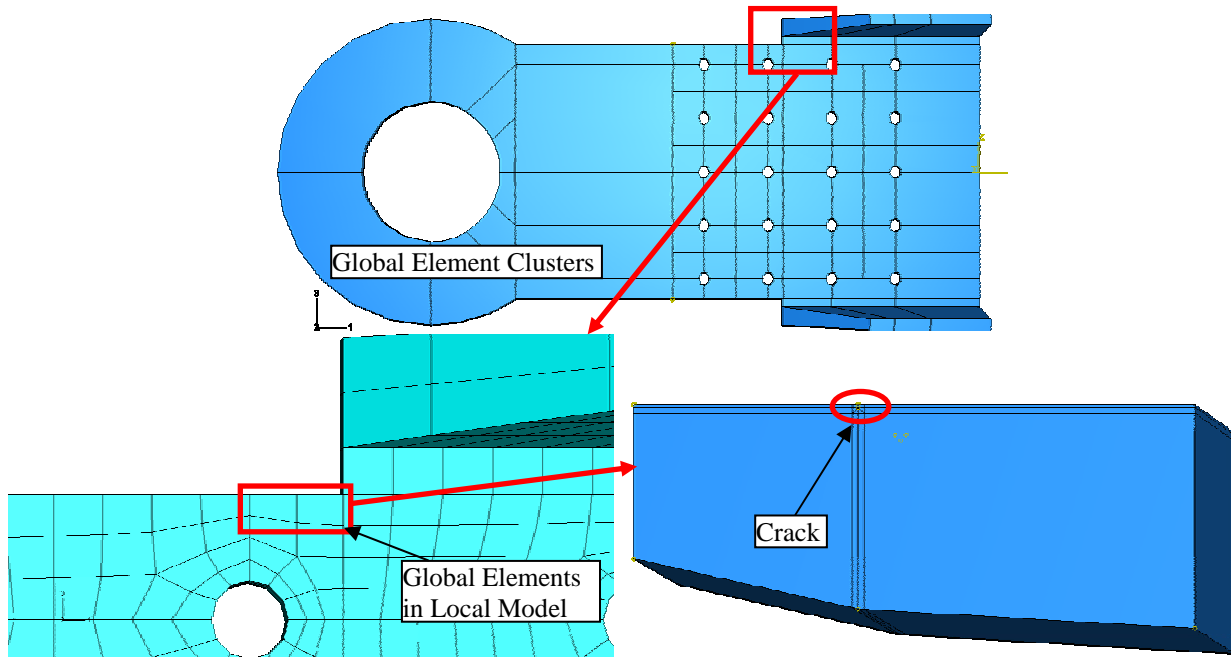


Figure 8.3 Local Model Relationship to Global Model

The local model also consists of 3-dimensional solid hexahedral elements. The number of elements is 8086 and the number of nodes 6912. The mesh of the local model is given in Figure 8.4.

The mesh at the crack tip for the model with a 0.005 in. long crack is given in Figure 8.5. It should be noted that the physical width of the crack was 0.001 in. and the radius of the crack tip was modeled as 0.0005 in.

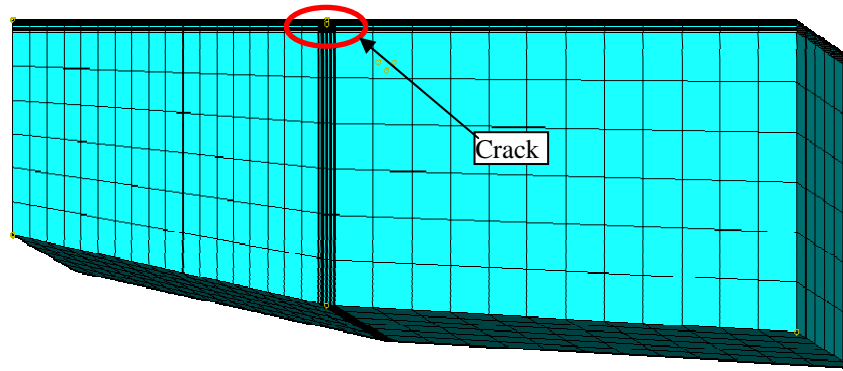


Figure 8.4 Three Dimensional Mesh of Local Model

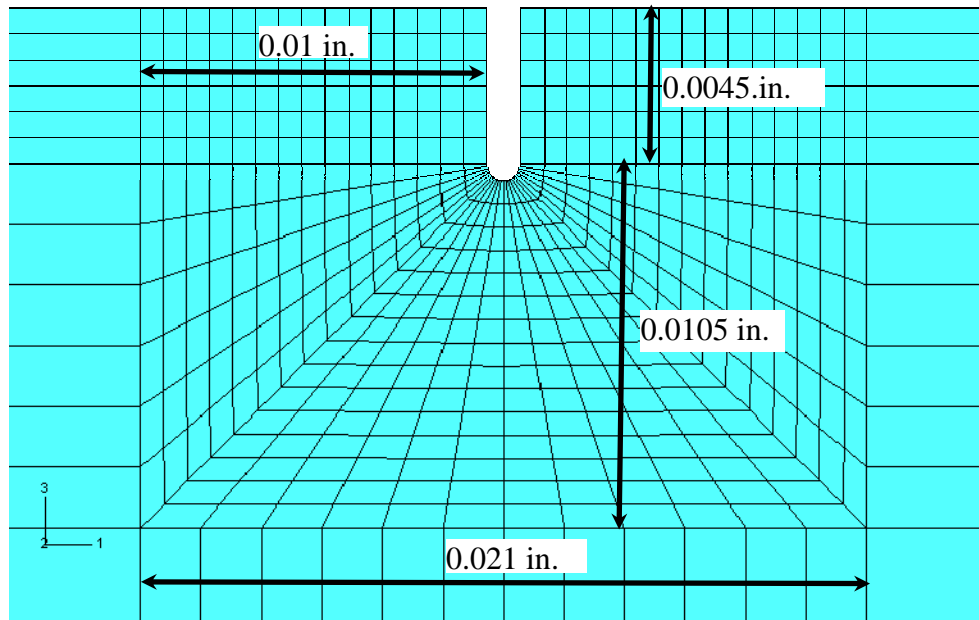


Figure 8.5 Mesh around Crack Tip of Local Model

### 8.3 FINITE ELEMENT MODEL LOADING

The material stress-strain curves developed in Section 3 of this report were used to model material behavior in the ABAQUS modeling. A Poisson's ratio,  $\nu=0.3$ , was used for calculations performed by the software. Loads were applied to the model corresponding to dead loads as well as traffic and thermal live loading. The values for traffic and thermal loads were obtained from the SAP 2000 analysis discussed in Section 7 of this report. As seen in Table 8.1, only 50% of the loads from Section 7.2 and Tables 7.2 and 7.3 were applied to the global model since it represents half of the failed strut. Seven specific loading cases were chosen for each crack length and are supplied in Table 8.1, with a description of the loading and the values of axial forces and moments applied.

Table 8.1 Loading Matrix for Chosen Test Cases

Load Case	Description	Temperature (°F)	Pin Condition	Axial Force (kip)	Moment (kip-in)
1	Dead + Live	60	unfrozen	145	0
2	Dead + Live	60	frozen	145	4250
3	Dead + Live + Thermal	30	frozen	169	19925
4	Dead + Live + Thermal	10	frozen	185	30375
5	Dead + Live + Thermal	0	frozen	193	35600
6	Dead + Live + Thermal	-10	frozen	200	40800
7	Dead + Live + Thermal	-30	frozen	215	51000

The combination of axial forces and moments were converted to distributed surface stresses applied on the top surface of the global model including the flanges. Figure 8.6 shows the dimensions where the stresses were applied to the global model. Figure 8.7 shows how the loads from axial forces and moments were combined and converted to stresses applied to the surface in Figure 8.6.

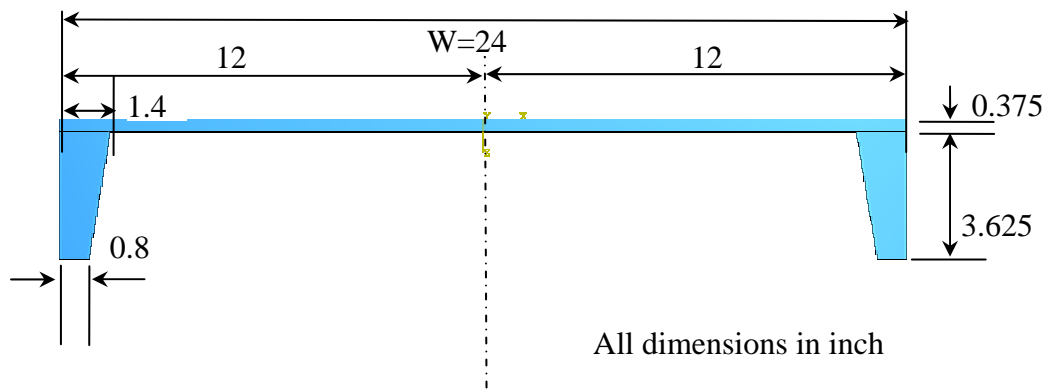


Figure 8.6 Cross Section Dimensions of Global Model

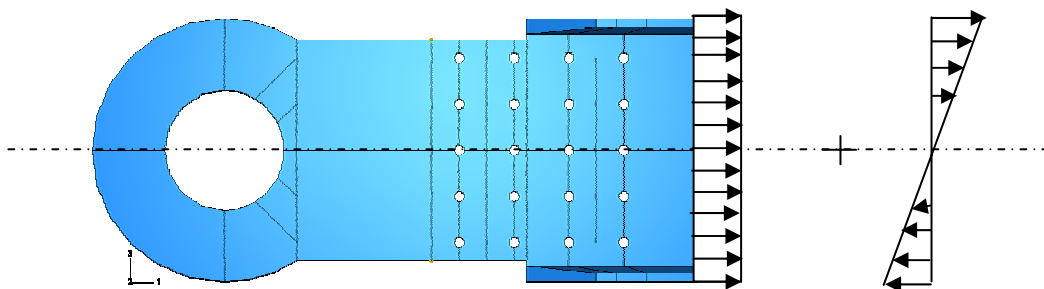


Figure 8.7 Illustration of Stress Application to the Global Model

Stresses at the boundaries of the local model, Figure 8.5, are found by first analyzing the global model, obtaining the resulting stresses corresponding to the boundaries of the elements in the local model and then applying those to the finer mesh of the local model.

## 8.4 J-INTEGRAL EVALUATION

To understand whether elastic analysis with  $K_I$  evaluation of the fracture process is sufficient, the limits of the validity of linear elastic fracture mechanics (LEFM) were checked. The limits require the conditions of Equation 8.1 be met.

$$a, B, (W - a) \geq 2.5 \left( \frac{K_I}{\sigma_y} \right)^2 \quad (8.1)$$

The term  $a$  represents crack length,  $B$  represents plate thickness. Based on the known yield stress,  $\sigma_y$ , and stress intensity factor,  $K_I$  for the given loading, the initial crack length would have to be a sufficient length to be considered valid. For example, for load case 1 in Table 8.1, the crack length,  $a$ , would have to be greater than 0.27 in. This was estimated by using a stress intensity factor equal to the stress concentration factor of 3.76 in value (see Section 4.4), and a yield stress of 36.2 ksi. The crack lengths modeled violate Equation 8.1. Other load cases in Table 8.1 were also checked and again indicated that significant plastic deformation has taken place. Therefore,  $K_I$  evaluation approach is not applicable and elastic-plastic analysis in ABAQUS was necessary to calculate the J-integral values.

The path-independent J-integral is a method of characterizing the stress-strain field at the tip of a crack by an integration path taken sufficiently far from the crack tip to be analyzed and then substituted for a path close to the crack-tip region. The J-integral, a mathematical expression, is applicable for either elastic or elastic-plastic behavior (Barsom et al., 1987). Hertzberg (1996) presents a definition for  $J$  as the pseudopotential energy difference between two identically loaded bodies possessing slightly different crack lengths.

J-integral evaluations were performed on the models and compared to threshold J integral values,  $J_{IC}$ . Sudden fracture occurs if the calculated J-integral value,  $J_I$ , is greater than the critical  $J$ , or  $J_{IC}$ .  $J_I$  is the driving force, which is a function of crack size and applied load, whereas  $J_{IC}$  is the resistance force, which is essentially a material property at the appropriate service temperature and loading rate (Barsom et al., 1987).

## 8.5 FINDINGS

Elastic-plastic analysis was performed for each of the seven load cases described in Table 8.1. Two crack lengths, 0.005 in. and 0.001 in., were considered. The crack length of 0.005 in. was selected because that is the smallest crack discernable with many test instruments. Table 8.2 shows the results of these analyses under 100% of design loads. Each analysis assumes that the load in the strut is completely transferred from pin to pin through the middle strut only. The critical  $J_{IC}$  values were calculated by Equation 8.2, found in Barsom (1987) for the condition of plane strain, using the values of predicted fracture toughness,  $K_{IC}$ , that were determined in Section 5.4. The calculated  $J_{IC}$  is also presented in Table 8.2.

$$J_{IC} = \frac{K_{IC}^2 (1 - \nu^2)}{E} \quad (8.2)$$

Table 8.2 Comparison of  $J_{IC}$  to  $J$  for Selected Load Cases (100% Loading)

Load Case	Temperature (°F)	Pin Condition	Experimental $J_{IC}$ (lb/in)	$J_I$ (lb/in) (0.005" defect)	$J_I$ (lb/in) (0.001" defect)
1	60	unfrozen	67	2.86	0.19
2	60	frozen	67	560	3.13
3	30	frozen	36	701	207
4	10	frozen	23	1068	262
5	0	frozen	21	1890	358
6	-10	frozen	19	2460	439
7	-30	frozen	-	2740	614

It is evident from Table 8.2 that if the pin were free to rotate, sudden fracture would never have happened even with an initial defect of 0.005 inches and low temperatures. For example, at a temperature of -10 °F, the  $J_I$  value (=2.86 lb/in) was still less than the critical value  $J_{IC}$ =19 lb/in. Thus, from findings in Figure 6.8 and Table 8.2, failure of the strut by fatigue can be ruled out.

On the other hand, the J-integral results in Table 8.2 indicated immediate fracture of the web of the strut as soon as the pin became mechanically frozen, even without thermal loading, so long as the initial crack length was at least 0.005 in. in length. Considering the stress concentration effect of the coping flange of the strut in numerical analysis, failure of the strut under dead plus live loads suggested by the numerical result seemed consistent with what was presented in Section 6.4. However, this result was not supported by the field-observed fact that indication for the frozen pin condition existed two months prior to the failure when the temperature was above 30 °F as seen in Figure 2.2 but fracture did not occur until the temperature dropped to -9.9 °F. Therefore, low temperature was a contributing factor to the failure of the strut though it was not the main reason and the assumption with an initial defect of 0.005 inches may be on the higher end.

The effect of an initial defect on the failure of the strut was further investigated with different analysis using a 0.001-inch defect. The numerical results included in Table 8.2 indicated sudden fracture at a temperature of 30 °F, which was once again different from the field observations. At this point, considering that the strut assembly actually consisted of a S24×120 section and four cover plates as shown in Figure 1.5, it was assumed that the plates riveted to the strut for bearing on the pins carried 50% of the load with the additional 50% transferred through the middle plate of the strut or web of the rolled section. The results of this analysis can be seen in Table 8.3 for two initial defects. It is clearly seen from Table 8.3 that sudden fracture occurred when the strut with an initial defect of 0.001 inches experienced a temperature below 10 °F, which agreed with the field observations. This analysis indicated that fracture would have occurred even though the fatigue detail around the coped flange of the strut had been improved.

The areas of plastic deformation on the middle plate of the strut for each load case analyzed, assuming the middle plate conveys 50% of the load to the pin, are presented in Figure 8.8. The figures were produced from Von Mises stress analysis in ABAQUS. The areas of plastic deformation, or areas with stress greater than the yield stress,  $\sigma_y$ , are outlined with bold black lines.

Table 8.3 Comparison of  $J_{IC}$  to  $J$  for Selected Load Cases (50% Loading)

Load Case	Temperature (°F)	Pin Condition	Experimental $J_{IC}$ (lb/in)	$J_I$ (lb/in) (0.005" defect)	$J_I$ (lb/in) (0.001" defect)
1	60	unfrozen	67	0.47	0.02
2	60	frozen	67	36.3	0.39
3	30	frozen	36	53.3	13.1
4	10	frozen	23	81.7	58.0
5	0	frozen	21	95.3	71
6	-10	frozen	19	231	180
7	-30	frozen	-	633	454

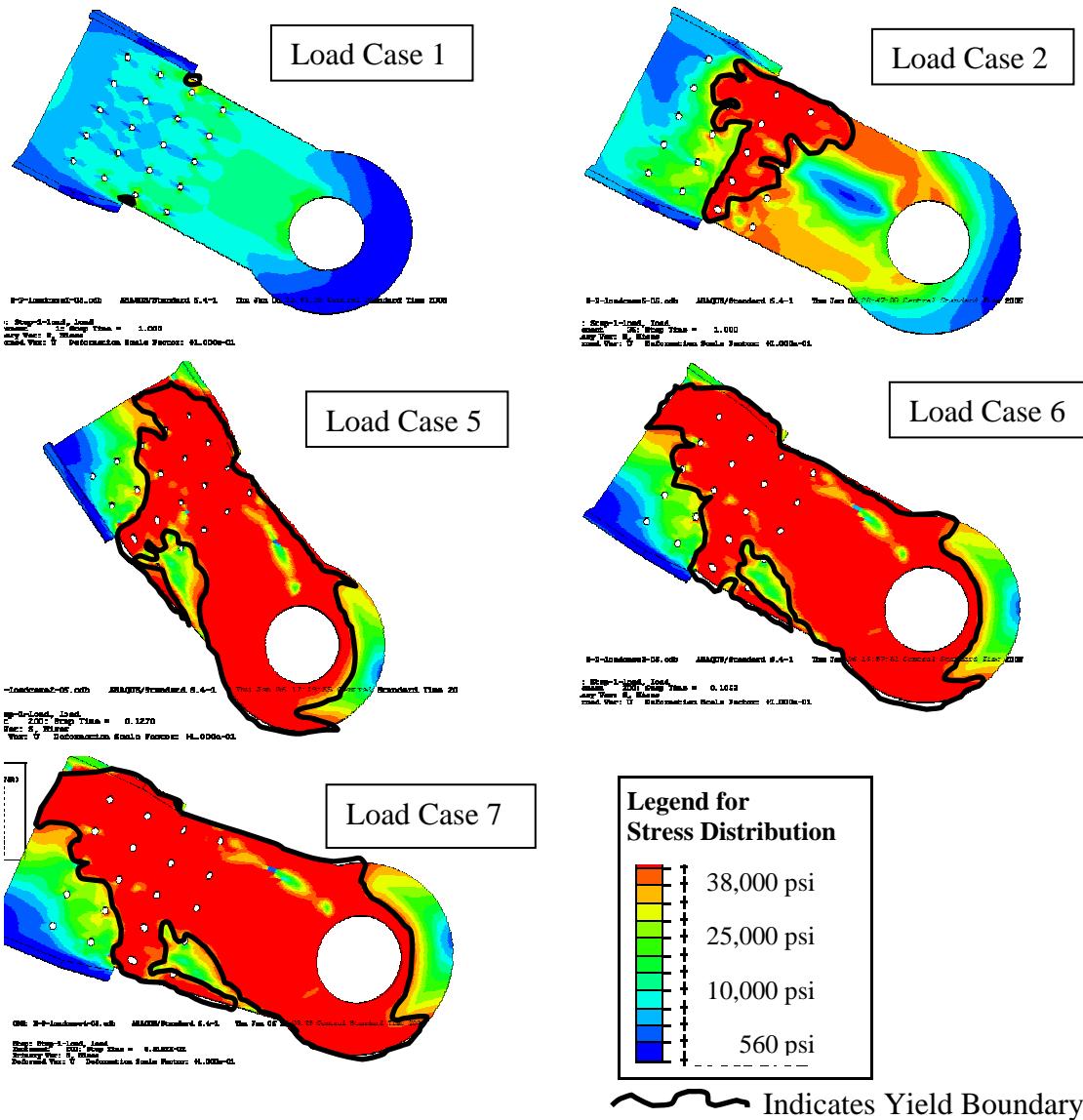


Figure 8.8 Progression of Plastic Deformation Areas for Selected Load Cases

To identify the location of crack initiation and propagation, a series of local models with various initial crack lengths were established in ABAQUS. Each model was analyzed for Load Case 1. When there is no initial flaw or crack, the stress contour is shown in Figure 8.9. It is observed from Figure 8.9 that crack is likely initiated near the flange coping area due to high stress concentration and propagated towards the closest hole. To further see the propagation of an initial crack, as shown in Figure 8.10, two additional models with a crack length of 0.5 in. for Crack Pattern 1 and 1.1 in. for Crack Pattern 2, respectively, were analyzed. Their corresponding stress contours are presented in Figure 8.11. As a result of the previous cracks, the maximum stress occurs in the opposite side of the hole near the flange coping area. To understand how sensitive the location of the maximum stress, the third crack pattern was introduced in Figure 8.10. Its corresponding stress contour is also presented in Figure 8.11. By comparing Crack Pattern 2 and Pattern 3, one can see that the locations of the maximum stress identified from the two models are practically the same. To finish up the analysis for crack propagation, the fourth crack pattern in Figure 8.10 was created and the stress contour is shown in Figure 8.11. By comparing Figure 8.11 with the actual fracture pattern, illustrated in Figure 8.12, one can conclude that the models accurately predict the crack initiation and propagation locations of the actual damage pattern.

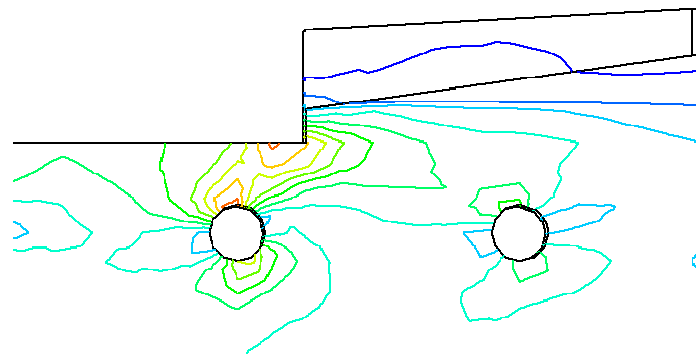


Figure 8.9 Mises Stress Contour in Load Case 1 for Crack Initiation Location Determination

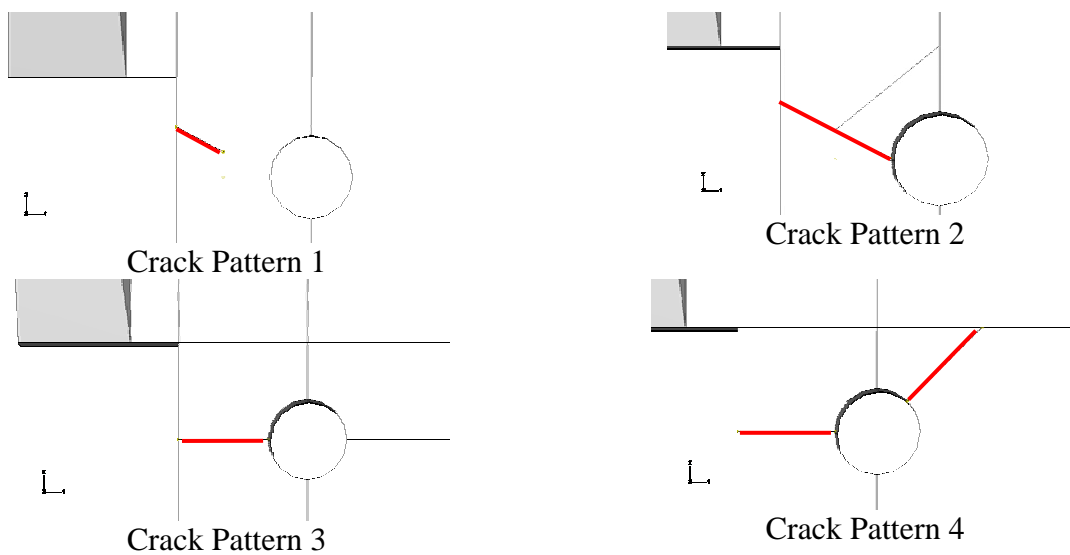


Figure 8.10 Crack Patterns

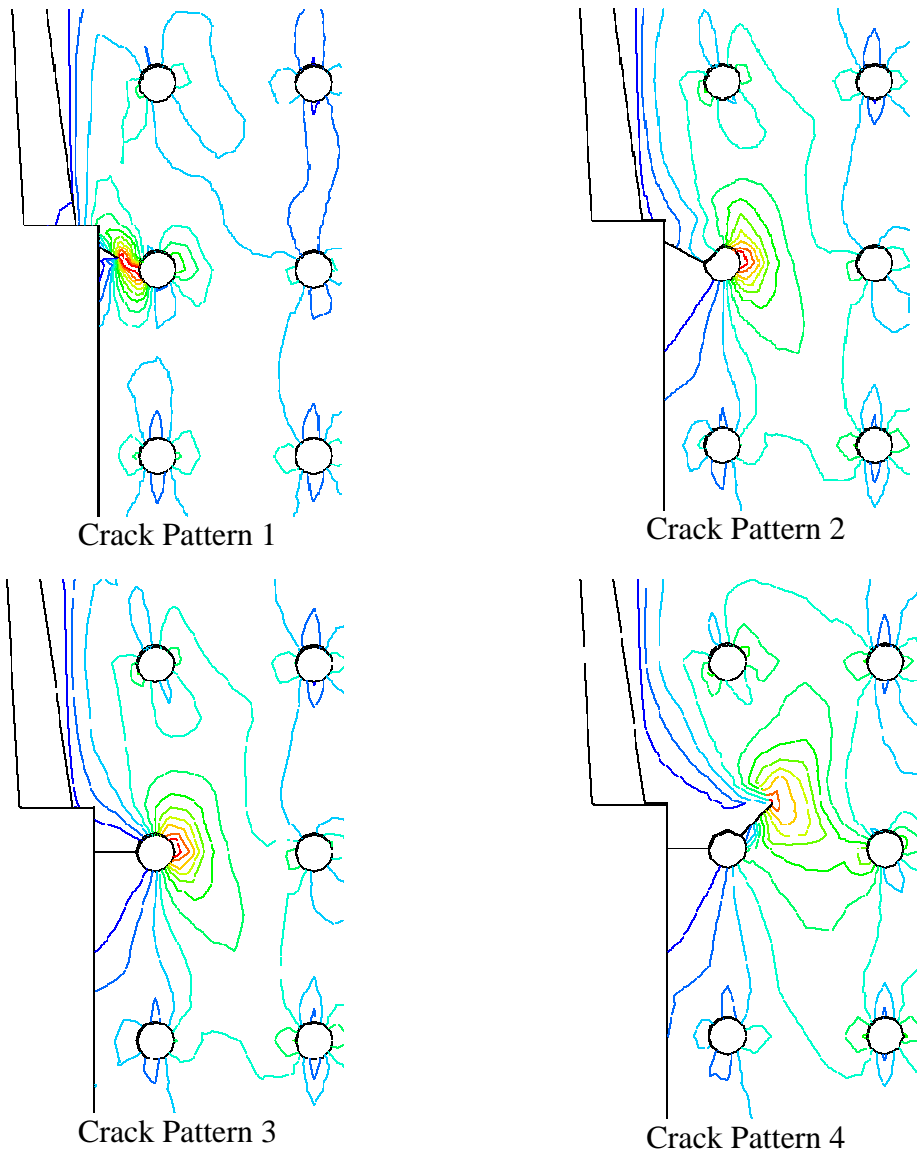


Figure 8.11 Mises Stress Distribution for Different Crack Patterns in Load Case 1



Figure 8.12 Actual Crack Propagation Pattern

## 9. CONCLUSIONS AND RECOMMENDATIONS

Based on the findings in this study, it can be concluded that the lack of access to the lower link pin, connecting the fractured strut to the bridge foundation, for proper preventative maintenance is the root cause of the failure of the Southeastern vertical strut of the Paseo Bridge. The failure occurred by sudden fracture shortly after the lower pin became completely frozen. Moments were generated from thermal contraction of the bridge as well as live loading once the pin was restrained from rotation. The struts were not designed to carry moment induced loading, rather axial forces only. Fracture initiated at the point where the flange of the rolled section S24×120 was coped from the web. The mechanical freezing of the lower link pin has been attributed to salt and sand accumulation in the lower link housing, discovered during the bridge inspection two months prior to failure. Specific scope of the work and findings presented in this report that lead to the conclusion include:

1. Determine basic material properties from static tensile testing. The stress-strain curve of the material used in the fractured strut has been established with testing of five specimens. The Young's modulus of the material is 28,500 ksi, the yield stress is 36.2 ksi, and the ultimate stress is 61 ksi. The material was identified as A36 steel.
2. Establish a stress and cycles-to-failure (S-N) relation for crack initiation life estimation, taking into account mean stress effects. The fatigue constants necessary to predict the residual crack initiation life of the bridge strut with the strain-life method have been determined with testing of 25 specimens. The fatigue strength coefficient and exponent are 70.71 ksi and -0.066, respectively, while the fatigue ductility coefficient is 0.0077 and the fatigue ductility exponent is -0.28. Fatigue tests on the failed strut material indicated an infinite life under normal service conditions when the strut were free to rotate, had no initial defects or small cracks inherent to steel structures.
3. Establish the relation between fracture toughness and temperature. The goal of this exercise would be to determine the critical flaw size at the design stress as a function of the operating temperature using a fracture mechanics criterion. Charpy impact testing was conducted at nine temperatures since the thickness of specimens would be prohibitively large for direct fracture toughness testing. Based on testing of 45 specimens at temperatures ranging from -10° to 136°F, the breaking energy of various specimens was related to the temperatures to which the specimens are exposed. The fracture toughness was then converted from the breaking energy with an empirical relation. It ranges from 24 to 110 ksi\*in<sup>1/2</sup>.
4. Establish crack growth rate for crack propagation life estimation. This information allows for determination of the life to fracture given an initial crack length and known loading conditions. Five compact tension specimens were tested to establish the Paris crack growth law with two material constants:  $C=7 \times 10^{-10}$  and  $m=2.8$ . It was found that nearly 1,000,000 cycles (approximately 12 years) of 100% design loading or over 2,500,000 cycles of 50% design loading are required for an initial defect of 0.005 inches in the strut to propagate to a critical length (over 1.3 or 2.4 inches) causing sudden fracture under normal loading conditions if the pin were free to rotate. Since no visual cracks were recorded during the inspection two months prior to the failure, crack propagation was unlikely the reason for the failure. On the other hand, sudden fracture occurred as a result of the mechanically frozen pin condition at the lower link of the southeastern strut.

5. Estimate service loading conditions and number of cycles. Dead load, live load, and thermal effects on the failed strut as a result of a frozen pin condition were estimated. The dead plus live load on the failed strut is 145 kips in tension only when the pin is free to rotate. With a frozen pin condition, the dead plus live load includes a tension force of 145 kips and a moment of 4,250 kip-in at a design temperature of 60°F. When the temperature drops to -10°F (when the strut failed), the thermal effects associated with the frozen pin condition amount the load on the strut to a total of 200 kips in tension and 40,800 kip-in in bending moment. From the recent traffic count records collected in the bridge area, each strut was subjected to approximately 230 cycles of live loading per day.
6. Establish a detailed finite element model and simulate the strut failure process. This allows for accurate calculation of the stress concentration (3.76) in the area of flange coping and the stress intensity factor as a function of crack length. Simulation results indicated that the strut would never have fractured even at low temperatures and with a 0.005-inch initial defect if the pin in the lower link were free to rotate. Low temperature makes the strut material behave more brittle with low fracture toughness and is thus a secondary contributor to the fracture of the strut after the pin was frozen. The load transferred through the web of the strut is likely 50% of design loading as supported by the fact that the strut did not fracture under the combined dead plus live load and thermal effect at a temperature of higher than 10°F during the bridge inspection in November, 2002. This fact also suggests that the initial defect (crack) in the coping flange area of the failed strut seems more than 0.001 inches.

Better design of lower link pin housing areas that allows preventative maintenance of the pins between vertical struts and the bridge foundation or special maintenance of the pins is required to prevent similar occurrences here or on other structures. The overstressing, thermal contraction, fatigue, and reduction in fracture toughness associated with low temperatures were all real conditions, but they would not have caused the failure if the preventative maintenance was done. They are contributory factors.

Several relatively simple recommendations to prevent similar incidences to other bridges and the new struts installed on the Paseo Bridge are provided:

1. Greasing the upper and lower pins during special pin inspections and maintenances to ensure continued free rotation of the struts. This would have prevented the freezing and allows for the free rotation. It is recognized that the design of the bridge had limited access to the lower link pin housing. Therefore, although the two cycle of inspection is adequate, special pin maintenance may be done over a longer time period such as every ten years.
2. Partial sealing the lower housings to prevent salt and sand accumulation near the pins or providing traps under the finger expansion joints to stop salt and sand debris from dropping to the lower link housing. These corrosive materials damage and/or clog free rotation.
3. Installation of a problem alarming device at a cost of less than \$10k to remotely monitor the rotation of all four vertical struts and immediately alert officials should the pins become mechanically frozen. In light of the limited access to the lower link area, greasing pins could be costly, and this recommendation can be a practical solution.

## 10. BIBLIOGRAPHY

- AASHTO, Standard Specifications for Highway Bridges, 15<sup>th</sup> ed., 1992.
- ASM, "What Does the Charpy Test Really Tell Us?" Proc. of the American Institute of Mining, Metallurgical and Petroleum Engineers. Denver, CO. February 27-28, 1978. American Society for Metals, Ohio, 1978.
- ASM Handbook, Mechanical Testing Vol. 8. American Society for Metals, USA, 1985.
- ASTM A36-04: Standard Specification for Carbon Structural Steel.
- ASTM A515-03: Standard Specification for Pressure Vessel Plates, Carbon Steel, for Intermediate- and Higher-Temperature Service.
- ASTM Committee E-28. Charpy Impact Test: Factors and Variables. STP 1072. American Society for Testing and Material, Philadelphia, PA, 1990.
- ASTM E399-90: Standard Test Method for Plane-Strain Fracture Toughness of Metallic Materials.
- ASTM E606-92: Standard Practice for Strain-Controlled Fatigue Testing.
- ASTM E647-00: Standard Test Method for Measurement of Fatigue Crack Growth Rates.
- ASTM E8-03: Standard Test Methods for Tension Testing of Metallic Materials.
- Bannantine, J.A., Comer, J.J., and Handrock, J.L., Fundamentals of Metal Fatigue Analysis. Prentice Hall, New Jersey, 1990.
- Barsom, J.M. and Rolfe, S.T., Fracture and Fatigue Control in Structures. 2<sup>nd</sup> Edition. Prentice Hall, New Jersey, 1987.
- Barsom, J.M., "Fatigue-Crack Propagation in Steels of Various Yield Strengths," *Transactions of the ASME, Journal of Engineering for Industry*, November 1971, pp. 1190-1196.
- Barsom, J.M., "The Development of AASHTO Fracture Toughness Requirements for Bridge Steels," U.S. Steel Corporation, August 1974.
- Barsom, J.M., and Rolfe, S.T., "Correlation Between  $K_{IC}$  and Charpy V-Notch Test Results in the Transition-Temperature Range," U.S. Steel Applied Research Laboratory, June 1969, AD 855832.
- Barsom, J.M., and Rolfe, S.T., "Fatigue and Burst Analysis of Hy-140(T) Steel Pressure Vessels," *Transactions of the ASME, Journal of Engineering for Industry*, February 1970, pp. 11-16.
- Boller, C. and Seeger, T., Materials Data for Cyclic Loading. Elsevier Science Publishers B.V., Amsterdam, The Netherlands, 1987.
- Bucher, J.H., "The Effect of Inclusions on the Brittle Fracture of Hot-Rolled Steel," *Journal of Materials*, Vol. 2, No. 2, June, 1967.
- Fisher, J.W., "Bridge Fatigue Guide – Design and Details," AISC, 1977.
- Fisher, J.W., Pense, A.W., Hausammann, H., and Irwin, G.R., "Quinnipiac River Bridge Cracking," *ASCE Journal of the Structural Division*, April 1980, pp 773-789.
- Fisher, J.W., Yen, B.T., and Frank, K.H., "Minimizing Fatigue and Fracture in Steel Bridges," *Transactions of the ASME, Journal of Engineering Materials and Technology*, Vol. 102, January 1980, pp. 20-25.
- Fisher, J.W., Yen, B.T., and Wang, D., "Fatigue of Bridge Structures-A Commentary for Design, Evaluation and Investigation of Cracking," ATLSS Report No. 89-02, Lehigh University, July 1989.

- Frank, K.A., "Mechanical and Chemical Properties of Selected Steels Used in Bridge Structures," Report No. FHWA-RD-75-79, Federal Highway Administration November 1974 PB-255-323.
- "Fracture Mechanics" Proc. of the Twelfth National Symposium on Fracture Mechanics, Washington University, St. Louis, MO, May 21-23 1979. ASTM Special Technical Publication 700. American Society for Testing and Materials, Philadelphia, PA, 1980.
- Frost, N.E., Marsh, K.J., and Pook, L.P. Metal Fatigue. Oxford University Press, London, 1974.
- Hertzberg, R.W., Deformation and Fracture Mechanics of Engineering Materials. 4<sup>th</sup> Edition. John Wiley and Sons, USA, 1996.
- Holt, J.M., Gibson, C., and Ho, C.Y. (eds.), Structural Alloys Handbook, Vol. 3, CINDAS/Purdue University, West Lafayette, IN, 1999.
- Little, R.E., Manual on Statistical Planning and Analysis for Fatigue Experiments. American Society for Testing and Materials, Philadelphia, PA, 1975.
- Little, R.E., and Jebe, R.H., Statistical Design of Fatigue Experiments. Halsted Press, USA, 1975.
- Manson, S.S., "Inversion of the Strain-Life and Strain-Stress Relationships for Use in Metal Fatigue Analysis." *Fatigue of Engineering Materials and Structures*, Vol. 1 pp. 37-57.
- Merritt, F.S. (ed), Structural Steel Designer's Handbook. McGraw Hill, USA, 1972.
- Mostovoy, S., Crosley, P.B., Ripling, E.J., "Use of Crack-Line –Loaded Specimens for Measuring Plane-Strain Fracture Toughness," *Journal of Materials*, Vol. 2, No. 3, September 1967.
- Orner, G.M., and Hartbower, C.E., "Sheet Fracture Toughness Evaluated by Charpy Impact and Slow Bend." Presented at AWS National Fall Meeting, Dallas, TX, Sept. 25-28, 1961. *Welding Research Supplement*, September 1961. pp 405s-416s.
- Parsons Engineering Group, "Paseo Bridge," 2002 Bridge Evaluation Report, Missouri Department of Transportation, April 2003.
- Phaal, K., Macdonald, K.A., and Brown, P.A., "Correlations Between Fracture Toughness and Charpy Impact Energy," *The TWI Journal*, Vol. 6, No. 3, 1997. pp. 454-538.
- Roberts, R., and Newton, C., "Interpretive Report on Small-Scale Test Correlations with  $K_{IC}$  Data," *Welding Research Council Bulletin* 265, February 1981. pp. 1-18.
- Roberts, R., Krishna, G.V., and Nishanian, J., "Fracture Behavior of A36 Bridge Steels," *Fracture Mechanics: Twelfth Conference, ASTM STP 700*. American Society for Testing and Materials, 1980. pp. 552-577.
- SAP 2000, Analysis Reference, Vol. 1, 1997.
- Schindler, H.J., and Morf, U., "A Closer Look at Estimation of Fracture Toughness from Charpy V-Notch Tests," *International Journal of Pressure Vessels & Piping*, 55, 1993. pp. 203-212.
- Smith, K.N., Watson, P., and Topper, T.H., "A Stress-Strain Function for the Fatigue of Metals," *Journal of Materials*, JMLSA, Vol. 5, No. 4, December 1970, pp. 767-778.

## APPENDIX A. STATIC TENSILE TESTING DATA

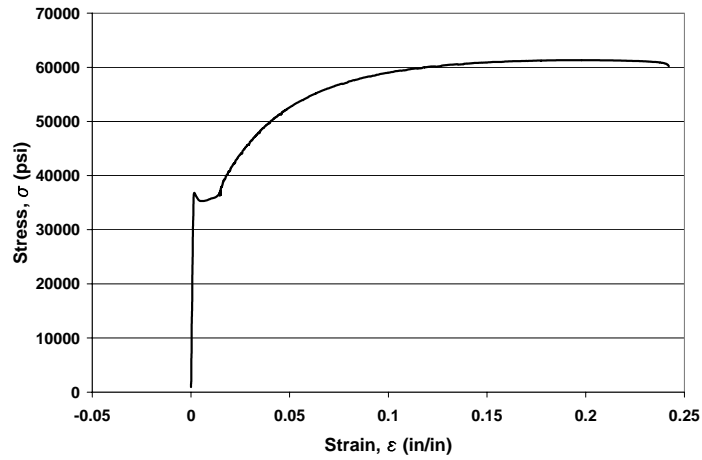


Figure A.1 Specimen 1 Engineering Stress-Strain Curve

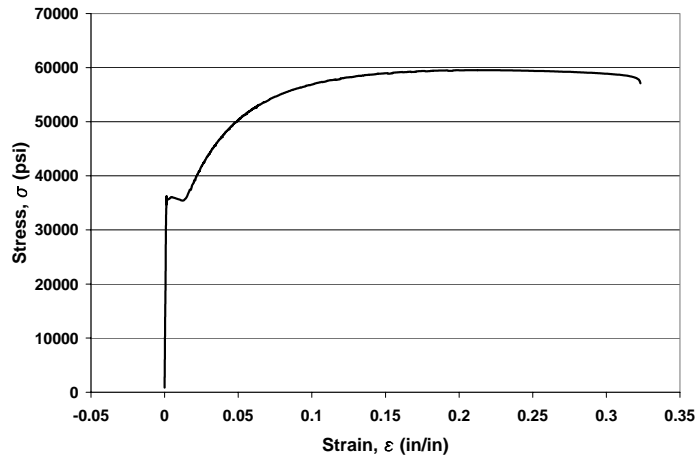


Figure A.2 Specimen 2 Engineering Stress-Strain Curve

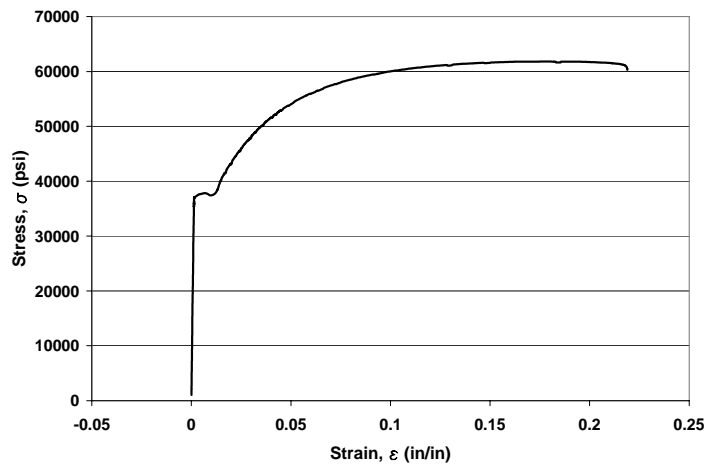


Figure A.3 Specimen 4 Engineering Stress-Strain Curve

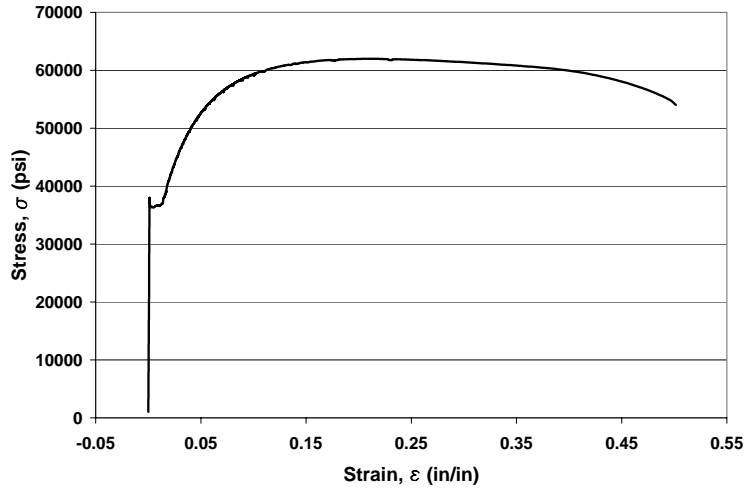


Figure A.4 Specimen 5 Stress-Strain Curve

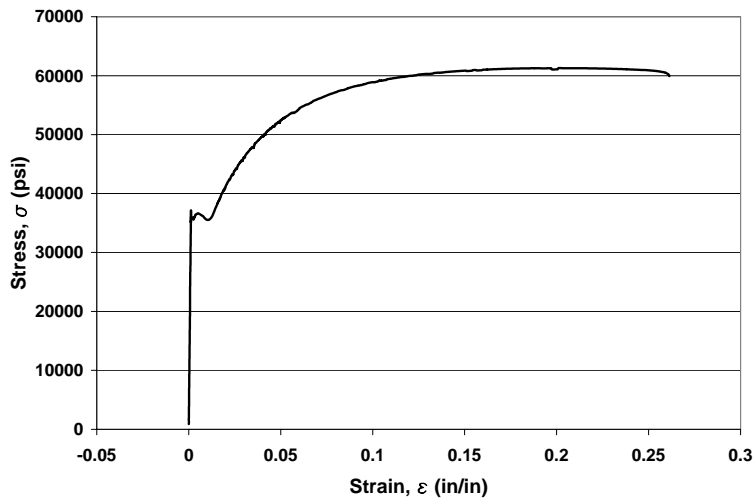


Figure A.5 Specimen 6 Engineering Stress-Strain Curve

Table A.1 Data Obtained from Automated Data Acquisition System

Specimen	Load at 0.2% Yield (lbf)	Stress at 0.2% Yield (psi)	Strain at 0.2% Yield (%)	Load at Peak (lbf)	Stress at Peak (psi)	Strain at Peak (%)	Stress at Break (psi)	Strain at Break (%)
1	5668	35173	0.365	9879	61308	20.8	50882	24.2
2	6610	35747	0.368	11010	59537	21.2	49268	32.3
4	5872	37551	0.354	9670	61842	18.3	52499	21.9
5	5618	36429	0.355	9557	61968	22.2	52048	51.3
6	6162	35957	0.290	10500	61275	20.3	50980	26.1
Mean	5986	36171	0.346	10123	61186	20.6	51135	31.2
S.D.	409	893	0.032	615	973	1.5	1251	11.9

## APPENDIX B. FATIGUE DATA

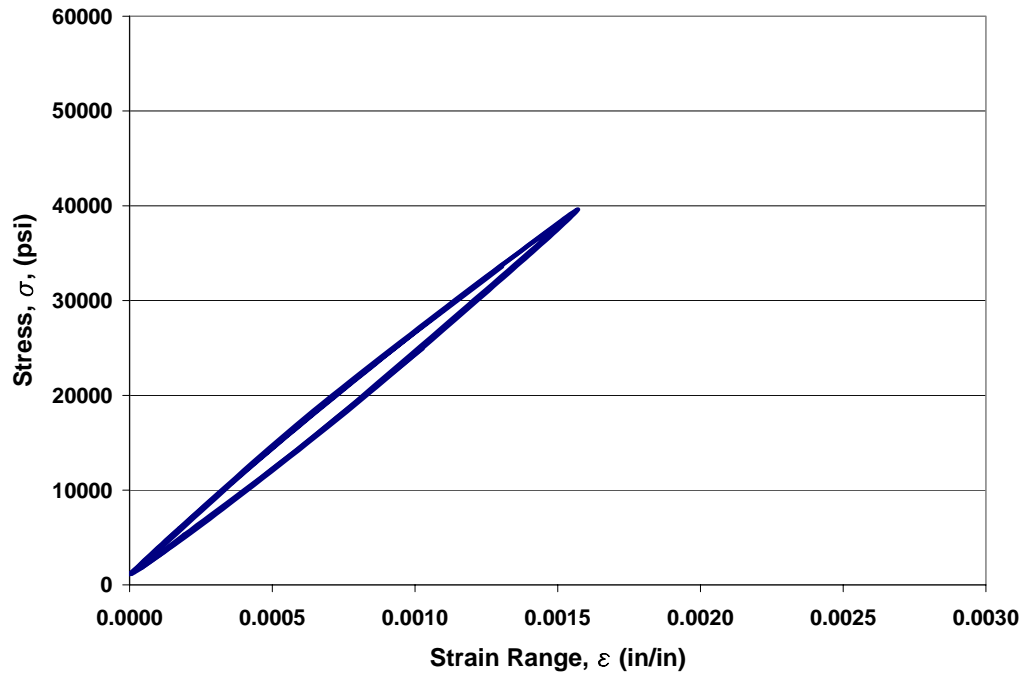


Figure B.1 Specimen 1 Hysteresis Loop

Table B.1 Specimen 1 Data

Cycle approximate	$\Delta\sigma$ (psi)	$\Delta\epsilon$ (in/in)	$\sigma_{\text{mean}}$ (psi)
1000	38520	0.00157	20290
1100	38360	0.00157	20390
1200	38450	0.00157	20330
1300	38420	0.00156	20320
1400	38450	0.00157	20350
1500	38450	0.00156	20300
1600	38530	0.00156	20250
1700	38420	0.00157	20380
1800	38400	0.00156	20300
1900	38490	0.00158	20350
2000	38450	0.00157	20380
2100	38420	0.00157	20300
<b>AVG.</b>	38450	0.00157	20330

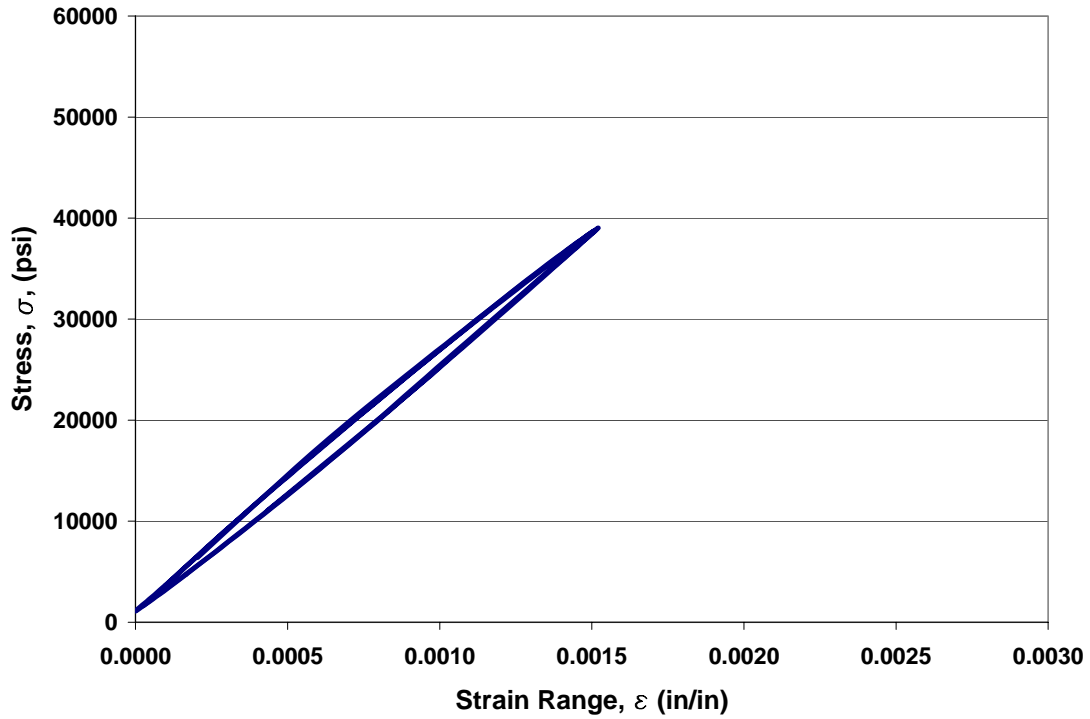


Figure B.2 Specimen 2 Hysteresis Loop

Table B.2 Specimen 2 Data

<b>Cycle approximate</b>	<b><math>\Delta\sigma</math> (psi)</b>	<b><math>\Delta\varepsilon</math> (in/in)</b>	<b><math>\sigma_{\text{mean}}</math> (psi)</b>
1000	37950	0.00152	20030
1100	37900	0.00152	20030
1200	37990	0.00152	20010
1300	38020	0.00152	20000
1400	37960	0.00152	20010
1500	37910	0.00152	20060
1600	38030	0.00151	20000
1700	37920	0.00152	20000
1800	37900	0.00153	19960
1900	38020	0.00153	20050
2000	38000	0.00152	20040
2100	37970	0.00151	20070
<b>AVG.</b>	37970	0.00152	20020

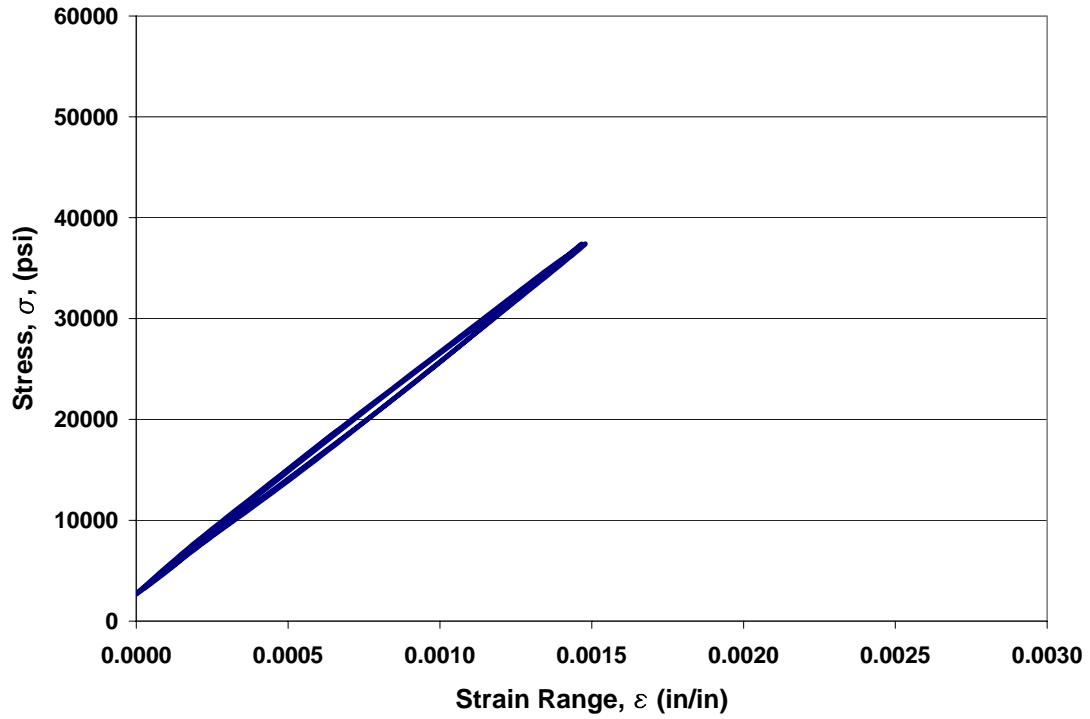


Figure B.3 Specimen 3 Hysteresis Loop

Table B.3 Specimen 3 Data

<b>Cycle approximate</b>	<b><math>\Delta\sigma</math> (psi)</b>	<b><math>\Delta\varepsilon</math> (in/in)</b>	<b><math>\sigma_{\text{mean}}</math> (psi)</b>
1000	34540	0.00147	19940
1100	34690	0.00148	20040
1200	34800	0.00149	19960
1300	34460	0.00147	20130
1400	34840	0.00149	19970
1500	34840	0.00148	20000
1600	34840	0.00147	20010
1700	34810	0.00148	19940
1800	34860	0.00148	19990
1900	34810	0.00148	20020
2000	34840	0.00148	20030
2100	34760	0.00147	20010
<b>AVG.</b>	34760	0.00148	20000

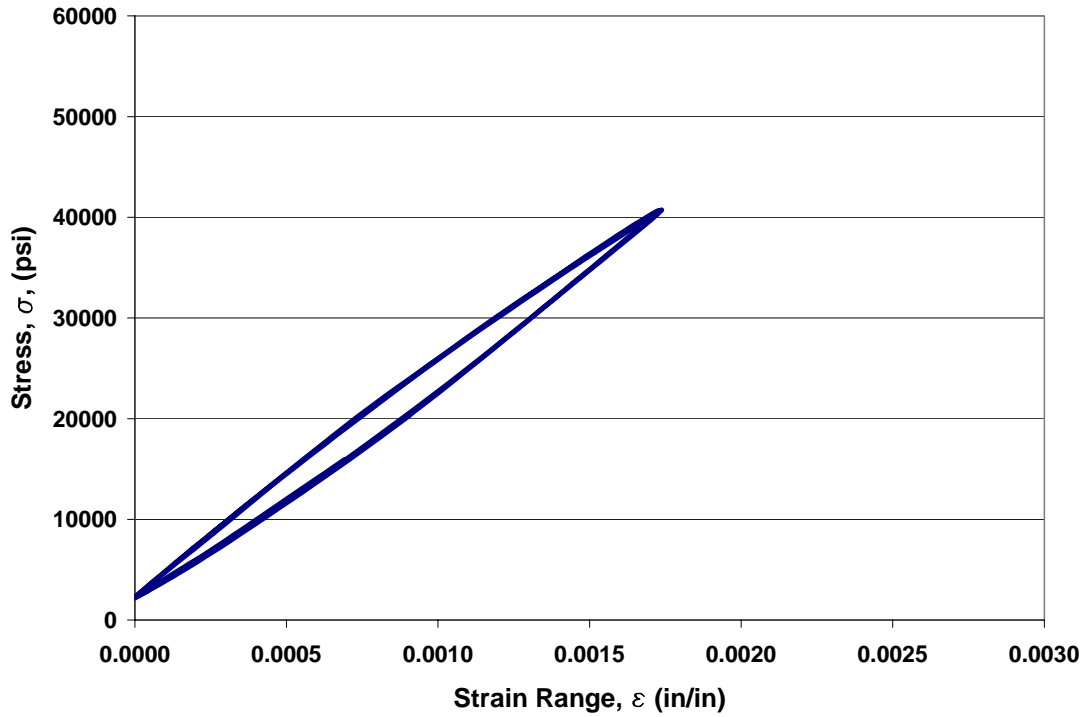


Figure B.4 Specimen 4 Hysteresis Loop

Table B.4 Specimen 4 Data

<b>Cycle approximate</b>	<b><math>\Delta\sigma</math> (psi)</b>	<b><math>\Delta\varepsilon</math> (in/in)</b>	<b><math>\sigma_{\text{mean}}</math> (psi)</b>
1000	38570	0.00174	21450
1100	38510	0.00173	21500
1200	38570	0.00174	21300
1300	38400	0.00174	21360
1400	38690	0.00174	21360
1500	38580	0.00174	21510
1600	38580	0.00173	21410
1700	38420	0.00173	21550
1800	38600	0.00174	21500
1900	38520	0.00174	21450
2000	38130	0.00172	21300
2100	38600	0.00173	21470
<b>AVG.</b>	38510	0.00174	21430

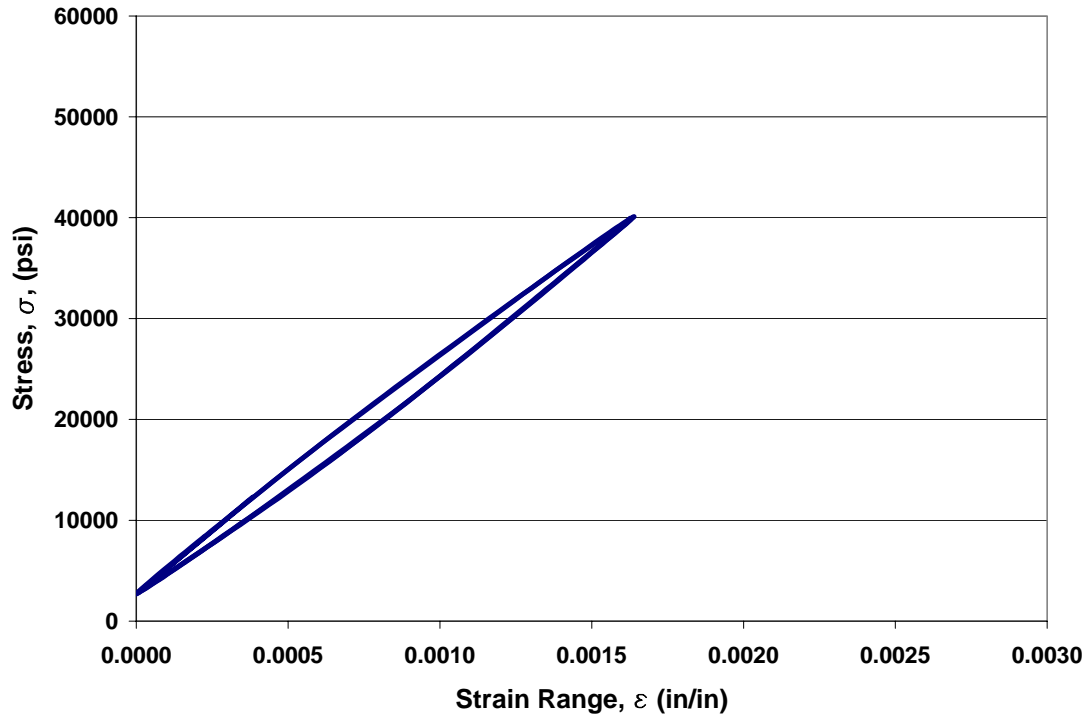


Figure B.5 Specimen 5 Hysteresis Loop

Table B.5 Specimen 5 Data

<b>Cycle approximate</b>	<b><math>\Delta\sigma</math> (psi)</b>	<b><math>\Delta\varepsilon</math> (in/in)</b>	<b><math>\sigma_{\text{mean}}</math> (psi)</b>
1000	37440	0.00164	21310
1100	37400	0.00164	21390
1200	37420	0.00164	21290
1300	37410	0.00164	21390
1400	37470	0.00165	21330
1500	37420	0.00165	21390
1600	37390	0.00164	21360
1700	37460	0.00164	21380
1800	37370	0.00164	21380
1900	37500	0.00164	21390
2000	37370	0.00163	21360
2100	37450	0.00164	21340
<b>AVG.</b>	37420	0.00164	21360

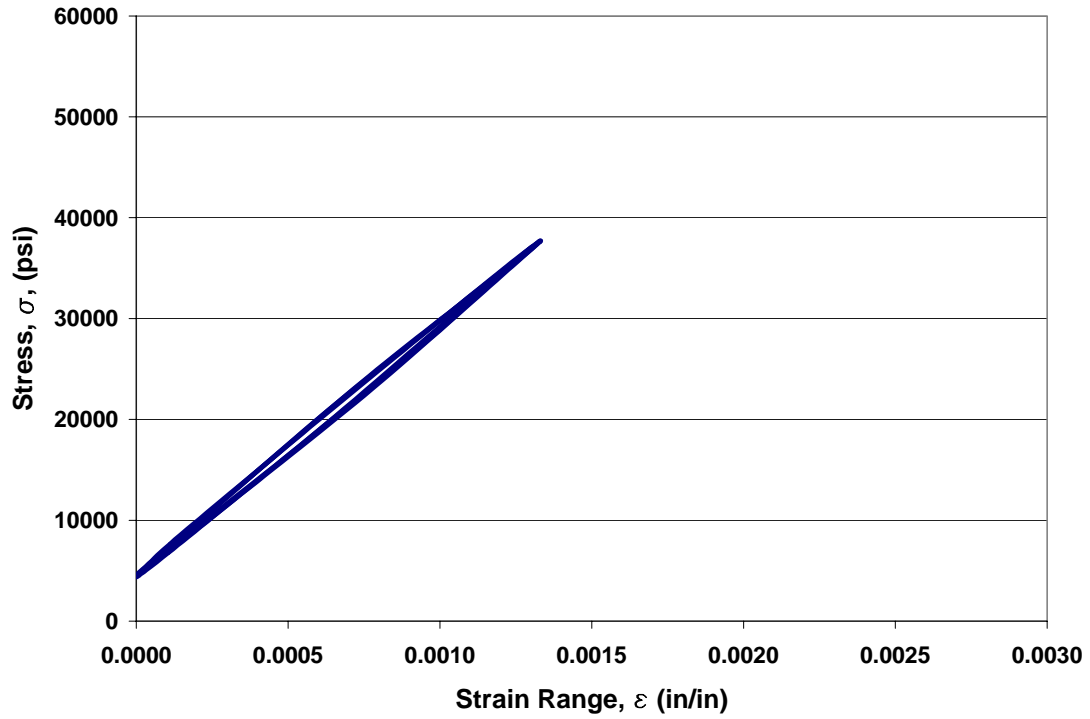


Figure B.6 Specimen 6 Hysteresis Loop

Table B.6 Specimen 6 Data

<b>Cycle approximate</b>	<b><math>\Delta\sigma</math> (psi)</b>	<b><math>\Delta\varepsilon</math> (in/in)</b>	<b><math>\sigma_{\text{mean}}</math> (psi)</b>
1000	33120	0.00133	21150
1100	33350	0.00135	21080
1200	33400	0.00134	21100
1300	33340	0.00134	21030
1400	33310	0.00134	21060
1500	33360	0.00134	21100
1600	33330	0.00133	21050
1700	33290	0.00134	21090
1800	33390	0.00134	21100
1900	33230	0.00133	21000
2000	33260	0.00134	21080
2100	33400	0.00134	21070
<b>AVG.</b>	33320	0.00134	21080

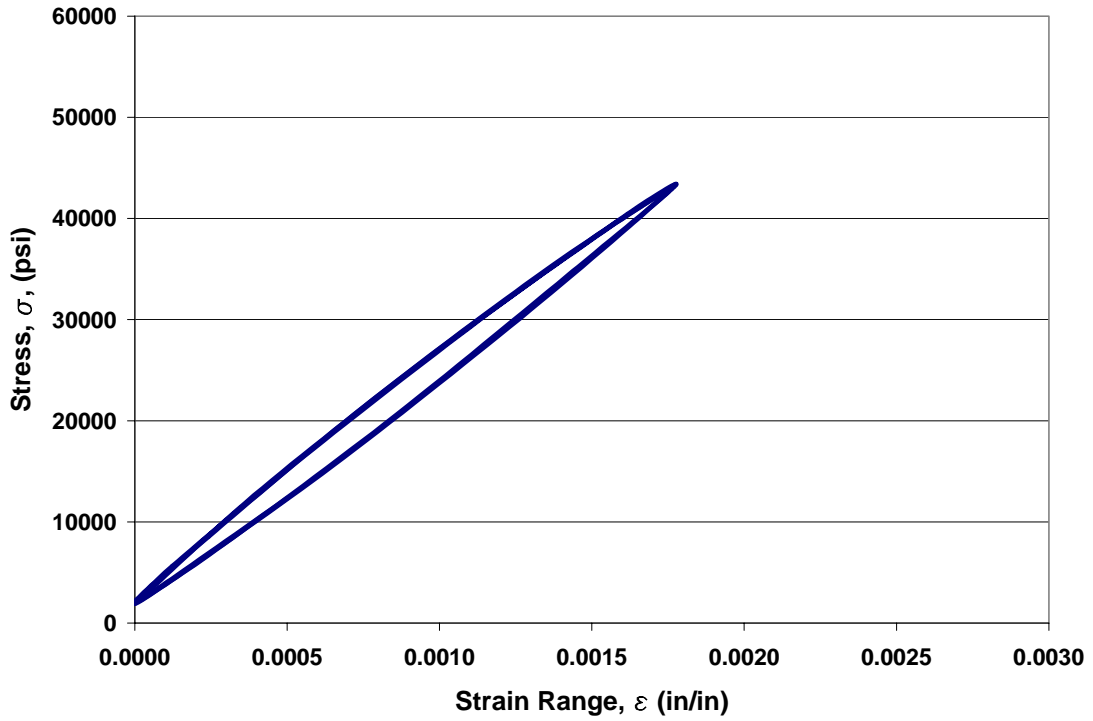


Figure B.7 Specimen 7 Hysteresis Loop

Table B.7 Specimen 7 Data

<b>Cycle approximate</b>	<b><math>\Delta\sigma</math> (psi)</b>	<b><math>\Delta\varepsilon</math> (in/in)</b>	<b><math>\sigma_{\text{mean}}</math> (psi)</b>
1000	41430	0.00178	22580
1100	41420	0.00178	22650
1200	41400	0.00177	22700
1300	41500	0.00176	22700
1400	41370	0.00176	22760
1500	41280	0.00177	22760
1600	41420	0.00178	22620
1700	41450	0.00178	22650
1800	41490	0.00178	22660
1900	41470	0.00178	22670
2000	41460	0.00178	22690
2100	41360	0.00178	22630
<b>AVG.</b>	41420	0.00177	22670

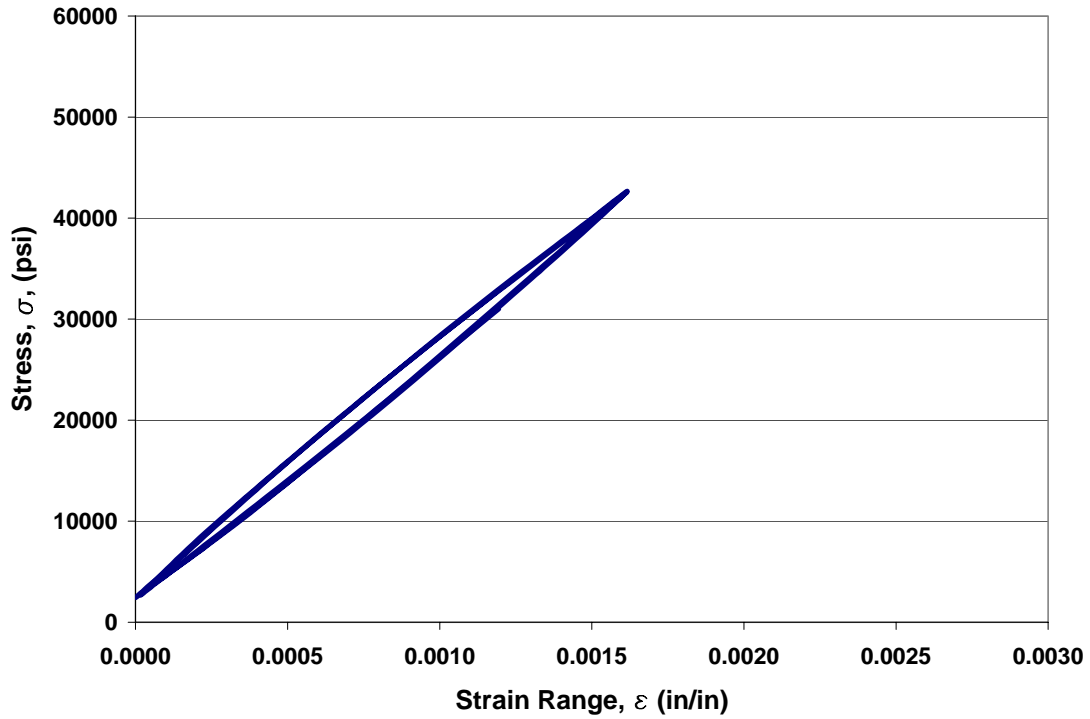


Figure B.8 Specimen 8 Hysteresis Loop

Table B.8 Specimen 8 Data

<b>Cycle approximate</b>	<b><math>\Delta\sigma</math> (psi)</b>	<b><math>\Delta\varepsilon</math> (in/in)</b>	<b><math>\sigma_{\text{mean}}</math> (psi)</b>
1000	40200	0.00161	22580
1100	40150	0.00161	22630
1200	40220	0.00161	22570
1300	40160	0.00162	22530
1400	40260	0.00162	22510
1500	40200	0.00161	22540
1600	40090	0.00161	22640
1700	40140	0.00161	22540
1800	40230	0.00162	22530
1900	40160	0.00161	22520
2000	39960	0.00160	22430
2100	40190	0.00161	22580
<b>AVG.</b>	40160	0.00161	22550

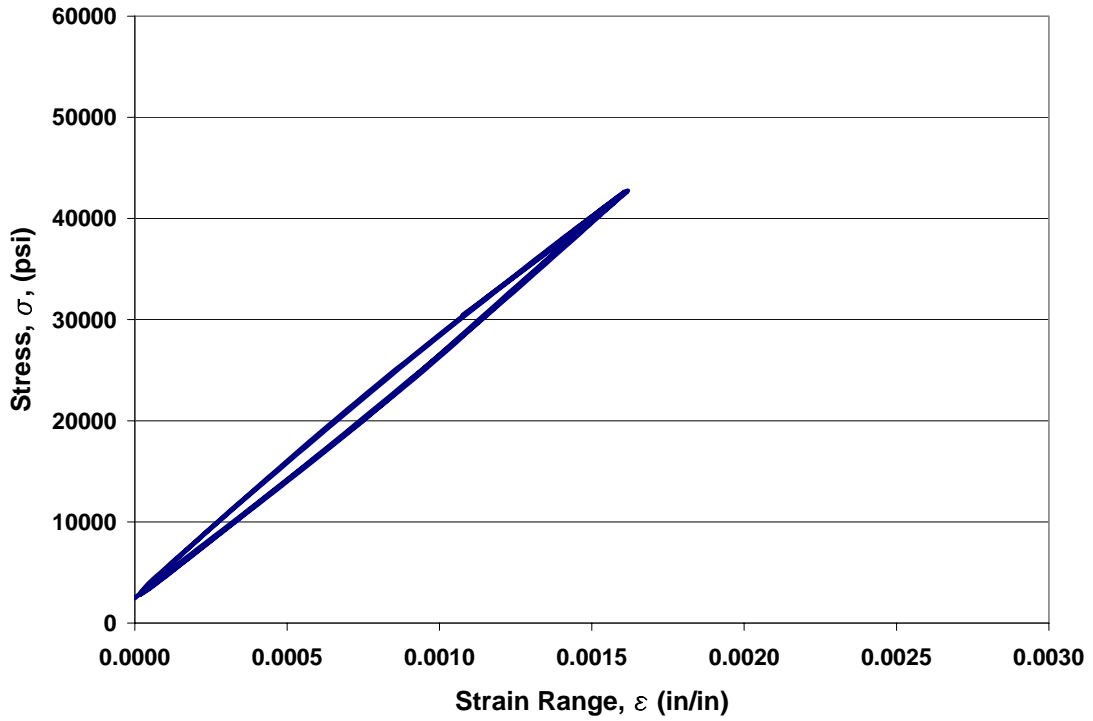


Figure B.9 Specimen 9 Hysteresis Loop

Table B.9 Specimen 9 Data

<b>Cycle approximate</b>	<b><math>\Delta\sigma</math> (psi)</b>	<b><math>\Delta\varepsilon</math> (in/in)</b>	<b><math>\sigma_{\text{mean}}</math> (psi)</b>
1000	40700	0.00219	22520
1100	40780	0.00220	22550
1200	40570	0.00266	22150
1300	40600	0.00252	22470
1400	40650	0.00229	22460
1500	40680	0.00223	22530
1600	40560	0.00219	22560
1700	40690	0.00213	22440
1800	40670	0.00212	22500
1900	40660	0.00226	22550
2000	40650	0.00228	22470
2100	40780	0.00225	22480
<b>AVG.</b>	40670	0.00228	22470

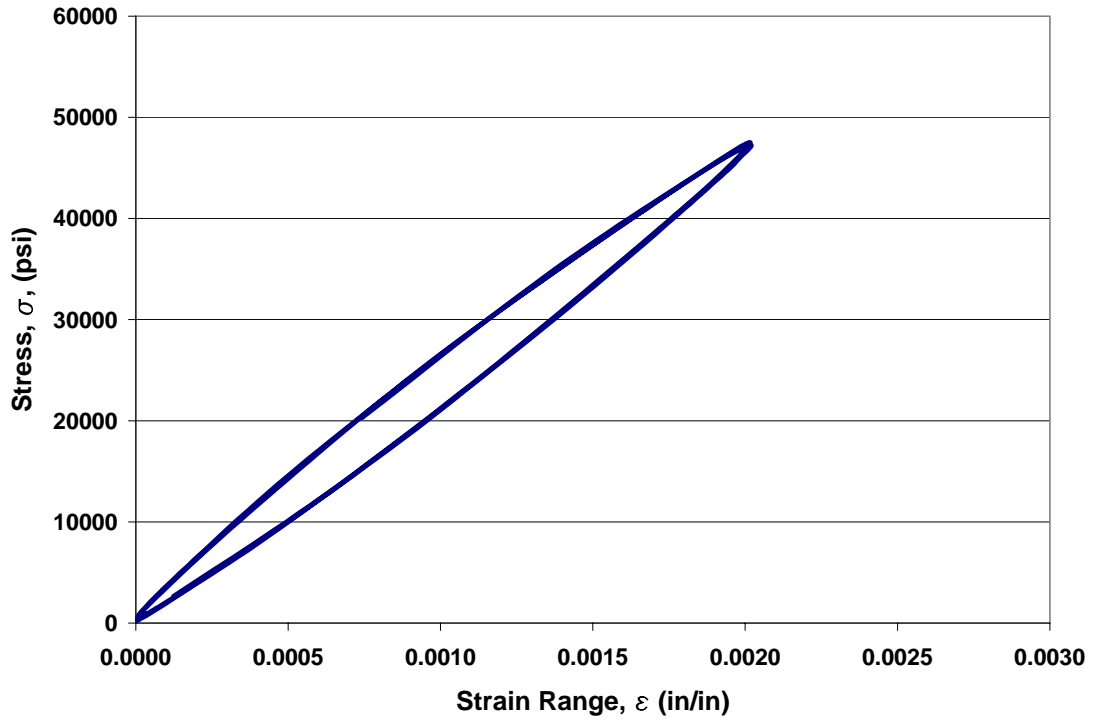


Figure B.10 Specimen 10 Hysteresis Loop

Table B.10 Specimen 10 Data

<b>Cycle approximate</b>	<b><math>\Delta\sigma</math> (psi)</b>	<b><math>\Delta\varepsilon</math> (in/in)</b>	<b><math>\sigma_{\text{mean}}</math> (psi)</b>
1000	47390	0.00205	23760
1100	47370	0.00204	23810
1200	47220	0.00203	23690
1300	47320	0.00204	23780
1400	47370	0.00204	23800
1500	47400	0.00205	23740
1600	47300	0.00205	23730
1700	47380	0.00205	23840
1800	47060	0.00202	23570
1900	47440	0.00205	23750
2000	47320	0.00203	23800
2100	47330	0.00202	23860
<b>AVG.</b>	47320	0.00204	23760

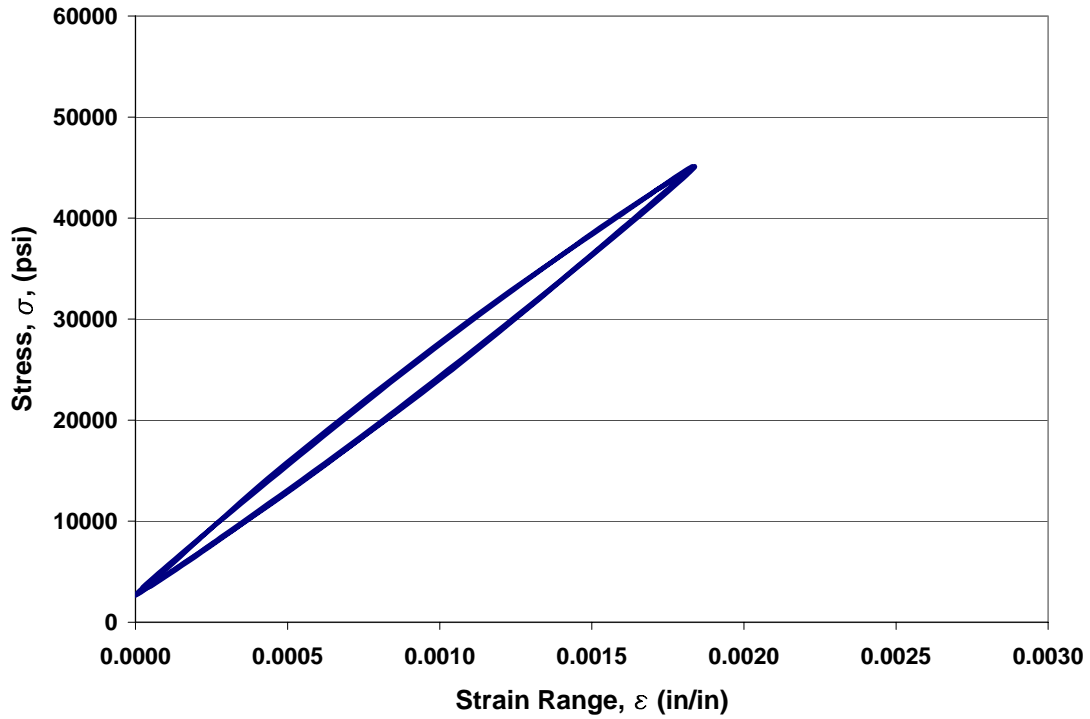


Figure B.11 Specimen 11 Hysteresis Loop

Table B.11 Specimen 11 Data

<b>Cycle approximate</b>	<b><math>\Delta\sigma</math> (psi)</b>	<b><math>\Delta\varepsilon</math> (in/in)</b>	<b><math>\sigma_{\text{mean}}</math> (psi)</b>
1000	42360	0.00182	23770
1100	42470	0.00184	23877
1200	42410	0.00183	23910
1300	42430	0.00182	23790
1400	42490	0.00184	23850
1500	42360	0.00184	23890
1600	42450	0.00185	23840
1700	42400	0.00183	23870
1800	42490	0.00184	23850
1900	42460	0.00184	23850
2000	42030	0.00183	24000
2100	42440	0.00184	23880
<b>AVG.</b>	42400	0.00184	23870

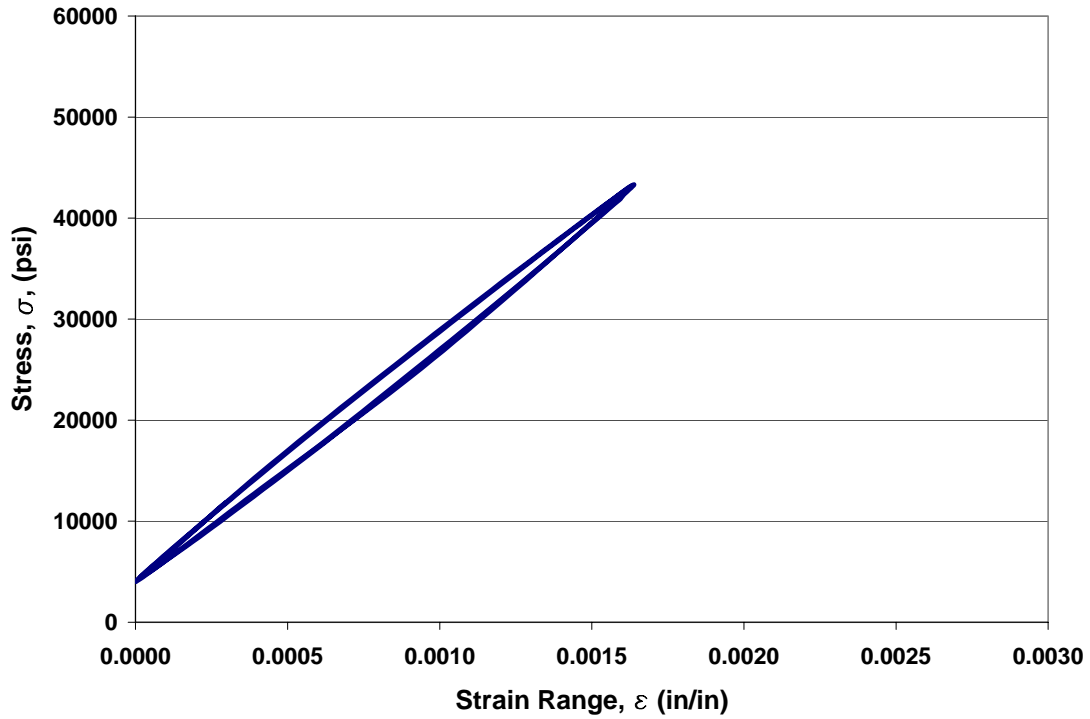


Figure B.12 Specimen 12 Hysteresis Loop

Table B.12 Specimen 12 Data

<b>Cycle approximate</b>	<b><math>\Delta\sigma</math> (psi)</b>	<b><math>\Delta\varepsilon</math> (in/in)</b>	<b><math>\sigma_{\text{mean}}</math> (psi)</b>
1000	39190	0.00164	23660
1100	39370	0.00164	23660
1200	39240	0.00163	23740
1300	39200	0.00165	23680
1400	39230	0.00164	23560
1500	39310	0.00164	23680
1600	39270	0.00163	23690
1700	39220	0.00165	23720
1800	39240	0.00165	23650
1900	39280	0.00165	23740
2000	38900	0.00162	23570
2100	39280	0.00163	23700
<b>AVG.</b>	39230	0.00164	23670

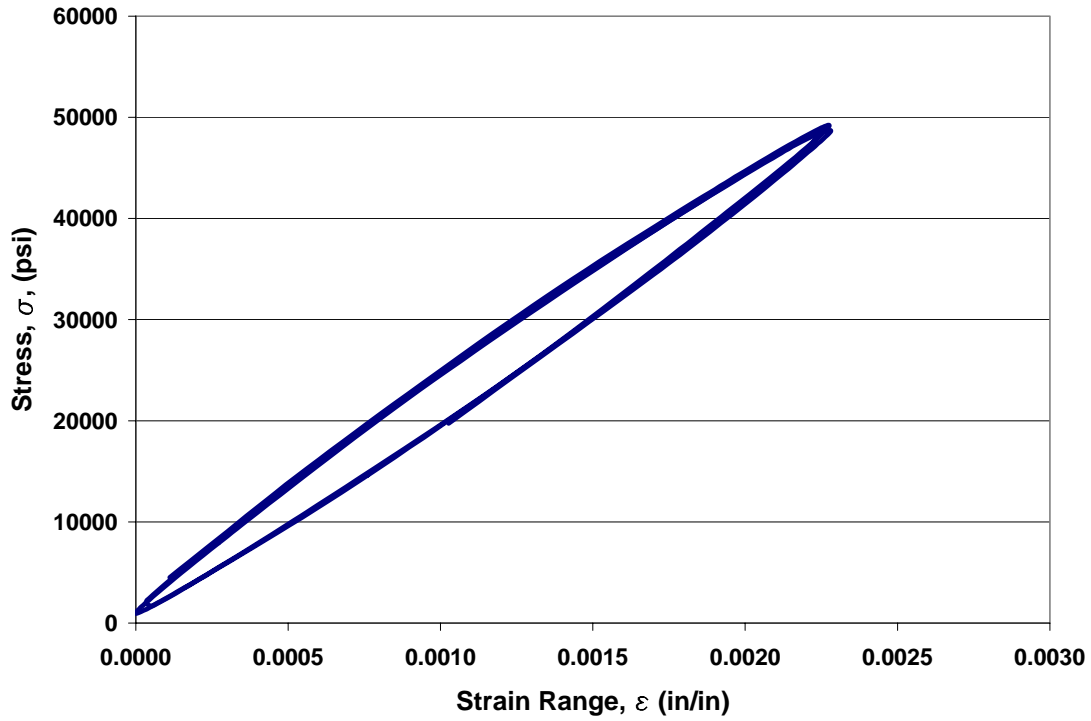


Figure B.13 Specimen 13 Hysteresis Loop

Table B.13 Specimen 13 Data

<b>Cycle approximate</b>	<b><math>\Delta\sigma</math> (psi)</b>	<b><math>\Delta\varepsilon</math> (in/in)</b>	<b><math>\sigma_{\text{mean}}</math> (psi)</b>
1000	48220	0.00229	25050
1100	48190	0.00230	25030
1200	48200	0.00226	25070
1300	48190	0.00229	25040
1400	48270	0.00229	25040
1500	48240	0.00229	25100
1600	47810	0.00228	24920
1700	48130	0.00228	25060
1800	48240	0.00231	25100
1900	48160	0.00228	25120
2000	48230	0.00231	25050
2100	47980	0.00226	24900
<b>AVG.</b>	48160	0.00229	25040

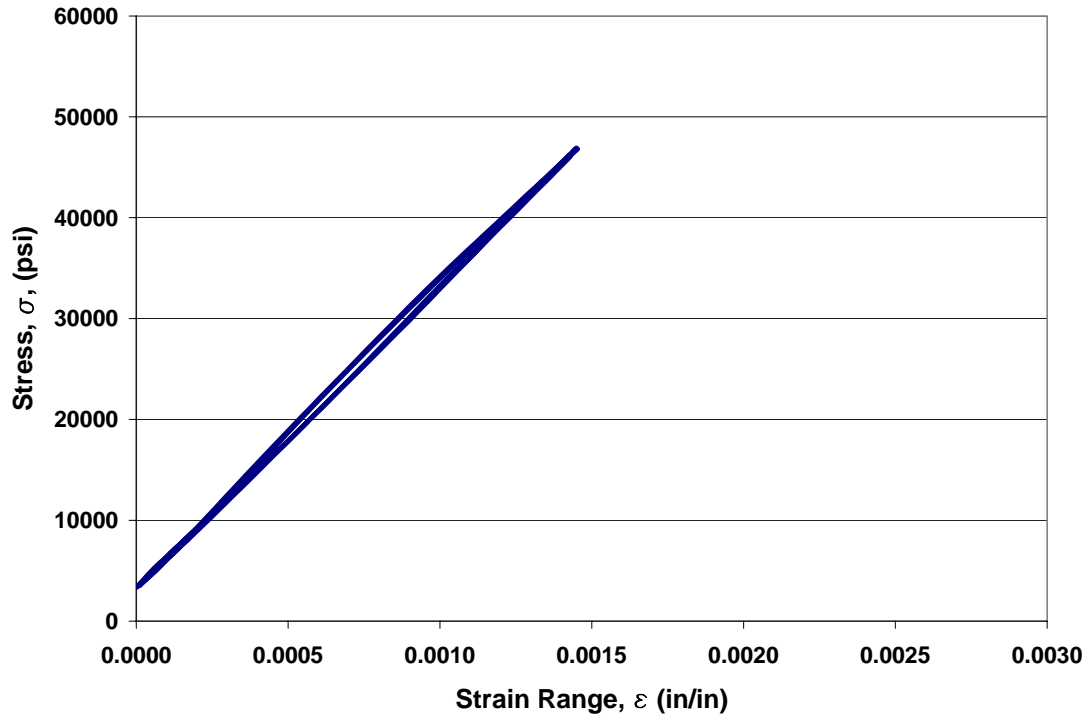


Figure B.14 Specimen 14 Hysteresis Loop

Table B.14 Specimen 14 Data

<b>Cycle approximate</b>	<b><math>\Delta\sigma</math> (psi)</b>	<b><math>\Delta\varepsilon</math> (in/in)</b>	<b><math>\sigma_{\text{mean}}</math> (psi)</b>
1000	43540	0.00146	25150
1100	43380	0.00145	25270
1200	43520	0.00146	25220
1300	43570	0.00147	25230
1400	43550	0.00146	25180
1500	43500	0.00145	25100
1600	43480	0.00145	25180
1700	43570	0.00145	25160
1800	43540	0.00146	25130
1900	43520	0.00145	25140
2000	43440	0.00145	25080
2100	43490	0.00145	25110
<b>AVG.</b>	43510	0.00145	25160

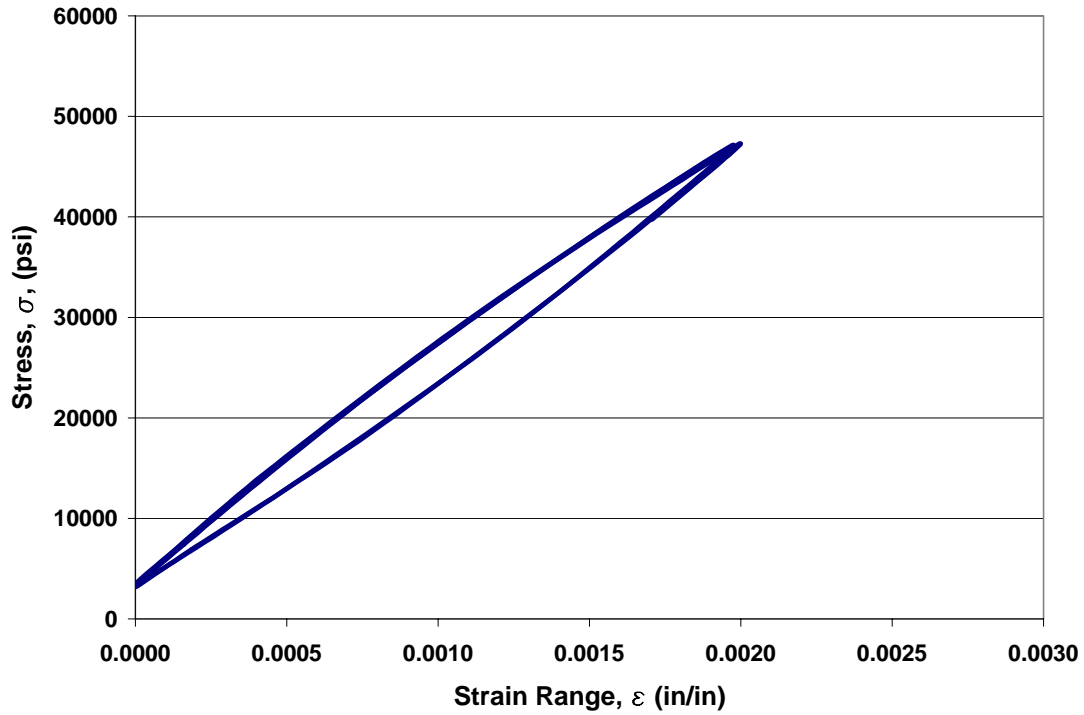


Figure B.15 Specimen 15 Hysteresis Loop

Table B.15 Specimen 15 Data

<b>Cycle approximate</b>	<b><math>\Delta\sigma</math> (psi)</b>	<b><math>\Delta\varepsilon</math> (in/in)</b>	<b><math>\sigma_{\text{mean}}</math> (psi)</b>
1000	43760	0.00200	25140
1100	44100	0.00200	25230
1200	44080	0.00201	25260
1300	44100	0.00200	25320
1400	43840	0.00197	25400
1500	44030	0.00200	25200
1600	44090	0.00200	25280
1700	44040	0.00200	25280
1800	44010	0.00200	25180
1900	44080	0.00201	25260
2000	44060	0.00200	25270
2100	44110	0.00200	25250
<b>AVG.</b>	44030	0.00200	25260

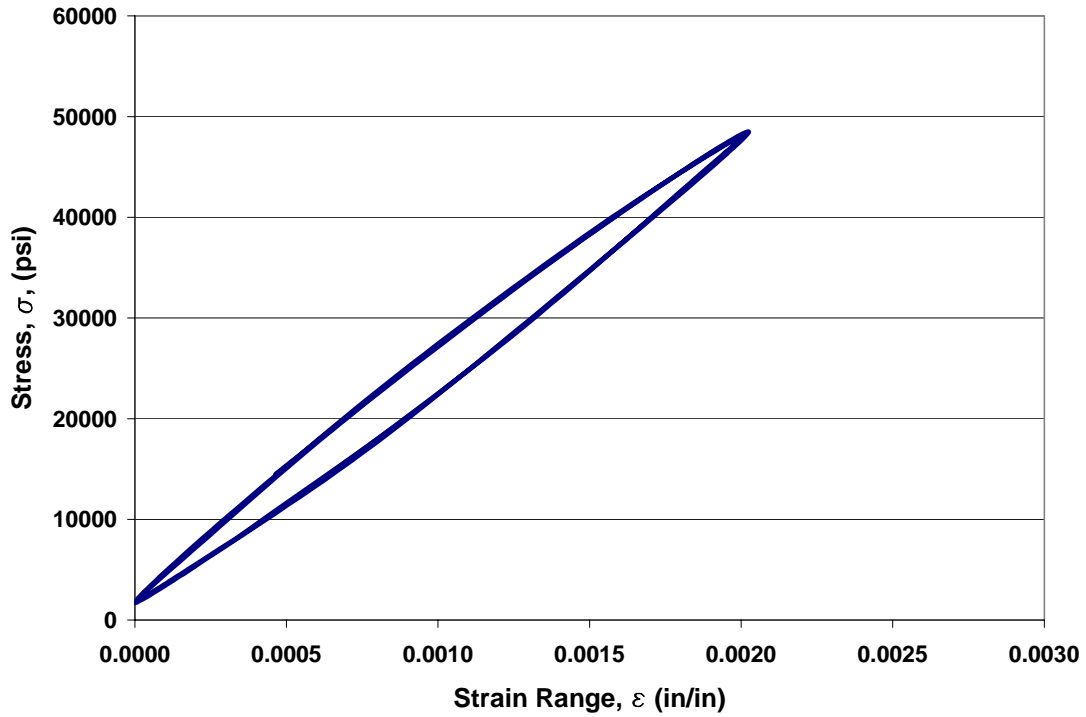


Figure B.16 Specimen 16 Hysteresis Loop

Table B.16 Specimen 16 Data

<b>Cycle approximate</b>	<b><math>\Delta\sigma</math> (psi)</b>	<b><math>\Delta\varepsilon</math> (in/in)</b>	<b><math>\sigma_{\text{mean}}</math> (psi)</b>
1000	46670	0.00202	25240
1100	46750	0.00202	25220
1200	46650	0.00202	25180
1300	46680	0.00202	25240
1400	46790	0.00202	25170
1500	46700	0.00202	25080
1600	46620	0.00202	25190
1700	46730	0.00202	25130
1800	46730	0.00203	25080
1900	46690	0.00201	25200
2000	46680	0.00202	25150
2100	46710	0.00202	25120
<b>AVG.</b>	46700	0.00202	25170

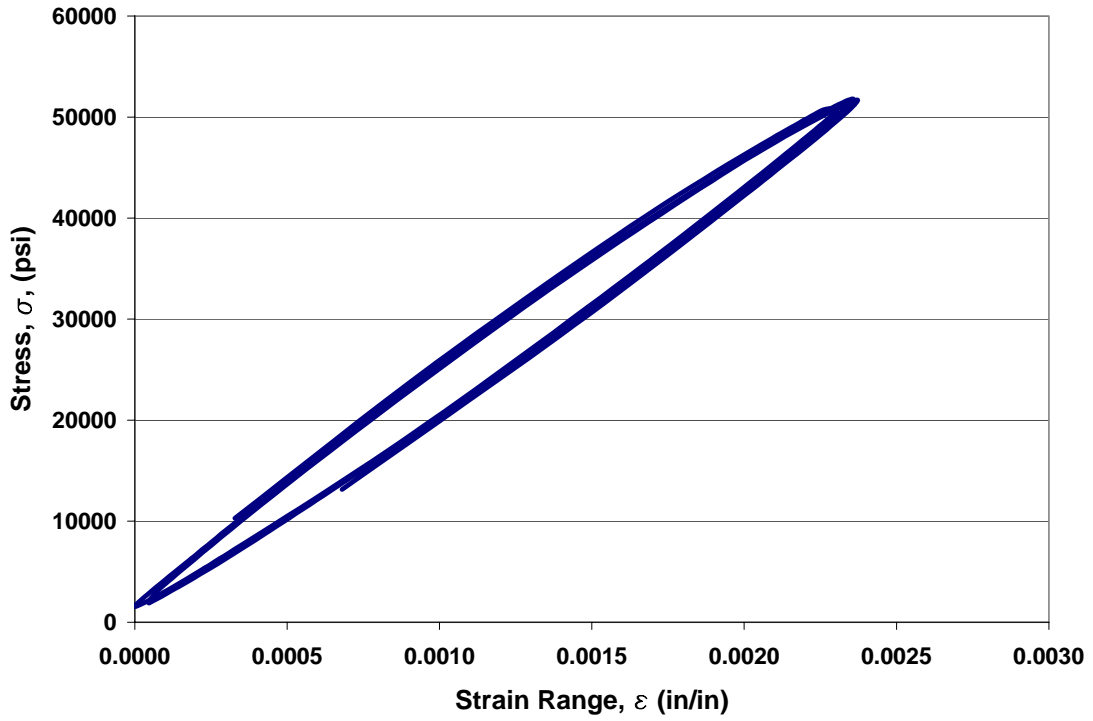


Figure B.17 Specimen 17 Hysteresis Loop

Table B.17 Specimen 17 Data

<b>Cycle approximate</b>	<b><math>\Delta\sigma</math> (psi)</b>	<b><math>\Delta\varepsilon</math> (in/in)</b>	<b><math>\sigma_{\text{mean}}</math> (psi)</b>
1000	50190	0.00234	26700
1100	50230	0.00236	26640
1200	50170	0.00233	26620
1300	50130	0.00237	26610
1400	50200	0.00238	26660
1500	50190	0.00238	26700
1600	49710	0.00235	26430
1700	50130	0.00236	26660
1800	50090	0.00238	26620
1900	49850	0.00233	26770
2000	50170	0.00237	26620
2100	50230	0.00234	26650
<b>AVG.</b>	50110	0.00235	26640

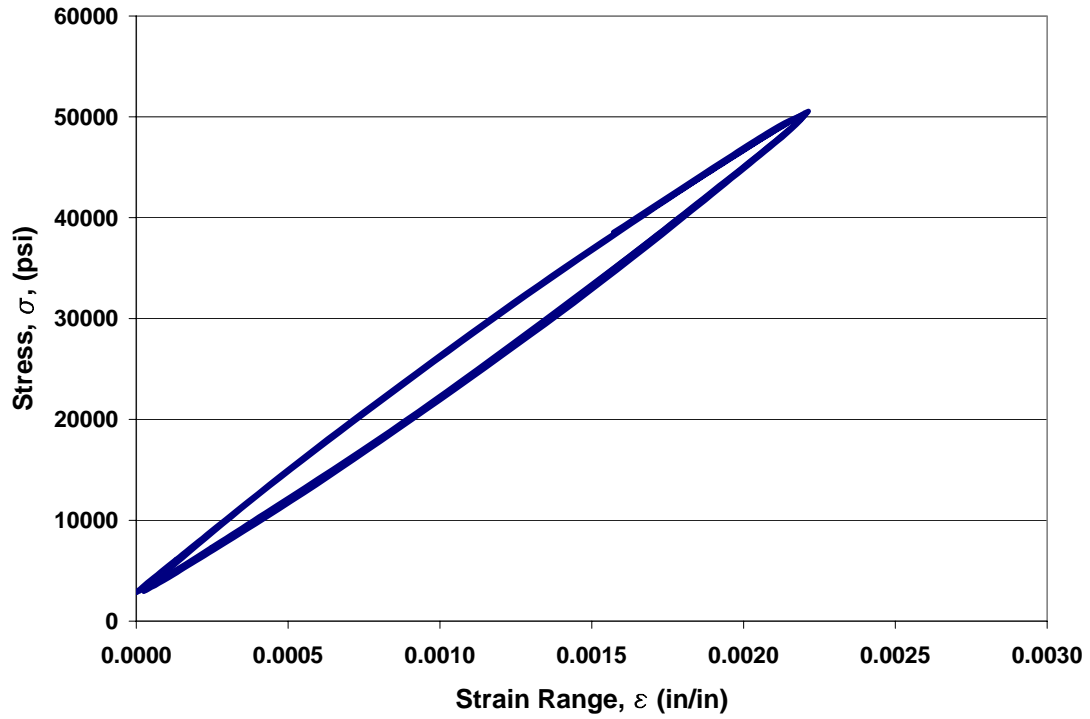


Figure B.18 Specimen 18 Hysteresis Loop

Table B.18 Specimen 18 Data

<b>Cycle approximate</b>	<b><math>\Delta\sigma</math> (psi)</b>	<b><math>\Delta\varepsilon</math> (in/in)</b>	<b><math>\sigma_{\text{mean}}</math> (psi)</b>
1000	47740	0.00221	26590
1100	47710	0.00221	26700
1200	47730	0.00223	26640
1300	47700	0.00220	26730
1400	47700	0.00221	26650
1500	47720	0.00221	26670
1600	47750	0.00222	26640
1700	47690	0.00221	26670
1800	47660	0.00221	26680
1900	47720	0.00222	26660
2000	47700	0.00221	26730
2100	47640	0.00221	26610
<b>AVG.</b>	47700	0.00221	26670

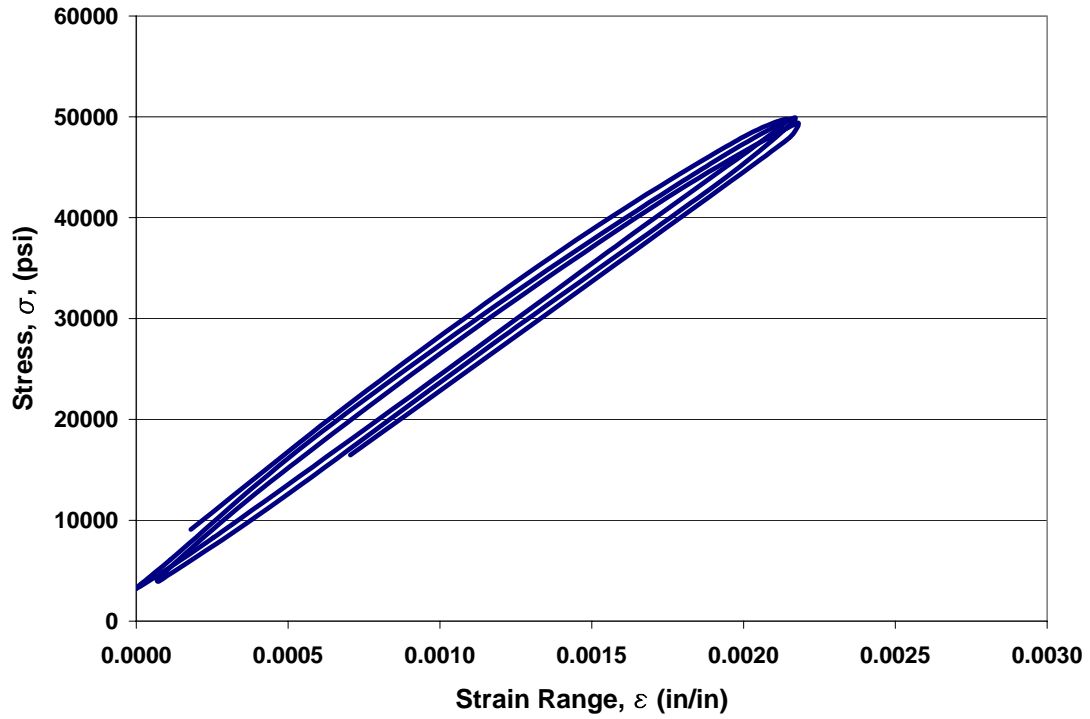


Figure B.19 Specimen 19 Hysteresis Loop

Table B.19 Specimen 19 Data

<b>Cycle approximate</b>	<b><math>\Delta\sigma</math> (psi)</b>	<b><math>\Delta\varepsilon</math> (in/in)</b>	<b><math>\sigma_{\text{mean}}</math> (psi)</b>
1000	46610	0.00227	26070
1100	46610	0.00225	26300
1200	46680	0.00220	26350
1300	46770	0.00227	26230
1400	46720	0.00225	26240
1500	46690	0.00223	26270
1600	46770	0.00217	26230
1700	46670	0.00227	26300
1800	46610	0.00231	26300
1900	46480	0.00228	26310
2000	46560	0.00223	26460
2100	46690	0.00231	26490
<b>AVG.</b>	46660	0.00225	26300

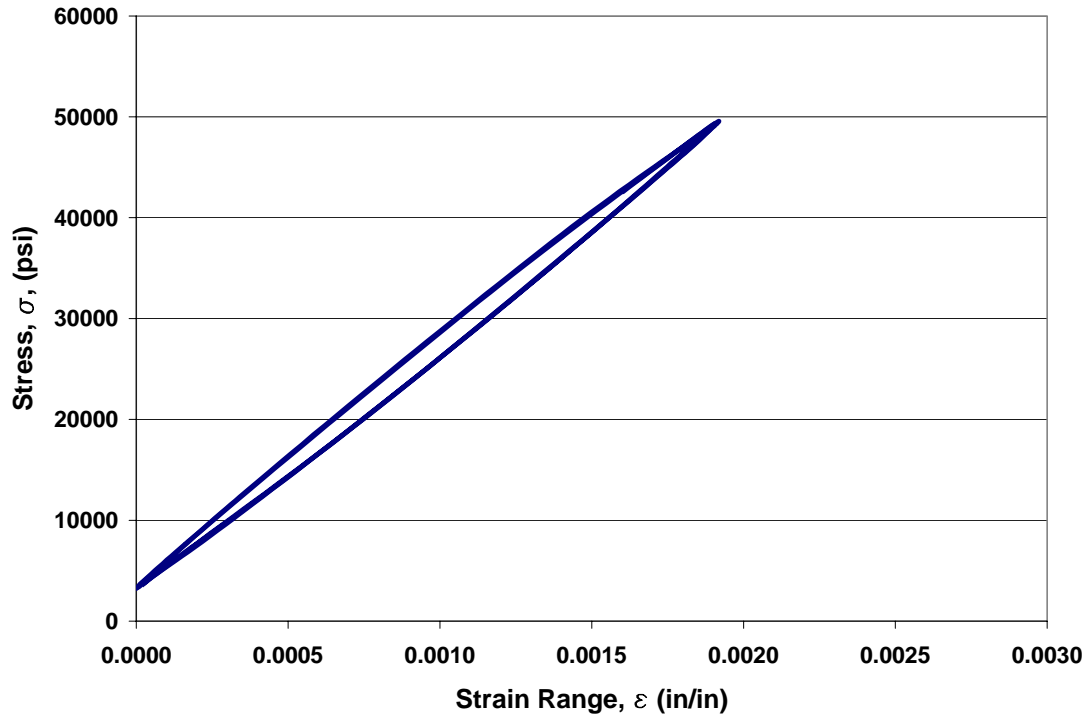


Figure B.20 Specimen 20 Hysteresis Loop

Table B.20 Specimen 20 Data

<b>Cycle approximate</b>	<b><math>\Delta\sigma</math> (psi)</b>	<b><math>\Delta\varepsilon</math> (in/in)</b>	<b><math>\sigma_{\text{mean}}</math> (psi)</b>
1000	46220	0.00192	26480
1100	46290	0.00191	26520
1200	45930	0.00192	26650
1300	46180	0.00192	26430
1400	46240	0.00192	26440
1500	46230	0.00192	26420
1600	46270	0.00191	26400
1700	46240	0.00192	26380
1800	46260	0.00192	26400
1900	45830	0.00189	26590
2000	46210	0.00191	26390
2100	46200	0.00192	26380
<b>AVG.</b>	46170	0.00191	26460

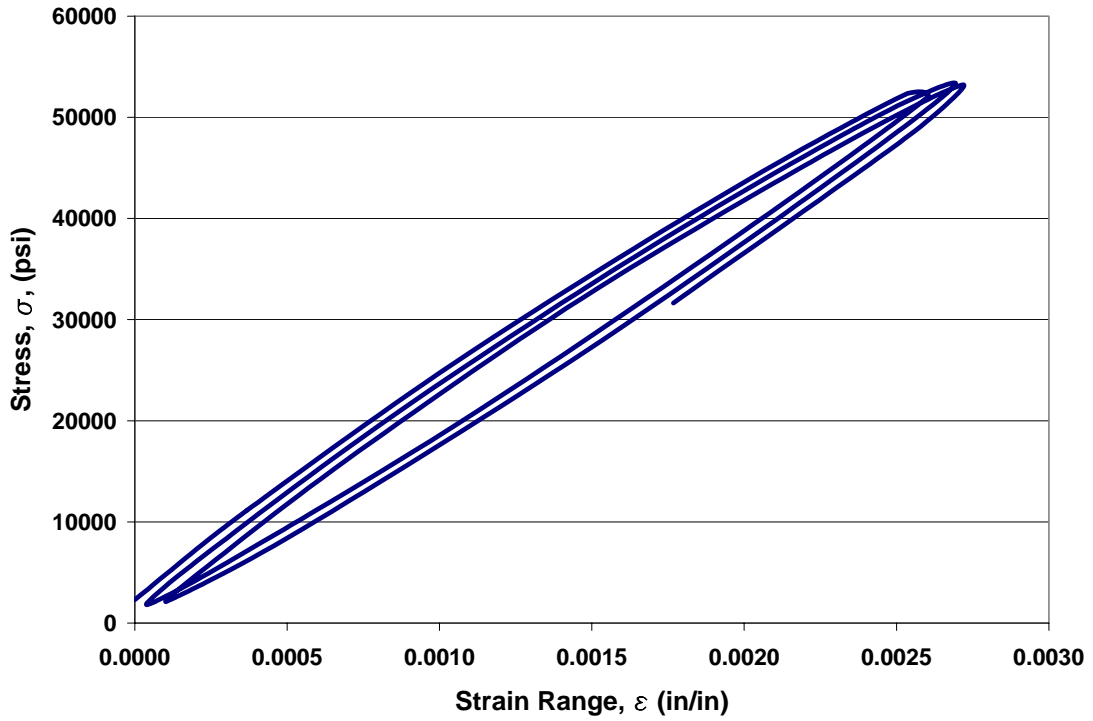


Figure B.21 Specimen 21 Hysteresis Loop

Table B.21 Specimen 21 Data

<b>Cycle approximate</b>	<b><math>\Delta\sigma</math> (psi)</b>	<b><math>\Delta\varepsilon</math> (in/in)</b>	<b><math>\sigma_{\text{mean}}</math> (psi)</b>
1000	51390	0.00271	27590
1100	51040	0.00264	27720
1200	51390	0.00272	27520
1300	51430	0.00274	27580
1400	51390	0.00269	27620
1500	51370	0.00269	27600
1600	51380	0.00262	27621
1700	51370	0.00457	27690
1800	51360	0.00223	27670
1900	51390	0.00211	27680
2000	50790	0.00202	27470
2100	51400	0.00207	27700
<b>AVG.</b>	51310	0.00265	27620

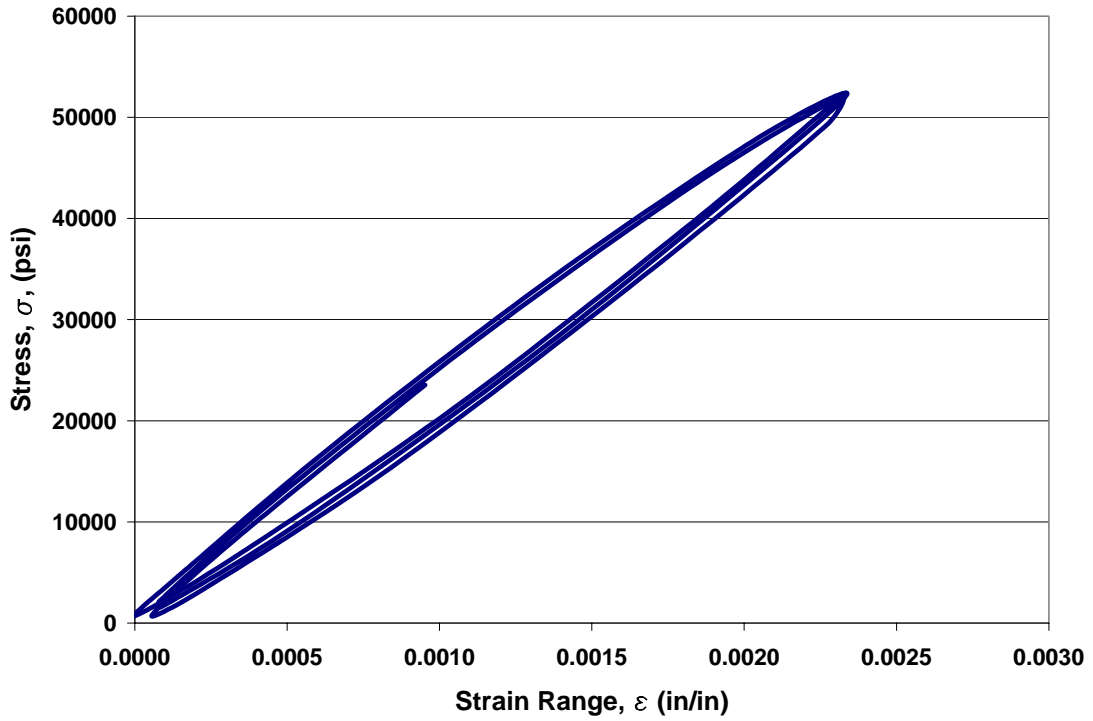


Figure B.22 Specimen 22 Hysteresis Loop

Table B.22 Specimen 22 Data

<b>Cycle approximate</b>	<b><math>\Delta\sigma</math> (psi)</b>	<b><math>\Delta\varepsilon</math> (in/in)</b>	<b><math>\sigma_{\text{mean}}</math> (psi)</b>
1000	51700	0.00268	26540
1100	51730	0.00256	26520
1200	51600	0.00252	26440
1300	51640	0.00255	26460
1400	51800	0.00261	26270
1500	51720	0.00253	26430
1600	51640	0.00261	26460
1700	51690	0.00267	26390
1800	51730	0.00265	26520
1900	51700	0.00253	26540
2000	51660	0.00257	26600
2100	51680	0.00254	26540
<b>AVG.</b>	51690	0.00258	26480

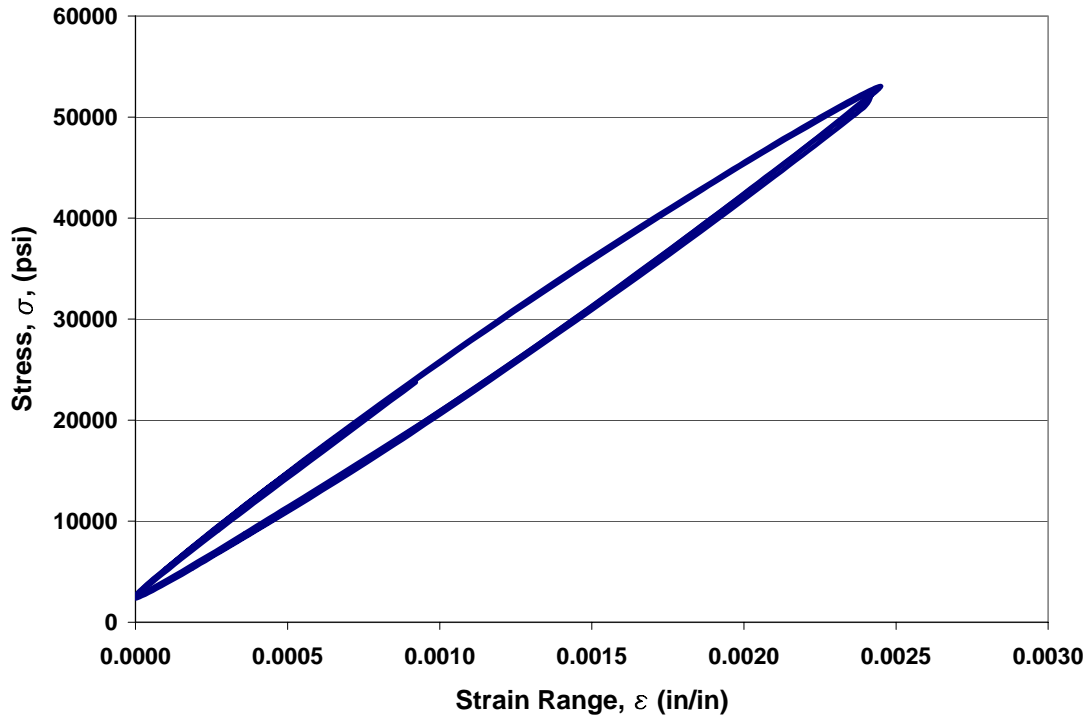


Figure B.23 Specimen 23 Hysteresis Loop

Table B.23 Specimen 23 Data

<b>Cycle approximate</b>	<b><math>\Delta\sigma</math> (psi)</b>	<b><math>\Delta\varepsilon</math> (in/in)</b>	<b><math>\sigma_{\text{mean}}</math> (psi)</b>
1000	50640	0.00249	27530
1100	50700	0.00250	27630
1200	50550	0.00241	27380
1300	50360	0.00246	27480
1400	50670	0.00249	27700
1500	50660	0.00245	27750
1600	50590	0.00248	27620
1700	50630	0.00247	27700
1800	50560	0.00246	27680
1900	50610	0.00248	27660
2000	50590	0.00247	27760
2100	50430	0.00247	27530
<b>AVG.</b>	50580	0.00247	27620

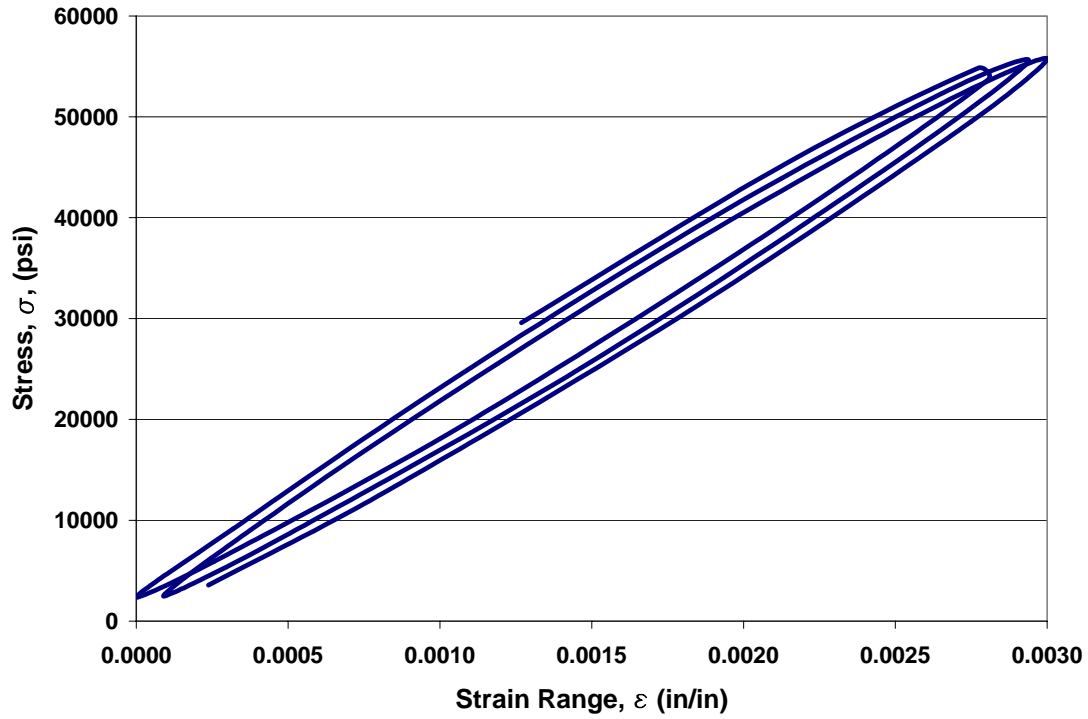


Figure B.24 Specimen 24 Hysteresis Loop

Table B.24 Specimen 24 Data

<b>Cycle approximate</b>	<b><math>\Delta\sigma</math> (psi)</b>	<b><math>\Delta\varepsilon</math> (in/in)</b>	<b><math>\sigma_{\text{mean}}</math> (psi)</b>
1000	53420	0.00288	29020
1100	53390	0.00297	28970
1200	53430	0.00292	29040
1300	53450	0.00295	29040
1400	53390	0.00296	28950
1500	53420	0.00302	29030
1600	53500	0.00302	29060
1700	53430	0.00297	28980
1800	53530	0.00292	29070
1900	53400	0.00300	29120
2000	52940	0.00292	29260
2100	53460	0.00301	29070
<b>AVG.</b>	53400	0.00296	29050

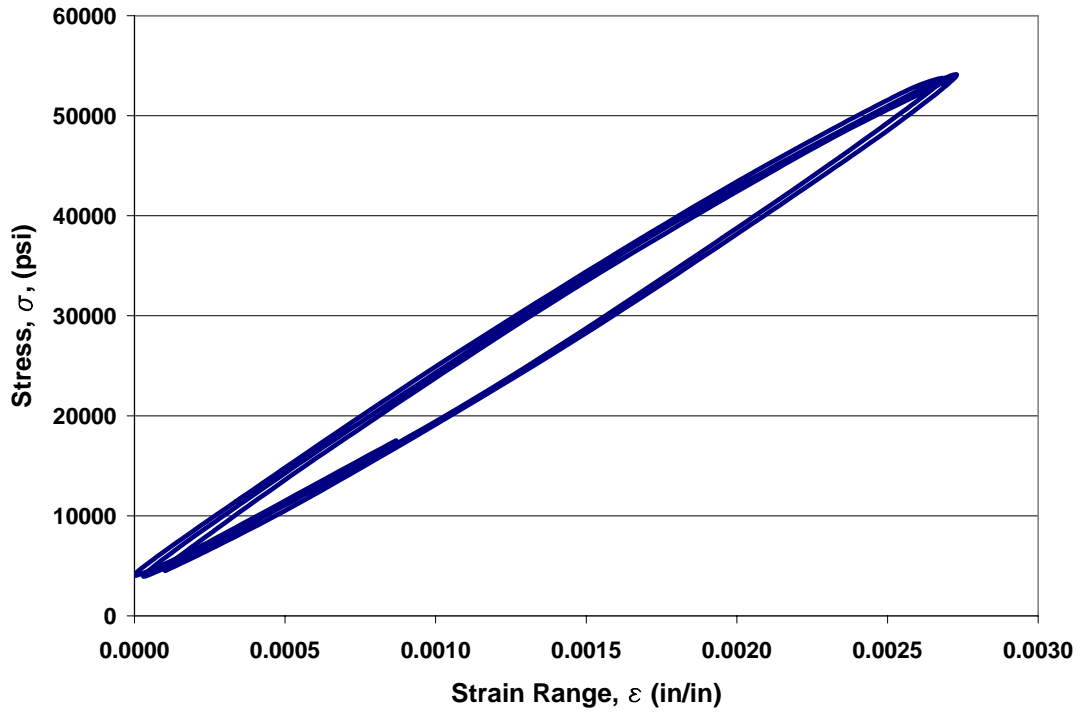


Figure B.25 Specimen 25 Hysteresis Loop

Table B.25 Specimen 25 Data

<b>Cycle approximate</b>	<b><math>\Delta\sigma</math> (psi)</b>	<b><math>\Delta\varepsilon</math> (in/in)</b>	<b><math>\sigma_{\text{mean}}</math> (psi)</b>
1000	50210	0.00271	29060
1100	50050	0.00273	29090
1200	49950	0.00269	28910
1300	50240	0.00270	28910
1400	50320	0.00267	28920
1500	50120	0.00271	29020
1600	50020	0.00267	29060
1700	50140	0.00273	28910
1800	50150	0.00273	29000
1900	50040	0.00268	29160
2000	50070	0.00269	28990
2100	49980	0.00270	29090
<b>AVG.</b>	50100	0.00270	29010

## APPENDIX C. CHARPY V-NOTCH IMPACT DATA

Table C.1 Charpy V-Notch Impact Data

Targeted Temperature (°F)	Measured Temperature (°F)	Absorbed Energy Cv (ft-lb)	Average for Targeted Temperature (ft-lb)
-10	-10.2	4.1630	4.11
	-10.0	4.1470	
	-9.9	3.8505	
	-9.8	3.7985	
	-9.8	4.5775	
10	9.8	5.1570	5.11
	9.9	4.2152	
	10.0	5.1570	
	10.1	5.7881	
	10.2	5.2095	
30	29.8	9.4668	7.89
	30.1	7.3240	
	30.4	8.8211	
	30.4	6.7927	
	30.7	7.0581	
50	49.1	13.2830	11.56
	50.2	13.0080	
	50.7	9.6827	
	50.9	13.3390	
	51.1	8.4991	
70	69.7	16.5080	17.03
	69.9	18.1980	
	70.1	17.2390	
	70.1	14.2780	
	70.3	18.9350	
90	85.9	26.8550	28.48
	86.2	24.0380	
	86.5	33.0130	
	86.6	32.2880	
	88.9	26.2060	
105	102.8	47.2070	49.96
	102.9	59.4880	
	104.0	53.5360	
	104.5	47.0170	
	105.6	42.5490	
110	108.9	54.6340	59.03
	109.1	53.7940	
	109.2	54.5760	
	109.5	55.0870	
	111.0	77.0760	
135	134.8	78.2940	84.57
	135.1	87.2140	
	135.7	81.7540	
	136.6	85.9820	
	137.6	89.6140	

## APPENDIX D. FATIGUE CRACK GROWTH DATA

Table D.1 Compact Tension Specimen 1 Data

N (cycles)	Measured Length (in)			da/dN $10^{-5}$ (in/cycle)	a (in)	a/W (in/in)	$\Delta K$ (ksi*in <sup>1/2</sup> )
	Front	Back	Avg.				
27000	2.075	2.079	2.077				
30000	2.146	2.142	2.144	2.23	1.144	0.286	38.9
33000	2.225	2.220	2.223	2.62	1.223	0.306	40.9
36000	2.296	2.290	2.293	2.35	1.293	0.323	42.8
39000	2.390	2.386	2.388	3.17	1.388	0.347	45.5
42000	2.494	2.485	2.490	3.38	1.490	0.372	48.6
45000	2.629	2.635	2.632	4.75	1.632	0.408	53.4
48000	2.897	2.886	2.892	8.65	1.892	0.473	63.9

Table D.2 Compact Tension Specimen 2 Data

N (cycles)	Measured Length (in)			da/dN $10^{-5}$ (in/cycle)	a (in)	a/W (in/in)	$\Delta K$ (ksi*in <sup>1/2</sup> )
	Front	Back	Avg.				
12000	1.892	1.888	1.890				
15000	1.910	1.920	1.915	0.833	0.915	0.229	33.3
18000	1.935	1.934	1.935	0.650	0.935	0.234	33.8
21000	1.960	1.955	1.958	0.767	0.958	0.239	34.3
24000	1.981	1.979	1.980	0.750	0.980	0.245	34.9
27000	2.000	1.999	2.000	0.650	1.000	0.250	35.3
30000	2.025	2.020	2.023	0.767	1.023	0.256	35.9
33000	2.090	2.088	2.089	2.22	1.089	0.272	37.5
36000	2.168	2.159	2.164	2.48	1.164	0.291	39.4
39000	2.250	2.241	2.246	2.73	1.246	0.311	41.5
42000	2.338	2.335	2.337	3.03	1.337	0.334	44.0
45000	2.475	2.463	2.469	4.42	1.469	0.367	48.0
48000	2.535	2.538	2.537	2.25	1.537	0.384	50.1
51000	2.715	2.703	2.709	5.75	1.709	0.427	56.2
54000	2.889	2.890	2.890	6.02	1.890	0.472	63.8

Table D.3 Compact Tension Specimen 3 Data

N (cycles)	Measured Length (in)			da/dN $10^{-5}$ (in/cycle)	a (in)	a/W (in/in)	$\Delta K$ (ksi*in <sup>1/2</sup> )
	Front	Back	Avg.				
12000	1.860	1.851	1.856				
15000	1.886	1.888	1.887	1.05	0.887	0.222	32.7
18000	1.899	1.913	1.906	0.633	0.906	0.227	33.1
21000	1.929	1.938	1.934	0.917	0.934	0.233	33.8
24000	1.996	2.008	2.002	2.28	1.002	0.251	35.4
27000	2.052	2.043	2.048	1.52	1.048	0.262	36.5
30000	2.080	2.130	2.105	1.92	1.105	0.276	37.9
33000	2.163	2.188	2.176	2.35	1.176	0.294	39.7
36000	2.212	2.230	2.221	1.52	1.221	0.305	40.9
39000	2.283	2.331	2.307	2.87	1.307	0.327	43.2
42000	2.390	2.424	2.407	3.33	1.407	0.352	46.1
45000	2.515	2.530	2.523	3.85	1.523	0.381	49.7
48000	2.690	2.723	2.707	6.13	1.707	0.427	56.1
51000	3.010	3.034	3.022	10.5	2.022	0.506	70.5

Table D.4 Compact Tension Specimen 4 Data

N (cycles)	Measured Length (in)			da/dN $10^{-5}$ (in/cycle)	a (in)	a/W (in/in)	$\Delta K$ (ksi*in <sup>1/2</sup> )
	Front	Back	Avg.				
12000	1.836	1.832	1.834				
15000	1.874	1.875	1.875	1.35	0.875	0.219	32.4
18000	1.901	1.911	1.906	1.05	0.906	0.227	33.1
21000	1.936	1.967	1.952	1.52	0.952	0.238	34.2
24000	1.972	1.980	1.976	0.817	0.976	0.244	34.8
27000	1.983	1.995	1.989	0.433	0.989	0.247	35.1
30000	1.992	2.006	1.999	0.333	0.999	0.250	35.3
33000	2.033	2.046	2.040	1.35	1.040	0.260	36.3
36000	2.118	2.123	2.121	2.70	1.121	0.280	38.3
39000	2.135	2.137	2.136	0.517	1.136	0.284	38.7
42000	2.189	2.204	2.197	2.02	1.197	0.299	40.2
45000	2.225	2.246	2.236	1.30	1.236	0.309	41.3
48000	2.278	2.310	2.294	1.95	1.294	0.324	42.9
51000	2.389	2.419	2.404	3.67	1.404	0.351	46.0
54000	2.536	2.537	2.537	4.42	1.537	0.384	50.1
57000	2.713	2.739	2.726	6.32	1.726	0.432	56.9
60000	3.066	3.080	3.073	11.6	2.073	0.518	73.4

Table D.5 Compact Tension Specimen 5 Data

N (cycles)	Measured Length (in)			da/dN $10^{-5}$ (in/cycle)	a (in)	a/W (in/in)	$\Delta K$ (ksi*in <sup>1/2</sup> )
	Front	Back	Avg.				
12000	1.862	1.893	1.878				
15000	1.893	1.927	1.910	1.08	0.910	0.228	33.2
18000	1.905	1.952	1.929	0.617	0.929	0.232	33.6
21000	1.940	1.980	1.960	1.05	0.960	0.240	34.4
24000	1.990	2.032	2.011	1.70	1.011	0.253	35.6
27000	2.047	2.080	2.064	1.75	1.064	0.266	36.9
30000	2.107	2.135	2.121	1.92	1.121	0.280	38.3
33000	2.190	2.255	2.223	3.38	1.223	0.306	40.9
36000	2.291	2.333	2.312	2.98	1.312	0.328	43.4
39000	2.409	2.473	2.441	4.30	1.441	0.360	47.1
42000	2.598	2.653	2.626	6.15	1.626	0.406	53.1
45000	2.931	3.117	3.024	13.3	2.024	0.506	70.6

## APPENDIX E. INFLUENCE LINES FOR SOUTHEASTERN STRUT

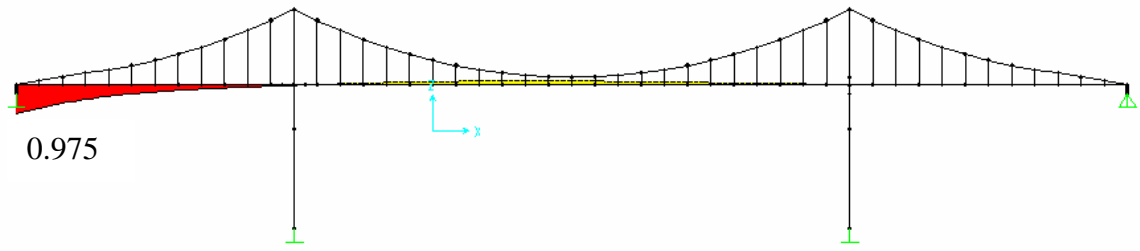


Figure E.1 Lane 1 Southeastern Strut Axial Load Influence Line

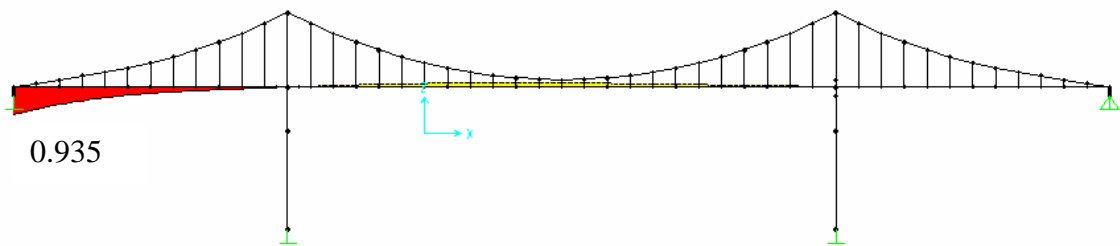


Figure E.2 Lane 2 Southeastern Strut Axial Load Influence Line

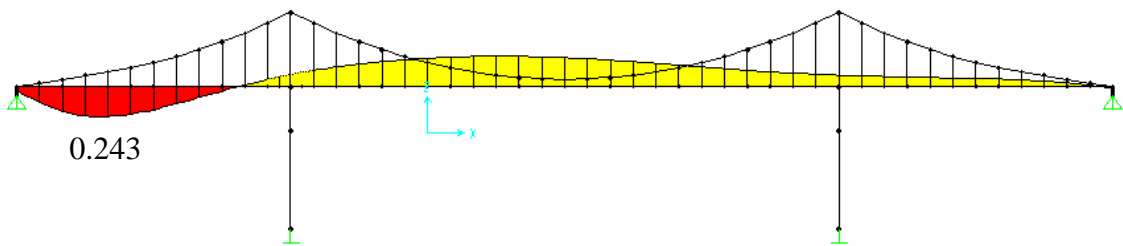


Figure E.3 Lane 3 Southeastern Strut Axial Load Influence Line

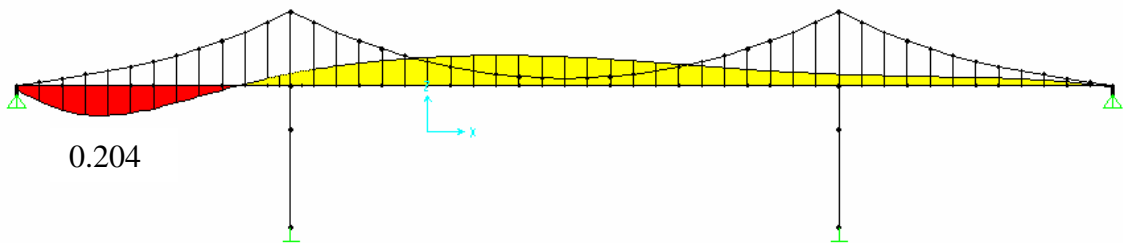


Figure E.4 Lane 4 Southeastern Strut Axial Load Influence Line

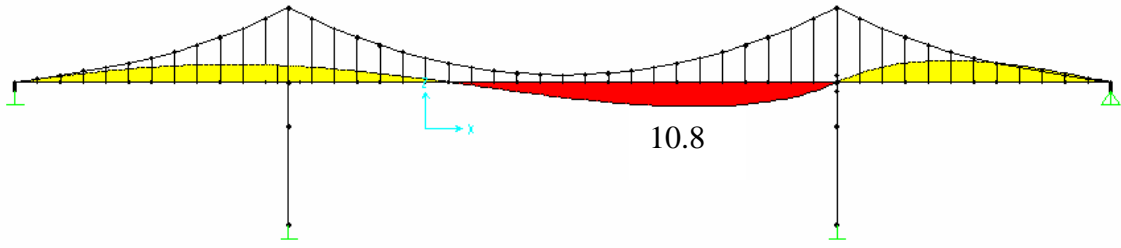


Figure E.5 Lane 1 Southeastern Strut Moment Influence Line

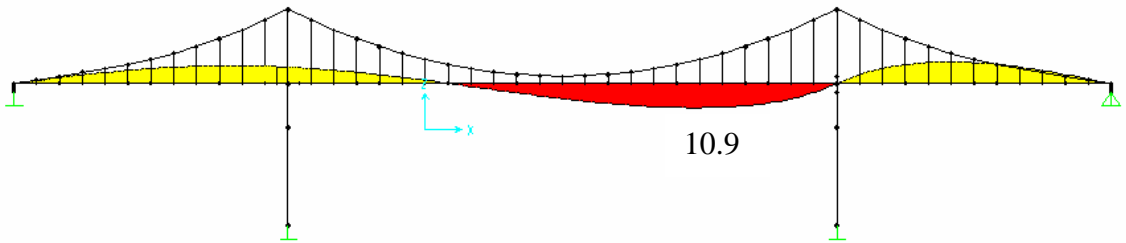


Figure E.6 Lane 2 Southeastern Strut Moment Influence Line

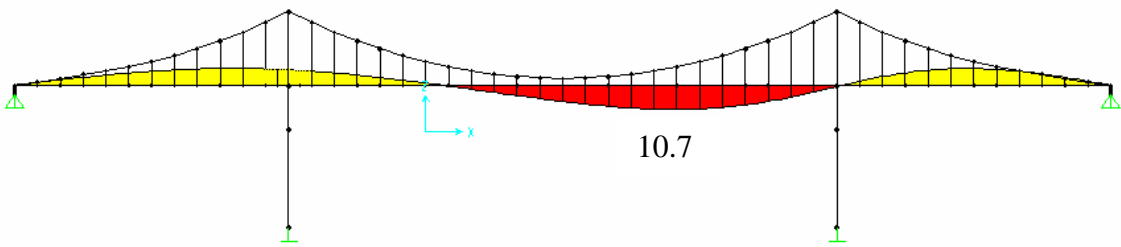


Figure E.7 Lane 3 Southeastern Strut Moment Influence Line

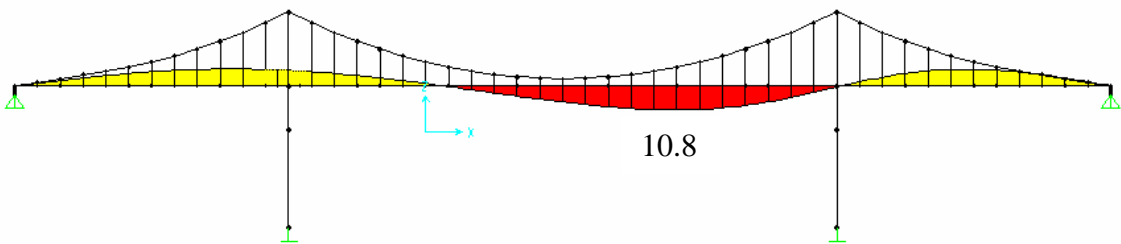


Figure E.8 Lane 4 Southeastern Strut Moment Influence Line

## APPENDIX F. SPECIFICATIONS FOR REMOTE TILTMETER

Table F.1 Items for Remote Tiltmeter Monitoring (January 2005 Prices)

Company	Item Description	Quantity	Price
Lucas Schaevitz	LSOP-30 Inertial Referenced tilt sensor	4	\$5,044.00
Campbell Scientific	CR10X Measurement & Control Module w/128K Memory, Wiring Panel, & Screwdriver	1	\$1,200.00
Campbell Scientific	ENC 16/18 Weather Resistant Enclosure 16 x 18 Inch	1	\$259.20
Campbell Scientific	ENC 16/18 Option W/1 Conduit for Cables	1	\$0.00
Campbell Scientific	CH100 12V Charger/Regulator	1	\$158.40
Campbell Scientific	Power Wall Adapter AC/DC 110VAC to 18VAC 1.2A, 6 Ft. Cable	1	\$28.80
Campbell Scientific	BP24 12V Sealed Rechargeable Battery, 24Ahr	1	\$134.40
Campbell Scientific	AM 16/32 16 or 32 Channel Relay Multiplexer	1	\$523.20
Campbell Scientific	Redwing100 Airlink Redwing CDMA Cellular Digital Modem for Verizon Systems	1	\$520.00
Campbell Scientific	Redwing & Raven Mounting Kit w/Cable	1	\$19.20
Campbell Scientific	Antenna Cellular 800MHz YAGI 8DBD W/Type N Female & Mounting Hardware, 10Ft. Cable	1	\$196.80
Campbell Scientific	SC932A CS I/O to 9-PIN RS-232 DCE Interface	1	\$81.60
Campbell Scientific	Freight	1	\$65.00
<b>*Total USD*</b>			<b>\$8,230.60</b>